A NANOPOROUS MEMBRANE BASED ELECTROCHEMICAL BIOSENSOR FOR BACTERIA DETECTION WITH NANOPARTICLE TAG AMPLIFICATION

TIAN FENG

M.Phil

The Hong Kong Polytechnic University

2016

The Hong Kong Polytechnic University

Interdisciplinary Division of Biomedical Engineering

A Nanoporous Membrane Based Electrochemical Biosensor for Bacteria Detection with Nanoparticle Tag Amplification

TIAN Feng

A thesis submitted in partial fulfilment of the requirements for the degree of Master of Philosophy

May 2016

Certificate of originality

I hereby declare that this thesis is my own work and that, to the best of my knowledge and belief, it reproduces no material previously published or written, nor material that has been accepted for the award of any other degree or diploma, except where due acknowledgement has been made in the text.

_____

TIAN Feng

Abstract

Nowadays, biosensing has attracted tremendous interests for its versatility in many fields including food safety, medical diagnosis, and prognosis, as well as environmental detection. Food poisoning is a critical issue which threatens lives through pathogenic bacteria which are naturally infectious or releasing toxins. Conventional detection methods consist of culture & colony counting method, electron microscopy method, immunological reaction based method and polymerase chain reaction (PCR). These methods have been demonstrated outstanding for detection of pathogenic bacteria or characteristic virulence genes expressed in them. However, these traditional methods have drawbacks such as long testing time, complex working procedures and high cost. Hence, the development of new detection methods is of great importance. Recently, various biosensors including optical biosensors, piezoelectric biosensors, and electrochemical biosensors have been developed for pathogenic bacteria detection. Among these three types of biosensors for pathogenic bacteria detection, electrochemical biosensors are very promising with advantages of low-cost, ease to operate, rapid response and portability, which highly meets the requirement of on-site bacteria detection in food or water. Moreover, the recent rapid development of nanomaterials injects new energy into electrochemical biosensors with better performance such as high sensitivity and specificity.

The research of this thesis is mainly focused on designing and fabricating nanoporous membrane based electrochemical biosensors with nanocatalyst-based signal

amplification for rapid and sensitive detection of pathogenic bacteria or characteristic virulence genes expressed in pathogenic bacteria. Nanoporous alumina membrane is an excellent biosensing platform for various biological species detection due to its tunable nanopore size as well as the high surface area to volume ratio which allows numerous oligonucleotide probes and antibody immobilization. Nanoporous alumina membrane based microfluidic chambers are designed as the electrochemical detecting platform. *E. coli O157:H7 genes* and *Salmonella enteritidis* bacteria are chosen as the representative food-borne pathogens to testify the functionality of this biosensor.

The first part of this thesis is to develop a nanoporous alumina membrane based electrochemical biosensor with platinum nanoparticle (PtNP) tags for *E. coli O157:H7* gene detection. Firstly, (3-glycidoxypropyl) trimethoxysilane (GPMS) silane was immobilized onto nanoporous alumina membrane surface followed by further immobilization of oligonucleotide probes through covalent binding. After oligonucleotide probes immobilization, nanoporous alumina membrane was integrated with a PDMS microfluidic chamber. The solution with target *E. coli O157:H7* gene was then dropped into the detection chamber and hybridized with oligonucleotide probes. Platinum nanoparticles (PtNPs) modified with secondary oligonucleotide probes were added and conjugated with target *E. coli O157:H7* gene to form sandwich structures. PtNPs then catalyzed soluble 4-Chloro-1-naphthol (4-CN) in the solution into insoluble products which were deposited on the nanoporous membrane, leading to blockage of nanopores and impedance signal increase. By

electrochemical impedance spectroscopy (EIS), the impedance signal increase was then measured. Various characterization methods including fluorescent labelling, electron microscopy and Zeta-potential measurement were used to confirm experimental steps. The hybridization time between target genes and probe genes as well as the precipitation catalyzing time were investigated by EIS. The specificity was also studied using non-target oligonucleotides and 6 bases mismatched oligonucleotides. As a result, this biosensor showed a good sensitivity and selectivity with a limit of detection (LOD) as low as 94 pM.

The second part of this thesis was to develop a nanoporous alumina membrane based electrochemical biosensor with graphene oxide (GO)/Hemin-Antibody composite amplification for the whole-cell bacterial detection of *Salmonella enteritidis*. Nanoporous alumina membrane was firstly integrated into microfluidic chambers and then *Salmonella enteritidis ompC* antibodies were immobilized onto membrane surface with GPMS silane as the chemical linker. Target *Salmonella enteritidis* bacteria were then captured by these antibodies on nanoporous membrane. Here, GO/Hemin-antibody was chosen as amplification tag was composites instead of PtNPs because of the high loading capacity of graphene oxide and the easy modification of hemin molecules and antibodies onto GO surface. Precipitation of 4-CN was then performed, leading to a significant increase of impedance for signal amplification. Both the detection time and specificity of this biosensor was studied for *Salmonella enteritidis*. The amplification effect on detection sensitivity was also explored. As a

result, this platform showed a good sensitivity and selectivity with a limit of detection (LOD) as low as 12 CFU/mL.

List of Publications

Journal Papers

[1] **Tian, F.**, Lyu, J., Shi, J., Tan, F., & Yang, M. (2016). A polymeric microfluidic device integrated with nanoporous alumina membranes for simultaneous detection of multiple foodborne pathogens. Sensors and Actuators B: Chemical, 225, 312-318.

[2] Chan, C. Y., Guo, J., Sun, C., Tsang, M. K., **Tian, F.**, Hao, J., ... & Yang, M. (2015). A reduced graphene oxide-Au based electrochemical biosensor for ultrasensitive detection of enzymatic activity of botulinum neurotoxin A. Sensors and Actuators B: Chemical, 220, 131-137.

Acknowledgements

First of all, I would like to give my sincere gratitude to my supervisor, Dr. Mo Yang, for his generous help and support. The invaluable advice and sustained encouragement gave a right direction and guided me to overcome problems during my research. His intelligence in finding and solving problems as well as the enthusiasm and optimism had a profound impact on my research career. The most prominent and impressive is the talent in grasping the principal aspects of issues.

Then I would like to thank Dr. Sheng Chen from Department of Applied Biology & Chemical Technology in the Hong Kong Polytechnic University for the *Salmonella enteritidi*s bacteria culture and *Salmonella enteritidis opmC* antibodies synthesis and preparation, as well as the characterization instrument supply. I would like to thank Dr. Hardy Lui from MRC for SEM characterizations and Dr. Wei Lu from MRC for TEM characterizations. Also I would like to thank professors and staffs in Interdisciplinary Division of Biomedical Engineering for their selfless encouragement and inspiration.

At last, I would like to thank all the labmates in our group, Dr. Weiwei Ye, Miss. Jingyu Shi, Miss. Jing Lyu, Dr. Chan Chun Yu, Dr. Fei Tan, Miss. Xiaoqian Su, Miss Gerile Oudeng and Miss Yadi Fan for the constructive and inspiring suggestions during my two years' M.Phil. study. Also I would like to thank my colleagues and friends in S104 and S106, Miss Qinjin He, Miss Shiyao Wang, Mr. Yu Zheng, Miss

Yangmin Lin, Mr. Yaoheng Yang, Mr. Zhihai Qiu, Mr. Cheng Liu and so on, for their friendship and accompanies of such fascinating and interesting life in Hong Kong.

Last but not least, I would like to thank my parents for their love and support without any reservation to help me go through difficult patches.

Table of Contents

Certificate of originality i

Abstract ii

List of Publications vi

Acknowledgements vii

Table of Contents ix

List of Figures xiv

List of Tables xviii

List of Abbreviations xix

Chapter 1 Introduction 1

1.1 Detection of Pathogenic Bacteria 1

1.1.1 Diseases Caused by Foodborne Pathogenic Bacteria 1

1.1.2 Traditional methods for Pathogenic Bacteria Detection 5

1.2 Biosensor for Pathogenic Bacteria Detection 7

1.2.1 Optical biosensor 8

1.2.2 Piezoelectric biosensor 9

1.2.3 Electrochemical biosensor 10

1.3 Electrochemical biosensor for bacteria detection 11

1.3.1 Introduction of electrochemical sensing 12

1.3.2 Electrochemical biosensor classification based on recognition mechanism 17

1.3.3 Why electrochemical biosensing.....21
1.4 Impedimetric biosensor.....23
1.4.1 Electrochemical impedance spectroscopy (EIS).....23
1.4.2 Factors for impedance variation.....27
1.4.3 Catalyzed precipitation and its applications in impedimetric biosensors.....30
1.5 Graphene and graphene derivative.....34
1.5.1 Graphene and its structure.....34
1.5.2 Synthesis of graphene and its properties.....36
1.5.3 Graphene based composites.....42
1.5.4 Electrochemistry of graphene materials.....44
1.5.5 Applications of graphene related materials in electrochemical biosensors.....46
1.6 Nanoporous alumina membrane.....53
1.6.1 Structure of nanoporous alumina membrane.....53
1.6.2 Properties of nanoporous alumina membrane.....54
1.6.3 Application of nanoporous alumina membrane in electrochemical biosensing.....55
1.7 Objectives of the study.....57
Chapter 2 Methodology.....59
2.1 Nanoporous alumina membrane based electrochemical biosensor with PtNPs tags for *E. coli O157:H7 gene* detection.....59

2.1.1 Materials and instruments 59

2.1.2 Surface silanization of nanoporous alumina membrane 61

2.1.3 Oligonucleotide probes immobilization 63

2.1.4 Fabrication of microfluidic chip integrated with nanoporous alumina 64

2.1.5 PtNPs synthesis 66

2.1.6 PtNP-oligonucleotide conjugation preparation 66

2.1.7 Target *E. coli O157:H7* gene capture 67

2.1.8 Formation of a sandwich structure and precipitation catalysis 68

2.1.9 Electrochemical impedance spectroscopy for target *E. coli O157:H7 gene* detection 70

2.1.10 Specificity study of this fabricated *E. coli O157:H7 gene* electrochemical biosensor 71

2.2 Nanoporous alumina membrane based electrochemical biosensor with GO/Hemin-Antibody tags amplification for *Salmonella enteritidis* detection 72

2.2.1 Materials and instruments 72

2.2.2 Antibody Immobilization on Nanoporous Alumina Membrane 73

2.2.3 Synthesis of GO/Hemin/-Antibody composites 75

2.2.4 *Salmonella enteridis* captured on nanoporous alumina membrane 77

2.2.5 Formation of a sandwich structure and precipitation catalysis 78

2.2.6 Electrochemical impedance spectroscopy for target *Salmonella enteridis* bacteria detection 80

Chapter 3 Results 81

3.1 Nanoporous alumina membrane based electrochemical biosensor with PtNPs tags for *E. coli O157:H7 gene* detection 81

3.1.1 Surface modification of nanoporous alumina membrane 81

3.1.2 Oligonucleotide probes immobilization on nanoporous alumina membrane 83

3.1.3 PtNP-oligonucleotide probes conjugation 85

3.1.4 Target *E. coli O157:H7 gene* captured by probes on nanoporous alumina membrane 87

3.1.5 Target *E. coli O157:H7* gene detection with PtNPs based precipitation via EIS 89

3.2 Nanoporous alumina membrane based electrochemical biosensor with graphene/hemin-antibody tags amplification for *Salmonella enteritidis* detection 99

3.2.1 Antibody immobilization on nanoporous alumina membrane 99

3.2.2 Synthesis of graphene-antibody/hemin composites 101

3.2.3 *Salmonella enteritidis* captured on nanoporous alumina membrane 104

3.2.4 Impedance sensing for Salmonella bacteria 106

Chapter 4 Discussion and future work 115

4.1 Immobilization of *E. coli O157:H7 gene* probes or *Salmonella enteritidis* bacteria antibodies on nanoporous alumina membrane....115
4.2 Nanopores size effect 118
4.3 Selection of amplification methods and tags....120
4.4 Synthesis of GO/Hemin-antibody composites 122
4.5 Sample volume and sensing area effects....125
4.6 Improvement to achieve fast detection....125
5. Conclusion 126
Reference....128

List of Figures

Figure 1.3.1 Two typical models of impedance 17

Figure 1.4.1 Simplified circuit model of charge transfer process controlled EIS 24

Figure 1.4.2 Nyquist plot of charge transfer process controlled EIS 25

Figure 1.4.3 Simplified circuit model of charge transfer/diffusion controlled EIS process 26

Figure 1.4.4 Nyquist plot of charge transfer/diffusion controlled EIS process. 27

Figure 1.4.5 Mechanism of the exonuclease III-assisted electrochemical hairpin-shaped DNA biosensor [44]. 29

Figure 1.4.6 Chemical structural formulas of soluble 4-CN (a) and insoluble product (b) 30

Figure 1.5.1 Structure of graphene (a) and typical functional groups on graphene oxide (b) 35

Figure 1.5.2 An overview of strategies for graphene synthesis [62] 36

Figure 1.5.3 Conjugation between gold pattern, functionalized graphene oxide nanosheets and EpCAM antibodies[112] 52

Figure 1.6.1 SEM images of nanoporous alumina nanotemplate. Plan view image of the membrane (a) and cross-section view of the membrane (b) [115] 54

Figure 2.1.1 Chemical structure of (3-Glycidyloxypropyl)trimethoxysilane (GPMS) 61

Figure 2.1.2 The whole process of surface silanization. 62

Figure 2.1.3 Image of Ramé-Hart goniometer (NJ, USA) equipment 63
Figure 2.1.4 Scheme of amino group modified oligonucleotide probes conjugation on GPMS modified nanoporous alumina membrane 64
Figure 2.1.5 Fabrication process of microfluidic chip integrated with nanoporous alumina membranes. 65
Figure 2.1.6 Formation of PtNP-oligonucleotide conjugates.....67
Figure 2.1.7 Sensing mechanism of *E. coli O157:H7 gene* detection 69
Figure 2.1.8 The set-up of whole detection system 71
Figure 2.2.1 Scheme for *S. enteridis ompC* antibodies immobilization.....74
Figure 2.2.2 Formation of GO/Hemin conjugates through π-π stacking [58].....77
Figure 2.2.3 Sensing mechanism of *S. enteridis* bacteria detection.....79
Figure 3.1.1 Change of nanoporous alumina membrane surface's water contact angle before (a) and after GPMS modification (b). 82
Figure 3.1.2 Average water contact angle before and after surface silanization. 83
Figure 3.1.3 Fluorescent images of oligonucleotide probes immobilized on GPMS modified nanoporous alumina membrane with (a) control group at a concentration of 2 μM; FAM modified oligonucleotide probes at concentrations of (b) 0.5 μM, (c) 1 μM and (d) 2 μM, respectively. 84
Figure 3.1.4 (a) TEM image of PtNPs dispersed in DI water with a scale bar of 50 nm; (b)TEM image of PtNPs dispersed in DI water with a scale bar of 10 nm.86
Figure 3.1.6 Zeta potential of bare PtNPs and PtNP-oligonucleotide probes in DI water. 87

Figure 3.1.7 Fluorescence images of (a) FAM labelled non-target oligos captured by bio-functionalized nanoporous alumina membrane; (b) FAM labelled non-target oligoes. Both of them adopted a concentration of 1μM. 88

Figure 3.1.8 Fluorescence intensity change for 1h, 2h, 3h, 4h, 5h and 6h incubation with FAM labelled target oligos. 89

Figure 3.1.9 SEM characterizations before and after the PtNPs catalyzed precipitation of nanoporous alumina membrane surface 90

Figure 3.1.10 Impedance spectra of nanoporous membrane based biosensor for various concentrations of target genes. 95

Figure 3.1.11 Normalized impedance change (NIC) from 1Hz to 10kHz with different concentrations of target *E. coli O157:H7 genes*. 96

Figure 3.1.12 Normalized impedance change (NIC) at 50 Hz with different target *E. coli O157:H7 gene* concentrations. 97

Figure 3.1.13 Impedance amplitude NIC for target gene, 6 base mismatch DNA and non-specific DNA 98

Figure 3.2.1 Fluorescent images of FAM-modified salmonella antibodies immobilized on GPMS modified alumina oxide membrane. The concentrations of FAM-modified antibodies were (a) 0 nM, (b) 50 nM, (c) 100 nM, (d) 200 nM, respectively. 100

Figure 3.2.2 TEM image of graphene oxide synthesized by Hummer's method 102

Figure 3.2.3 Zeta potential of GO and GO-antibody composites 102

Figure 3.2.4 UV-Vis spectrum of GO, Hemin, and GO-antibody/hemin composites 103

Figure 3.2.5 Fluorescent image of (a) no salmonella bacteria captured by nanoporous alumina membrane (b) 10^5 CFU/mL Salmonella bacteria captured by nanoporous alumina membrane. 105

Figure 3.2.6 (a) SEM of bare nanoporous alumina membrane and (b) nanoporous alumina membrane with captured salmonella bacteria 106

Figure 3.2.70 Normalized impedance change (NIC) from 1Hz to 10 kHz with different concentrations of target salmonella bacteria after precipitation.....111

Figure 3.2.8 Impedance amplitude NIC for target salmonella and non-specific *E. coli O157:H7* bacteria. 114

Figure 4.3.1 Sensing principle of nanoporous membrane impedance sensor based on silver enhancement amplification. (a) (b) (c) and (d) show the impedance gradually decreases in each experimental step and each the largest after silver enhancement reaction [122]. 121

Figure 4.4.1 Skeletal formula of hemin molecule.....124

Figure 4.4.2 Three strategies to synthesize GO/Hemin-Antibody composites.....124

List of Tables

Table 1.1.1 A summary of estimated foodborne illnesses, hospitalizations and deaths caused by selected pathogens in the US annually as calculated by the USDA's economic research service [1] 2

Table 1.1.2 Pathogenic bacteria, diseases they cause, toxins they secrete, infection sources and mortality rates for humans infected by microorganisms used as biological warfare agent (BWA) [2] 5

Table 1.2.1 Some current biosensors for bacteria related detection 11

List of Abbreviations

(3-aminopropyl) triethoxysilane	APTES
(3-glycidoxypropyl) trimethoxysilane	GPMS
1-ethyl-3-(3-dimethylaminopropyl) carbodiimide hydrochloride	EDC
4-chloro-1-naphthol	4-CN
Amino group	$-NH_2$
Anodic alumina oxide	AAO
Antibody	Ab
Antigen	Ag
Ascorbic acid	AA
Atomic force microscopy	AFM
Biological warfare agent	BWA
Bovine serum albumin	BSA
Carbon nanotubes	CNTs
Carboxyl group	-COOH
Carcinoembryonic antigen	CEA
Catalase	CAT
Chemical Vapor Deposition	CVD
Chemically reduced graphene oxide	CRGO
Cyclic voltammetry	CV

Cytochrome c	Cyt c
Differential pulse anodic stripping voltammetry	DPASV
Differential pulse voltammetry	DPV
Dithiothreitol	DTT
Dopamine	DA
Electrochemical impedance spectroscopy	EIS
Enzyme-linked fluorescent assay	ELFA
Enzyme-linked immunosorbent assay	ELISA
Epithelial cell adhesion molecule	EpCAM
Epoxy group	-C-O-C-
Escherichia coli	*E. coli*
Fluorescein amidite	FAM
Fluorescence resonance energy transfer	FRET
Glassy carbon electrode	GCE
Glucose oxidase enzyme	GOx
Gold nanoparticles	AuNPs
Graphene oxide	GO
Graphene quantum dots	GQDs
Hemoglobin	Hb
Heterogeneous electron transfer	HET
Horseradish peroxidase enzyme	HRP

Hydrogen peroxide	H_2O_2
Hydroxyl group	-OH
Ion-selective electrode	ISE
Limit of detection	LOD
Manganese oxide	MnO_2
N-hydroxysuccinimide	NHS
Normalized impedance change	NIC
Phosphate buffered saline	PBS
Platinum	Pt
Platinum nanoparticles	PtNPs
Poly(styrenesulfonate)	PSS
Polydimethylsiloxane	PDMS
Polymerase chain reaction	PCR
Potassium permanganate	$KMnO_4$
Potentiometric stripping analysis	PSA
Reduced graphene oxide	rGO
Refractive index	RI
Salmonella enteritidis	*S. enteritidis*
Scanning electron microscope	SEM
Scanning probe microscopy	SPM
Silver/silver chloride	Ag/AgCl

Single-strand DNA	ssDNA
Single-strand RNA	ssRNA
Sodium borohydride	$NaBH_4$
Sodium sodecyl sulfonate	SDS
Sulfuric acid	H_2SO_4
Surface plasmon resonance	SPR
Systematic evolution of ligands by exponential enrichment	SELEX
Tetramethylbenzidine	TMB
Tetra-*n*-butylammonium	TBA
Thiol group	-SH
Transmission electron microscope	TEM
Uric acid	UA
α-teroprotein	AFP

Chapter 1 Introduction

1.1 Detection of Pathogenic Bacteria

1.1.1 Diseases Caused by Foodborne Pathogenic Bacteria

There is a huge family for foodborne pathogenic bacteria. They generally exist in food which can cause foodborne illness by secreting toxins entering human bodies. Since they are naturally infectious and can secret toxin in food or in human bodies, cases of foodborne diseases are emerging and continuously growing in recent years. **Table 1.1.1** shows a summary of the estimated foodborne illnesses, hospitalizations and deaths caused by selected pathogens in the US annually [1]. From this table, it is observed that typical types of foodborne pathogenic bacteria include *salmonella*, *listeria monocytogenes*, *campylobacter spp*. *Escherichia coli (E. coli) O157:H7*, *clostridium perfringens* and *staphylococcus*. Among them, *salmonella* bacteria and *campylobacter spp.* occupy the first two places.

Bacteria types	Estimated annual cases	Estimated annual hospitalizations	Estimated annual deaths	Onset	Infectious dose (CFU)

Salmonella	1,342,532	16,102	556	6 h to 28 days	10^4–10^7
Listeria monocytogenes	2493	2298	499	A few days to 3 weeks	400–10^3
Campylobacter spp.	1,963,141	10,539	99	2–5 days	400–10^6
Escherichia coli(0157:H7 and other types)	173,107	2785	78	12 h to 3 days	10^1–10^2
Clostridium perfringens	248,520	41	7	18–36 h	>10^8
Staphylococcus food poisoning	185,060	1753	2	1–7 h	>10^6

Table 1.1.1 A summary of estimated foodborne illnesses, hospitalizations and deaths caused by selected pathogens in the US annually as calculated by the USDA's economic research service [1]

A detailed introduction to various types of bacteria including related diseases, secreted toxins, sources of infections as well as the mortality rates is shown in **Table**

1.1.2 [2]. Generally, diseases caused by bacteria vary a lot with different secreted toxins, and the main infection sources are from meat, milk, and rice. Due to a large number of types of bacteria, it is not possible to conduct detection for all of them. Among these main bacteria related to foodborne disease, *E. coli O157:H7* and *Salmonella enteritidis* are selected as representative target bacteria for this MPhil study, which are the common foodborne bacteria in Hong Kong and Asia region.

Bacteria	Disease	Toxin	Infection sources	Mortality
Bacillus anthracis	Anthrax	Edema factor	Milk or meat, BWA	Fatal
Brucella melitensis	Brucellosis	–	Milk or meat, BWA	Low
Campylobacter jejuni	Diarrhea dysentry	–	Dairy products, meats, mushrooms	–
Clostridium botulinum	Botulism	Neurotoxin	Food	–
Coxiella burnetti	Pneumonia	–	BWA	Low
Corynebacterium diphtheriae	Diphtheria	Diphtheria toxin	BWA	Low

Bacteria	Disease	Toxin	Infection sources	Mortality
Escherichia coli	Gastroenteritis	Enterotoxin	Meats, fish, milk, rice, vegetables	–
Francisella (*Pasteurella*)*tularensis*	Tularemia	–	BWA	Low
Mycobacterium tuberculosis	Tuberculosis	–	BWA	High
Rickettsia rickettsi	Rocky Mountain-spotted fever	–	BWA	High
Salmonella paratyphi	Paratyphoid	–	Fecal contamination, eggs, milk, meats	–
Salmonella typhi	Typhoid fever	–	BWA	High
Shigella dysenteriae	Bacillary dysentry	Neurotoxin	Fecal contamination	–

Bacteria	Disease	Toxin	Infection sources	Mortality
Staphylococcus aureus	Pneumonia	Enterotoxin	Human carriers	–
Streptococcuspneumoniae	Pneumococcal pneumoni	Erythrogenic toxin	Human carriers	–
Treponema pallidum	Syphilis	–	Infected exudate or blood	–
Vibro cholerae	Cholera	Enterotoxin	Fecal contamination	High
Yersinia pestis	Bubonic plague	Plague toxin	BWA	Fatal

Table 1.1.2 Pathogenic bacteria, diseases they cause, toxins they secrete, infection sources and mortality rates for humans infected by microorganisms used as biological warfare agent (BWA) [2]

1.1.2 Traditional methods for Pathogenic Bacteria Detection

To avoid the wide-range infections of pathogenic bacteria, early detection of pathogenic bacteria is needed before potential pathogenic sources such as contaminated water or food entering human bodies. Bacteria, as well as their specific

DNA sequences, are the main detecting targets. For bacteria detection, direct and indirect counting methods are employed to obtain the concentration information. Direct counting methods consist of culture & colony counting method and electron microscopy method. On the other hand, indirect counting method is based on immunological reaction such as antibody-antigen interactions. Specific gene sequences of bacteria are also considered and regarded as another type of target to confirm the dose such as polymerase chain reaction (PCR), which is mostly used for determination of target oligonucleotides.

Culture & colony counting method. It is the oldest as well as the gold-standard method. Briefly, the procedure consists of bacteria culturing, isolation, enrichment, and plating. Since one pathogen can grow into a large bacterial colony which can be observed directly, this method is very reliable and visualized [3]. However, this method is also time and labor consuming, limiting its application for fast pathogen detection [4].

Electron Microscopy method. Unlike previous culture counting method which focuses on the amounts of target pathogens, electron microscopy method primarily concerns the morphology of specific bacteria types. Scanning electron microscope (SEM) is utilized for counting and size judging[5], while transmission electron microscope (TEM) pays attention to cell volume and dry morphology of target bacteria [6, 7]. Scanning probe microscopy (SPM) is often employed simultaneously with antibody arrays, which can provide specific detection [8]. Atomic force microscopy (AFM) has a high resolution on both lateral and vertical dimensions, resulting in that a tiny

variation in topography can be monitored. However, these methods are limited by the high cost and the need for professional operators.

Immunological reaction based methods. These methods are all correlated with antibody-antigen recognition as well as enzyme assays. Target bacteria could be captured on the substrate specifically, and enzyme modified secondary antibodies will be attached on them, resulting in fluorescent or chromatic signal changes. Enzyme-linked immunosorbent assay (ELISA) [9] and enzyme-linked fluorescent assay (ELFA) [10] are the main representatives. Drawbacks still exist as they are all high-cost and long-time detections.

Polymerase chain reaction (PCR). For detections of specific gene sequences, PCR is mostly often performed. A typical PCR contains cycle amplification of target gene sequence to achieve a high sensitivity detection. PCR is continuously developed and as a result, real-time PCR[11] and multiplex PCR emerged [12] for the realization of rapid and multiple detections. Despite the high sensitivity and selectivity, PCR methods are still severely limited by the long assay time.

1.2 Biosensor for Pathogenic Bacteria Detection

Since numerous drawbacks of traditional detecting methods exist, more advanced methods are highly in need to achieve a fast, low-cost, stable and repeatable detection with high sensitivity and selectivity. Plentiful efforts have been reported in recent years such as developing biosensors for bacteria detection. A typical biosensor

commonly consists of a sensitive biological element which can specifically recognize the targets (oligonucleotides, protein, cells, et.al), and a transducer which can transform the resulting signal caused by previous recognition into a detectable signal, and then analyzed by a reader instrument. Classification of biosensors relies on the resulting signals, and three types are widely accepted: optical biosensor, piezoelectric biosensor and electrochemical biosensor [13].

1.2.1 Optical biosensor

For pathogenic bacteria detections, optical biosensors have been well developed because of their versatile advantages. In a typical optical strategy, when target bacteria are captured or separated selectively, relevant optical signals (light absorption, reflection, fluorescence, luminescence, et.al) change and are then measured by particular instruments. Surface plasmon resonance (SPR) technique is one of the optical methods which is based on resonant oscillation of conduction electrons at the interface. As targets are adsorbed onto planar metal or metal nanoparticles, the resonance condition changes which can be acquired by detectors. Wasna and co-workers fabricated a SPR biosensor for *E. coli O157:H7* detection [14]. In this SPR biosensor, antibodies are firstly modified on gold surface and then exposed to LED light. When target *E. coli O157:H7* bacteria were captured, refractive index (RI) changed and signals were obtained by SPR detector. A low LOD of 10^2-10^3 CFU/mL was achieved.

Fluorescence resonance energy transfer (FRET) based optical sensor is another popular strategy which is rapidly developed recent years. When a fluorescent donor molecule is getting close to a fluorescent acceptor molecule in nanoscale and the emission spectrum of fluorescent donor overlaps the excitation spectrum of the fluorescent acceptor, a FRET effect happens, leading to the energy transfer from a donor to an acceptor [15]. Fluorescence emission spectra will be shifted or fluorescence quenching will appear, which can be monitored by photoluminescence spectrometer. Our group has established a FRET biosensor based on graphene quantum dots (GQDs) and gold nanoparticles (AuNPs) for the detection of mecA gene sequence of *Staphylococcus aureus* [16]. In this platform, GQDs acted as a fluorescent donor while AuNPs were the fluorescent acceptor. Both of them were modified with probe oligonucleotides and could get close as target gene sequences hybridized with probes on nanoparticles, resulting in FRET effect. The detection limit of 1nM was achieved.

1.2.2 Piezoelectric biosensor

Crystals have their oscillations under a particular electric field. The oscillating frequency is based on the electric field frequency. When the shape or weight of a crystal changes, oscillating frequency will change correspondingly which can be detected. For real biosensing applications, bacteria can be detected by the changes in shape and weight due to target bacteria adsorption. Su's group reported a piezoelectric biosensor for *E. coli O157:H7* detection [17]. Antibodies were firstly immobilized on

Au electrode surface. When target bacteria were captured, oscillating frequency decreased. The relative decrease was proportional to target bacteria, and a detection range from 10^3 to 10^8 CFU/mL was achieved in 30-50 minutes.

1.2.3 Electrochemical biosensor

Electrochemical biosensor is also an excellent choice for pathogenic bacteria monitoring because it is low-costive, easy to operate, fast, environmental friendly and portable, which highly meets the requirement of bacteria detection in food or water. Compared to optical biosensors, electrochemical biosensors have no interference from the particles or colors presented in samples. While compared to piezoelectric biosensors, electrochemical biosensors are portable and do not need large equipment. In this thesis, both the detection of *E. coli O157:H7* gene sequence and Salmonella enteritidis are based on electrochemical biosensors and detained introduction of electrochemical biosensor and related principles, materials and techniques are launched in the following sections.

Receptor	Analyte	Target Pathogen(s)	Signal Amplification method	Sensing Approach	Assay Time	Detection Limit
DNA	DNA	*E. faecium*, *S. aureus*, *Vibrio vulnificus*, *Stenotrophomonas maltophilia*	NA	SERS	NA	10 fM pathogenic DNA
Aptazyme	Whole cell	*E. coli*	Magneto signal amplification	Colorimetry	1-2 h	5×10^2–5×10^3 CFU/assay
Antibiotics	Whole cell	*S. aureus*, *P. aeruginosa*	NA	Fluorescence	NA	1.0~3.1 × 10^4 CFU/mL
DNA	DNA	*S. aureus*, *Vibrio vulnificus*, *Salmonella*, *S. epidermidis*, *E. faecalis*, *Klebsiella oxytoca*, *N. gonorrhoeae*	NA	LSPR	NA	10 fM (50 zmol) of pathogenic DNA
Aptamer	Whole cell	*P. aeruginosa*, *S. typhimurium*,	NA	LSPR	NA	30 CFU/assay
Aptazyme	Whole cell	*Salmonella paratyphi*	Luminol oxidation-based signal amplification method	Chemiluminescence	NA	1.0 × 10^3 CFU/mL
Bacteriophage	Whole cell	MRSA, *E. coli* O157: H7	NA	SPR	15 min	1.0 × 10^3 CFU/mL

Table 1.2.1 Some current biosensors for bacteria related detection

Table shows some reported biosensors in recent years. The limit of detection (LOD) varies from several CFU/mL to thousands of CFU/mL, depending on the design of the biosensors as well as the detecting time. The LOD of bacteria related oligos detection varies from

1.3 Electrochemical biosensor for bacteria detection

As mentioned in previous section, the electrochemical biosensor is extraordinarily good for bacteria detection, and thus is chosen as the main technique in this thesis. Before going into details of electrochemical biosensors, an introduction of electrochemistry was firstly given. Electrochemistry, a concept in physical chemistry, is actually a chemical process with charge transfer and separation [19]. Since the

charge is all about the electron, an electrochemical process is essentially the variation of electrons. Because of this nature, the way to explore mechanism and kinetics of electrochemical process is to identify and quantify the electronic change presented by species studied or the medium where species are dissolved. With the development of electrochemistry, sensing based on this mechanism has been performed as an efficient tool for qualitative and quantitative analysis of various chemicals since the early 20th century. A complete electrochemical sensing system generally consists of electrodes, electrolytes, and measurement devices. When electrochemical sensing is regarded as a tool, questions of the selectivity, sensitivity, stability and the repeatability are unavoidable [20].

In the following sections, a brief introduction of the electrochemical biosensor is given and its classification follows. Typically, electrochemical biosensors are classified into amperometric biosensor, potentiometric biosensor, conductometric biosensor and impedimetric biosensor. The principles and the applications of them are introduced as well. At last, the advantages and disadvantages of electrochemical sensing over other physical or chemical sensing methods are discussed as well.

1.3.1 Introduction of electrochemical sensing

Electrochemical sensing has a long history since the first time in Galvani's experiments at the end of 20th century. In that experiment, an electric stimulus on frog's legs was carried out, resulting in a current response as a recognition in frog's

biological system. It was the discovery of electrochemical phenomena and invention of galvanic cell. Soon afterwards in 1799, Volta's attempted to pile up zinc and copper sheets with a H_2SO_4 sopped woolen as segregation, and achieved the first electrochemical power source: the electric piles. This trail realized the conversion of chemical energy into electric energy. In 1800, inspired by Volta's success, NichoMn and Krlislc utilized electric piles to achieve water electrolysis, making it possible to transfer electric energy into chemical energy. These experiments aroused great interests at that time and promoted the establishment of electrochemical theory. With the help of electric piles, scientists started the research on phenomena of galvanic conductors in both physical and chemical aspects, respectively, and ohm's law and faraday's law were the outcomes of them. Faraday's law illuminated the quantitative relationship between the mass of the substance liberated at an electrode and the total electric charge passing through the substance. This law can apply to all redox reactions on electrodes and is regarded as basic quantitative law in electrochemistry. During that period, periodic table was established and numbers of elements were extracted [21]. The development of electrochemistry reveals that an electrochemical process is essentially an oxidation-reduction process, which forced electrochemical sensing to become an effective method for chemical analysis. Electrochemical sensing mainly focuses on the electric signal change of analytes on the electrode surface or in the aqueous medium, in a quantitative way [19]. Typically, three electrochemical methods are involved, potentiometry, voltammetry conductimetry and impedimetry [22].

1.3.1.1 Potentiometry

Potentiometry is commonly used in ion detection. Generally, a potentiometric measurement is to detect the equilibrium potential of an indicator electrode against another reference electrode with no significant current [23]. These two electrodes are separated by ion permselective membrane. After target ions are introduced into the ion-selective electrode (ISE) system, the potential between indicator and reference electrodes is directly proportional to the logarithm of ion concentration [24]. The earliest application of potentiometric devices was pH glass electrode in the early 20th century [25]. After abundant research work, various types of ion or gas potentiometric sensor emerged on the basis of Nernst equation. However, several drawbacks still exist. One important limitation is about the selectivity. Although the ion-membrane is claimed to be permselective, indicating that non-target ions have low potentiometric selectivity coefficients at ideal conditions, interferences still proportionally exert influence and result in wrong signals on the potential in practice. The other limitation is about the stability. The degradation of the membrane is very critical when the electrodes are immersed in flowing liquid. Corrosion happens on the electrode surface, making the whole system unstable and calibration needed all the time.

1.3.1.2 Voltammetry

Voltammetry is the most developed electrochemical sensing method and used to indicate the current-voltage profile. In a voltammetric process, a sweep of potential is

applied and the corresponding current is recorded to obtain the voltage-current curve. Also the sweep can be applied in a continuous current and the object registered is the potential. Unlike potentiometry, voltammetry is a representative strategy of probing dynamic processes based on redox reactions [23]. From the sensing perspective, the analytes are either in the solution which can be oxidized or reduced at a specific potential, or fixed on the electrode surface which will accelerate or hinder the redox reaction of the redox probes in the solution. Both of them show a positive or negative correlation between the current/voltage value and the concentration of analytes, depending on the actual sensing platform design. The voltammetric sensing platform operates in a cell of three electrodes: a working electrode, a reference electrode, and an auxiliary/counter electrode. Various types of working electrodes have been developed, and generally they can be classified into mercury electrodes, solid electrodes, and chemically modified electrodes. Solid electrodes are a huge family which are frequently employed such as glassy carbon electrode (GCE) [26], gold electrode [27], platinum electrode [28]. For the counter electrode, the platinum electrode is a common choice while silver/silver chloride (Ag/AgCl) electrode is used as the reference electrode, regularly.

1.3.1.3 Conductimetry

Conductimetry is the strategy which concerns the resistance between electrodes. If the charge in solution decreases, the related conductance will reduce accordingly. Compared to other electrochemical methods, conductimetry is the simplest one to

operate. However, it is also the least versatile one due to the non-specificity of species to be detected.

1.3.1.4 Impedimetry

Compared to conductimetry, impedimetry shows more functionalities. The impedance between the working electrode and the reference electrode is the main parameter, which is theoretically the reciprocal of the conductance. However, impedimetry is not only composed of solution and electrode surface resistance, but also of a combination of capacitance, inductance, and so on. From the view of mathematics, the expression of impedance (Z) is divided into a real compartment R and an imaginary compartment X, and the mathematical expression is $Z = R+jX$. Because the direction of R is along X axis while that of X is along Y axis, there exists an angle θ of the impedance Z. From the view of physics, real part R is the resistance while imaginary part X is the result of inductance and capacitance. Z_m is the absolute value of the impedance and θ is the phase of impedance. **Figure 1.3.1** shows two typical models of impedance. Further introduction of impedimetric biosensors is in section 1.4.

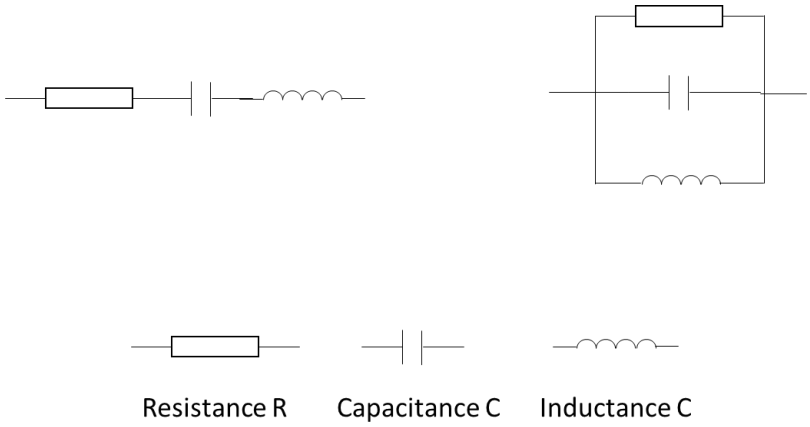

Figure 1.3.1 Two typical models of impedance

1.3.2 Electrochemical biosensor classification based on recognition mechanism

Traditionally, electrochemical biosensors are classified based on the modes of signal transduction (potential, conductance, impedance or voltammetry) as mentioned in the previous section. The classification of electrochemical biosensors can also be based on the biological specificity-conferring mechanism. In another word, varieties of the targets or the biology recognition involved with targets are the prime concerns. Based on this mechanism, electrochemical biosensors are classified based on biocatalysis recognition or bioaffinity recognition.

1.3.2.1 Biocatalysis based electrochemical biosensor

In this type of biosensor, catalytic reaction is the basis for biosensing. Generally, two classes of catalysts are employed including the natural biocatalysts such as

enzyme, cells (cell organelles), tissues which are previously isolated or manufactured, and the inorganic materials which intrinsically has the catalytic ability such as platinum nanoparticles (PtNPs). According to Thévenot and co-workers, an enzyme catalytic reaction commonly has one or two substrates S and S' [22]. Once the enzyme or enzyme-like substances are introduced, analytes will be reacted into one or several products, P and P'. The reaction scheme can be generalized as follow:

$$S + S' \xrightarrow{enzyme\ or\ enzyme-like\ substance} P + P'$$

Ways vary for the quantification of substrate S including monitoring of co-substrate S' or product P consumption, detecting the change of enzymatic activity, or directly reading the output of electron transfer from the enzyme fixed on the electrode surface to the electrochemical transducer. To reach a more versatile and sensitive biosensing platform, multiple enzymes can be modified onto the electrode surface. For example, several enzymes could be performed simultaneously to improve the sensitivity through reducing the non-specific influence [29]. Another group used several enzymes for multistage catalytic reactions where the products of the last step were the substrates of next step [30]. This permitted a much wider range of detection because it was no longer confined to one enzyme reaction. Through several steps of reactions, the performance of this biosensor would be enhanced. New inorganic catalysts or enzyme-mimicking biomacromolecules are the new trends in replacing the traditional enzyme which are costly, inconvenient for tagging, unstable against hydrolysis and heat treatment. New inorganic catalysts are mainly nanomaterials, e.g., platinum

nanoparticles (PtNPs) [31], gold nanoparticles (AuNPs) [32], and the enzyme-mimicking biomacromolecules are represented by DNAzymes. PtNPs are imported in the first project of this thesis, and detailed introduction of PtNPs for electrochemical biosensors is performed in section 1.5. DNAzymes, formed by nucleic acids with catalytic functions, are synthesized by the systematic evolution of ligands by exponential enrichment process (SELEX). One of the most used DNAzyme is hemin/G-quadruplex DNAzyme, which is a good substitution of HRP for H_2O_2 catalytic cracking [33].

1.3.2.2 Bioaffinity based electrochemical biosensor

Bioaffinity recognition based electrochemical biosensors are another big group of electrochemical biosensors operated with specific biological identification. Unlike biocatalysis recognition which is a dynamic process, the targets detected by bioaffinity recognitions are commonly in steady state.

Antibody-related interactions. Antibody-antigen interaction is most common used based on an immunochemical reaction. In this reaction, antibodies (Ab) can specifically bind to corresponding antigens (Ag). The binding force is strong and the binding efficiency is high. However, some drawbacks limit the use of Ab, e.g., the binding efficiency of Ab varies significantly with temperature and ionic strength in solution. Beyond that, Ab tends to degrade as time goes on, making the reproducibility

of sensing system uncertain. Also, another shortcoming hardly ignored is that the cost of Ab is quite high and the synthesis time is pretty long.

Nucleic acid related interactions. DNA or RNA hybridization is well known and extensively employed for single-strand nucleic acid detection. Typically, the single-strand DNA or RNA (ssDNA or ssRNA) probes are firstly attached onto working electrode surface, and some may fold into a G-quadruplex or hairpin structure and modified with enzyme or fluorescent labels [34]. After the probes contact with target single-strand nucleic acids, hybridization takes place, resulting in electrochemical signal change. Hybridization of nucleic acid is a fast process with high stability, and the structure of nucleic acids themselves is intrinsic firm against temperature and ions. Another application of nucleic acid related interaction is based on aptamer which is a DNA or RNA ligand with the abilities to combine with proteins and receptors such as thrombin [35, 36], and some small molecules including ATP or Adenosine [37-39]. Aptamers are obtained by SELEX. Roughly, SELEX is a PCR process which reserves the single-strand nucleic acids bound to target molecules and wash away the unbound ones. Finally, nucleic acid remained during numbers of amplifications are selected as aptamers which have a strong affinity with target molecules [40]. Compared to Ab-Ag interaction, Aptamer-target molecule interaction has a wider range of usage in biosensing because of the low cost, high stability of oligonucleotides and the simplicity of oligonucleotides synthesis [41].

1.3.3 Why electrochemical biosensing

Numerous criteria should be assessed before choosing appropriate electrochemical methods for biological detections. First of all, it is important to see if it is necessary to use electrochemical sensing and whether the advantages of electrochemical sensing are over the disadvantages. Furthermore, what is the optimal type of electrochemical sensor and which electrochemical technique will be appropriate to reach the best detection. Electrochemical sensing has a certain of advantages which make it suitable for bacteria related detections [19]. 1) Selectivity can be enhanced by choosing appropriate electrode materials. In potentiometric sensors, the specificity is achieved by the ion-selective material of the electrodes. In voltammetric sensors, the overpotential of some species in the solution is partially influenced by the electrode material. Therefore the separation of these species with similar redox characteristics can be realized by choosing the appropriate electrode material. 2) Higher sensitivity and selectivity by using electroactive species through redox reactions. Electroactive species with particular redox potentials are welcome in electrochemical sensing and redox reactions are very common in biological systems. Generally, in a voltammetric biosensor, the amplitude of a characterization peak at a certain voltage represents the sensitivity while the position of that shows the selectivity. Particularly, during the cyclic sweep, the formation of a new peak often indicates a chemical process which is helpful for monitoring of speciation. 3) Extra signal transducer is not needed. Signals of an electrochemical process are electrically

intrinsically. Therefore complicated instrumentation can be readily applied for the generation of electric waves and analysis of the correspondence. Functions of working electrodes can be tuned by surface modification, leading to an easy immobilization of bio-probes such as antibodies and oligonucleotides. 4) Unlike other optical biosensors which need complex and expensive instrumentation for analysis of fluorescent or luminescent signals, electrochemical sensors can be portable, cheap and simple. Electrochemical sensors can be assembled into flow systems such as microfluidic systems. Since some biomolecule reagents are very expensive, importing microfluidic techniques could significantly reduce dosage and save cost.

One limitation of the electrochemical biosensor is the need of sufficient, inert electrolytes in the solution to provide the current between working electrode and counter electrode. In our two projects, fortunately, biomolecules involved such oligonucleotides and antibodies are originally solved in phosphate buffered saline (PBS), which was also a good electrolyte to carry electrochemical currents. Therefore, this limitation will not influence the performance of electrochemical biosensor in our oligonucleotides and bacteria detections. The impedimetric biosensor was chosen as the sensing approach for the two projects of this thesis and detailed introduction of impedimetric biosensors is in the next section.

1.4 Impedimetric biosensor

A short introduction of impedimetric signals has been given in section 1.3.1.4. A deep discussion of the impedimetric biosensor is given in this section, including the basic principle, typical approaches, as well as biological applications.

1.4.1 Electrochemical impedance spectroscopy (EIS)

Electrochemical impedance spectroscopy (EIS) is one of the popular electrochemical techniques to apply a series of small amplitude AC voltage waves with different frequencies on the electrochemical system. Through the measurement of output current signals, spectroscopy of the system impedance is obtained from the specific value of AC input voltage and AC output current. Various impedance parameters such as Z_m, R, X and θ can be acquired within a wide frequency range for analysis of the kinetics of electrode process, the double electrode layer, electrode material and surface modification [42].

Typically, two types of EIS spectrums are used for analysis including Nyquist plot and Bode plot (**Figure 1.2**). In Nyquist plot, the real part of impedance (R) is plotted along X axis while the imaginary part (X) is plotted along the Y axis. Every sweep of EIS in different frequency is regarded as a parameter, leading to a plot in the Cartesian coordinates. In Bode plot, two variables are expressed along the Y axis. The left Y axis is the absolute value of impedance (Z_m) while the right one is the phase (θ). The logarithm of the frequency is along the X axis. Hence, two curves will exist in the

coordinate system: one shows the relationship between Z_m and log(f), and the other one shows the relationship between θ and log(f).

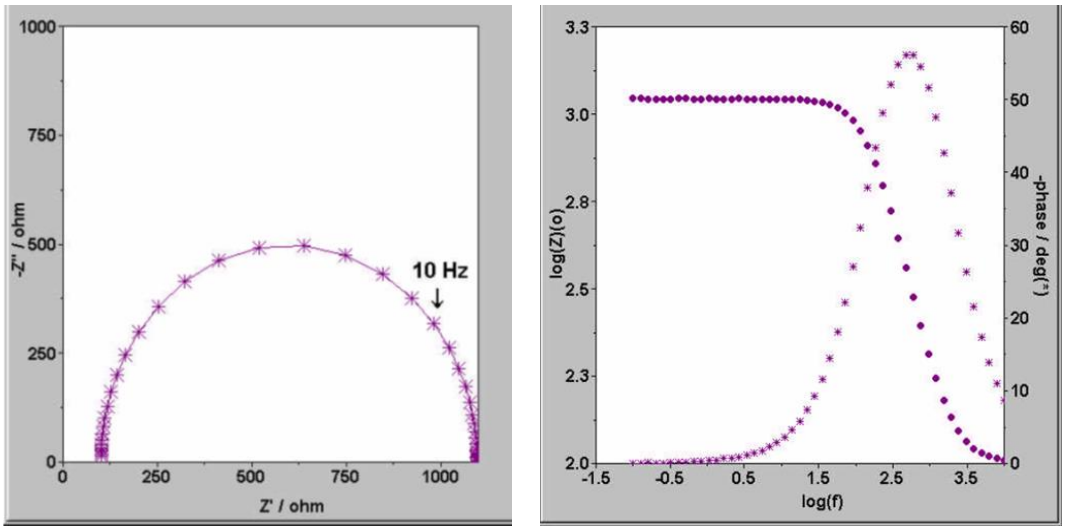

Typical diagrams of Nyquist plot and Bode plot

There are two basic models for EIS processes: charge transfer process and charge transfer/diffusion process. The first process is a simplification of electrode process where charge transfer mainly takes charge. The impedance caused by diffusion process can be negligible. The simplified circuit model of the electrochemical system is in **Figure 1.4.1**:

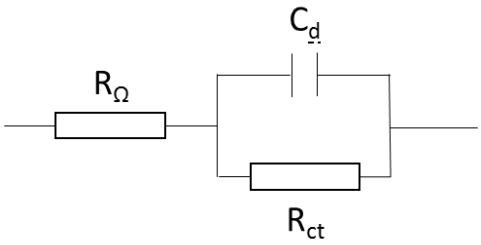

Figure 1.4.1 Simplified circuit model of charge transfer process controlled EIS

The impedance signal of this spectrum is expressed as the following equation:

$$Z = R_{\Omega} + \frac{1}{j\omega C_d + \frac{1}{R_{ct}}}$$

In this equation, R_Ω is the resistance of solution between working and counter electrodes. The combination of C_d and R_{ct} is the parallel connection of electron transfer resistance and electrical double-layer capacitance at the electrode/solution interface. After the mathematical derivation, EIS of this model consists of many circular plots with the radius of $\frac{R_{ct}}{2}$ and the center point at ($R_{\Omega} + \frac{R_{ct}}{2}$, 0) (**Figure 1.4.2**).

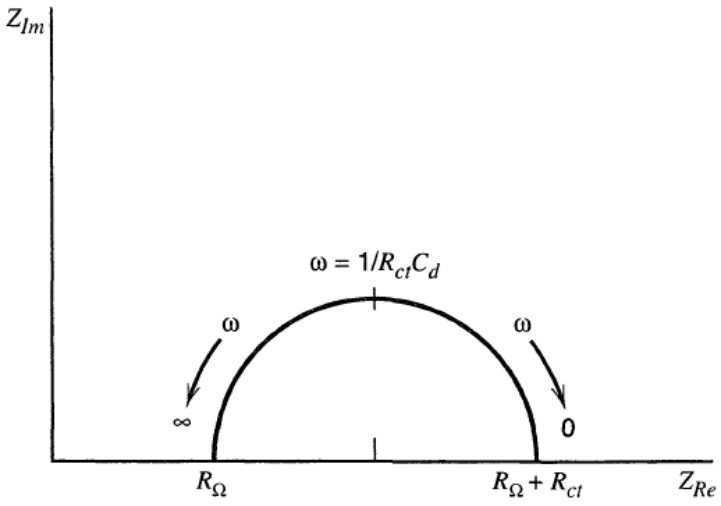

Figure 1.4.2 Nyquist plot of charge transfer process controlled EIS

The second EIS spectrum is a cooperative control of charge transfer and charge diffusion. Charge transfer indicates the influence of electrochemical polarization and the charge diffusion shows the existence of concentration polarization. The simplified

circuit model of the electrochemical system for charge transfer/diffusion is in **Figure 1.4.3**:

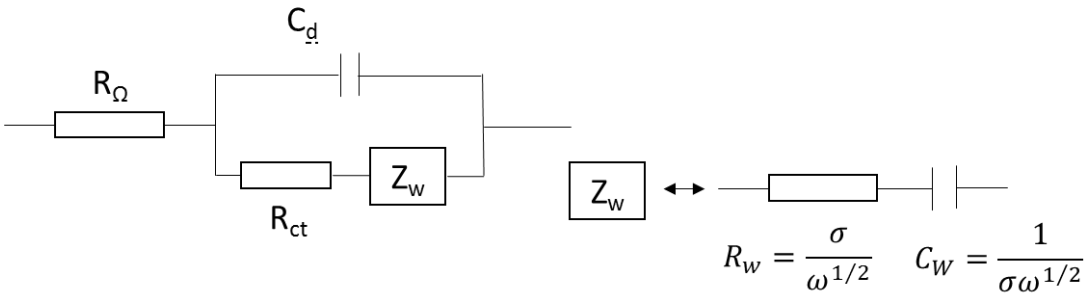

Figure 1.4.3 Simplified circuit model of charge transfer/diffusion controlled EIS process

The impedance signal of this spectrum is expressed as

$$Z = R_\Omega + \frac{1}{j\omega C_d + \frac{1}{R_{ct \div \sigma\omega^{-1/2}(1-j)}}}$$

In this equation, R_Ω is the resistance of solution between working and counter electrodes. Z_w is the impedance caused by a diffusion process. The combination of C_d and R_{ct}/Z_w is the parallel connection of electron transfer resistance, electron diffusion impedance and electrical double-layer capacitor at the electrode/solution interface. After the mathematical derivation, EIS of this model is divided into two parts: circular plots at high-frequency region with the radius of $\frac{R_{ct}}{2}$ and the center point at ($R_\Omega + \frac{R_{ct}}{2}$， 0), and a 45 degrees of straight line at low frequency region (**Figure 1.4.4**). For most cases of the electrochemical biosensor, the second model is commonly used because it is closer to the actual situation.

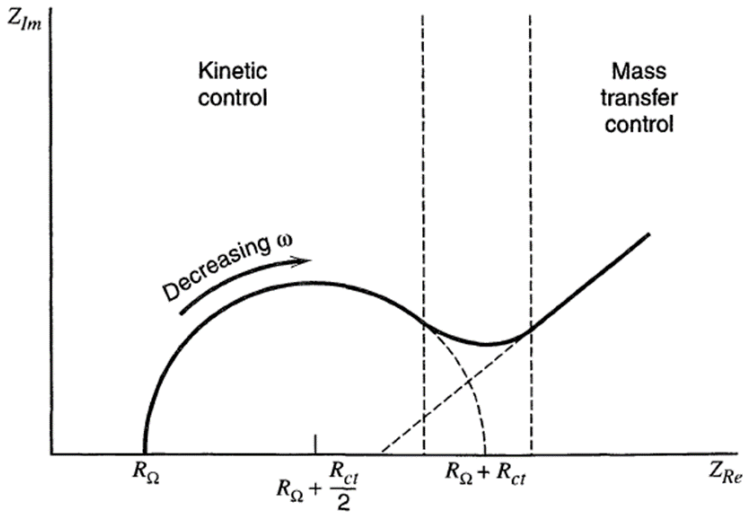

Figure 1.4.4 Nyquist plot of charge transfer/diffusion controlled EIS process.

1.4.2 Factors for impedance variation

Many factors may lead to impedance variation in electrochemical systems. In a nutshell, any changes of interfacial properties caused by biorecognition events can be regarded as the possible reasons. Similar to that of other electrochemical biosensors, impedimetric biosensors can be classified into bioaffinity recognitions and biocatalysis recognitions as well.

Antibody-antigen and nucleic acid related interactions on the interface between working electrode and electrolyte solution cover most cases of bioaffinity recognitions. The concept of antibody-antigen reaction is generalized which means any immune affinities, small to biomolecules or large to whole cells, can be regarded as antibody-antigen recognitions. Common antibodies are initially immobilized onto the sensing

surface. Once antibodies and antigens integrate with each other, immune complexes are formed, resulting in a block layer which can alter the electron transfer resistance on the interface. Nucleic acid related reactions are similar. One differentia of nucleic acid related reactions is that they may not only lead to complexes formation (DNA hybridization or aptamer-antigen binding) , but result in some conformational changes. For instance, as reported by Ferapontova and co-workers, the structure of aptamers before and after binding to target theophylline in serum molecules can be totally different [43]. Even though in simple DNA hybridizations, a pin-shape probe ssDNA due to self-hybridization can dehybridize and hybridize again into chain-shape dsDNA [44]. If some high charged molecules are modified at one end of probe ssDNAs, the electronic transfer rate may significantly change during such nucleic acid reactions since redox probes in solution are intrinsic charged.

Biocatalysis recognitions are based on enzymes, no matter protein based enzymes or synthesized DNAzymes. In impedimetric assays, enzymes may be originally immobilized onto electrode surface or exist in electrolytic solution. The function in the former one is to catalyze target molecules presented in solution such as glucose [45] or H_2O_2 [46]. During the catalyzing process, redox reactions result in electron transfer change and can be detected by electrochemical impedance spectroscopy. The function in the later one is to assist bioaffinity recognitions and signal enhancement. Xuan et.al reported a DNA electrochemical biosensor based on enzyme digestion for signal enhancement [44]. Firstly, target oligonucleotides were hybridized with

hairpin-shaped probes attached on the electrode surface. Exonuclease III enzymes were imported to specifically cleave hybridized oligonucleotide probes and release the target oligonucleotides. The released target oligonucleotides could hybridize with other free probes and be released by enzymes again. This process recycled for several times, resulting in large numbers of hairpin-shaped probes being cleaved and released from the electrode surface. As the attached probes could hinder the electron transfer of electrodes, exonuclease III enzymes were essentially an assistance for electrochemical signal enhancement (**Figure 1.4.5**).

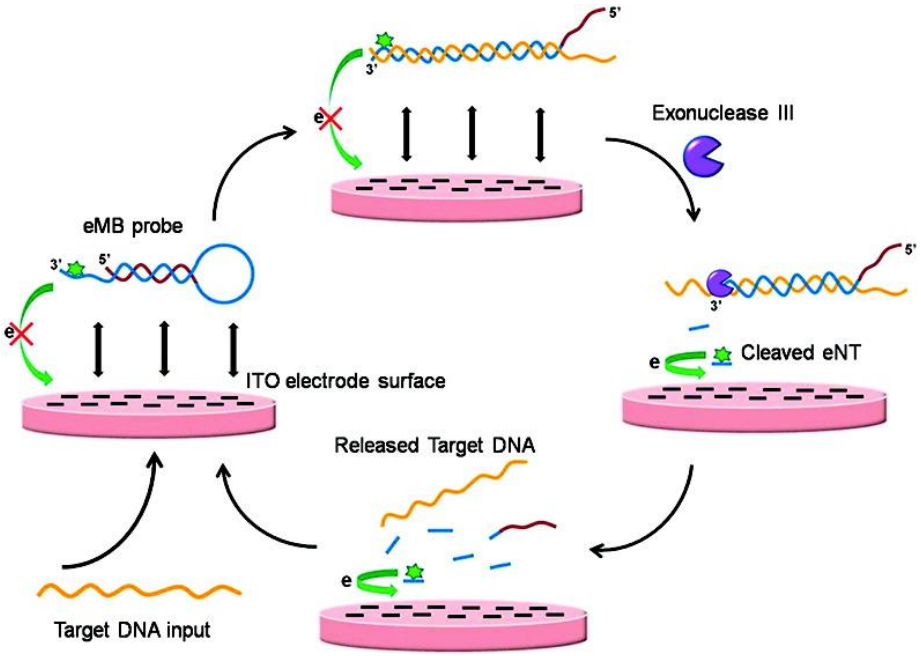

Figure 1.4.5 Mechanism of the exonuclease III-assisted electrochemical hairpin-shaped DNA biosensor [44].

The mechanism in above study was actually a combination of bioaffinity recognitions and biocatalysis recognitions. The enzymes originally existed in the electrolytic solution. In another case, when enzymes are initially attached to

oligonucleotide or antibody probes to form a sandwich structure, biocatalyzed precipitation is often conducted to achieve a hindrance of electron transfer. Biocatalyzed precipitation is a complicated process involving reagents such as hydrogen peroxide (H_2O_2), catalase or catalase-like molecules and 4-chloro-1-naphthol (4-CN) [47]. 4-CN is natively soluble. However, when 4-CN is dissolved with H_2O_2 together with catalases, H_2O_2 will be catalyzed into H_2O and O_2, and O_2 will oxidize soluble 4-CN into insoluble products. Chemical structural formulas of soluble and insoluble 4-CN are shown in **Figure 1.4.6**. Such biocatalyzed precipitation process is significative in impedimetric sensing methods. When 4-CN is oxidized and precipitates in situ, insoluble block layers is generated at the interface. The insoluble products are non-conductive. Hence the electron transfer will be hindered, resulting in impedance increase.

Figure 1.4.6 Chemical structural formulas of soluble 4-CN (a) and insoluble product (b)

1.4.3 Catalyzed precipitation and its applications in impedimetric biosensors

Traditional biocatalysts for hydrogen peroxide were mainly proteins. These proteins are mostly hemeproteins and have a common structure that iron centered

porphyrins are inserted. These functional groups can undergo redox reactions due to the active property of the centered iron [48]. For instance, Horseradish peroxidase (HRP) is one representative which can specifically catalyze H_2O_2 into H_2O and O_2, which has been widely used in bioanalysis such as ELISA assay. In a typical ELISA assay, HRPs are previously modified onto second antibodies, and will catalyze tetramethylbenzidine (TMB) into blue products in the presence of H_2O_2. Other enzymes like catalase (CAT), cytochrome c (Cyt c) and hemoglobin (Hb) are also in this Heme proteins family. However, although applications of heme proteins have been quite mature, some drawbacks still exist. The stability and cost are the major problems due to the nature of proteins. Enzymes are easily inactivated under high or low pH conditions as well as unstable temperatures. During the modification of these enzymes, catalytic properties may be lost because of the formation of covalent bindings. Hence, many efforts have been made to seek replacements, and the achievements contain metal nanoparticles, carbon nanomaterials, DNAzymes and small molecule like hemin.

Platinum (Pt) [49] and manganese oxide (MnO_2) [50] are main representatives of enzyme-like metal. Actually many oxides of transition metal have been demonstrated electrocatalytic activities to hydrogen peroxide such as cobalt oxide [51], copper oxide [52], iridium oxide [53] and titanium oxide [54]. One crucial problem limiting wide applications in biosensing is that the catalysis of traditional metal oxide is not strong enough compared to specific enzymes. Fortunately, the development of

nanotechnology solves this problem as metal nanoparticles can be synthesized in a controllable nanosize with various modifications. Due to the large surface-volume area of nanomaterials, catalytic effects are enormously enhanced. Compare to the same amount of a bulk of metal, metal-based nanoparticles have many orders of magnitude more surface areas. This remarkable property enables metal or metal oxide nanoparticles excellent catalyst comparable to or even better than H_2O_2 enzymes, without those drawbacks such as unstable and expensive.

Carbon-based nanomaterials such as carbon nanotubes (CNTs) or graphene are also reported to be effective H_2O_2 catalysis. For instance, Wang and coworkers decorated CNT/Teflon composites onto glass carbon electrode, and demonstrated such composites good catalysts for both H_2O_2 oxidation and reduction [55]. Zhou's group fabricated a H_2O_2 sensor based on chemically reduced graphene oxide (CRGO) and inferred that the electrocatalytic activity is most likely due to high amounts of defects on plane and edges [56].

DNAzyme is another alternate for heme protein enzymes and has attracted numerous attentions in biosensing field. DNAzymes are synthesized oligonucleotides with enzyme-like properties. For H_2O_2 catalysis, one DNAzyme molecule consists of a single-strand DNA and a hemin molecule. In the presence of hemin, specific ssDNA can integrate with hemin, folding into G-quadruplex, and showing excellent catalytic activities to H_2O_2. Oligonucleotides are inherently stable than proteins against high temperature and excess acid or alkali. Hence DNAzyme is a good alternative for

protein enzymes. Many biosensors have been reported using DNAzyme as H_2O_2 catalyst. Hou and coworkers fabricated a PSA impedimetric immunosensor using DNAzyme-functionalized gold-palladium nanocomposites for the catalysis of H_2O_2 and 4-CN [57]. DNAzyme catalyzed the oxidation of 4-CN, while gold-palladium provided large surface area for DNAzyme attachment, and promote the oxidation process as well.

Hemin, which is used as a component in DNAzyme, can intrinsically catalyze H_2O_2 oxidation itself. Hemin is a porphyrin with iron in the middle. Hence, it is very similar to heme proteins. However, the catalytic property of hemin is not as prominent as those of heme proteins or metal nanoparticles. To increase the catalytic ability, nanomaterials with large surface areas are introduced for large loading of hemin molecules. Graphene is a good selection because it can easily absorb hemin on the plane due to π-π interaction. As reported by Xue et.al, large amounts of hemin were attached onto graphene surface, and excellent catalytic characteristics were demonstrated to be more than two orders of magnitude better than free hemin [58]. Another good performance of GO/Hemin composites is that the abundant functional groups guarantee versatile modifications such as antibodies or aptamers. This method was applied in our second project.

1.5 Graphene and graphene derivative

1.5.1 Graphene and its structure

Graphene is a one-atom-thick free-standing sheet consisting of sp^2–bonded carbon atoms which are ordered in a two-dimensional honeycomb lattice (**Figure 1.5.1a**). Graphene is considered as a hypothetical structure which could not be stable in nature until the year of 2004, Andre Geim and Konstantin Novoselov at the University of Manchester completed the isolation of two-dimensional graphene, which made them win the Nobel Prize in Physics in 2010. Since then, tremendous interests across many fields of materials science, physics, chemistry, and nanotechnology have been attracted to its highly conductivity, high surface-volume ratio, and high mechanical strength [59].

Graphene oxide (GO), a 2D atomically thin structural deriving from graphene with carboxyl groups (-COOH) exposed on the edges and hydroxyls and epoxies groups (-OH, -C-O-C-) on the basal plane, differentiate it from graphene with the only carbon atoms (**Figure 1.5.1b**). Different from the mechanical exfoliation obtained pure graphene, massive synthesis of GO is facile to be achieved by utilizing Brodie, Staudenmaier, and Hummer's methods, involving the oxidation of graphite to obtain the hydrophilic groups. Due to the presence of oxygen-containing groups, GO is non-conductive with the electron transfer inhibited and dissolvable in water and other

solvents, but still mechanically strong and biocompatible. GO is a precursor of reduced graphene oxide (rGO) as well.

Reduced graphene oxide (rGO), which removes the oxygenated groups from GO, can be synthesized through electrochemical, thermal, or chemical approach. These synthesis methods are regarded as facile, low-cost, and large-production routes to obtain relative-pure graphene [60]. However, as the irreversibility of oxidation of graphite, rGO is inevitably doped with a variety of oxygen-containing groups [61]. In contrast to GO, rGO is more electrically conductive and compared to pure graphene, rGO is more promising in electrochemical sensing area because the chemical groups on the surface make it facile to bind with biomolecules, antibodies or aptamers. Moreover, among all the types of graphene derivatives, the remained oxygen-related defects exhibit the positive effect on electrochemical properties.

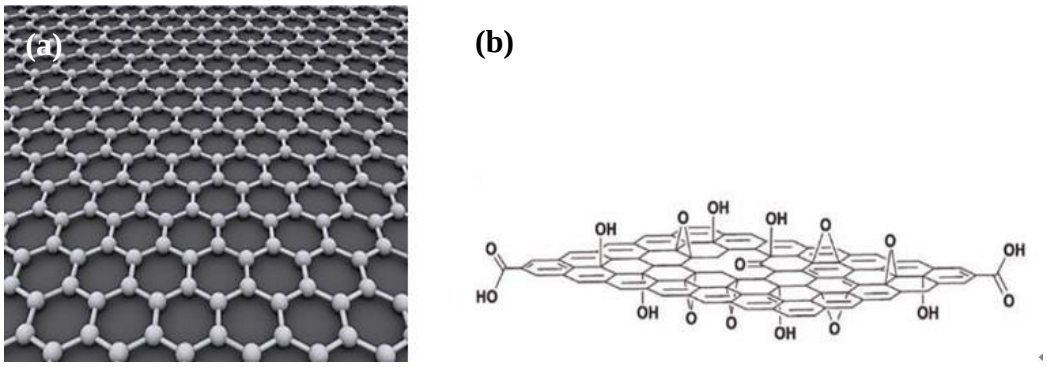

Figure 1.5.1 Structure of graphene (a) and typical functional groups on graphene oxide (b)

1.5.2 Synthesis of graphene and its properties

As briefly mentioned in Section 1.5.1, numerous methods have been developed for the synthesis of graphene and graphene-related materials. A summary will be given in this section. The preparation methods are commonly classified into top-down and bottom-up methods (**Figure 1.5.2**). Products of different methods present very different chemical construction, which makes the properties of the obtained graphene varies distinctly. In this thesis, one of the top-down methods, chemical oxidation strategy is selected to obtain graphene material.

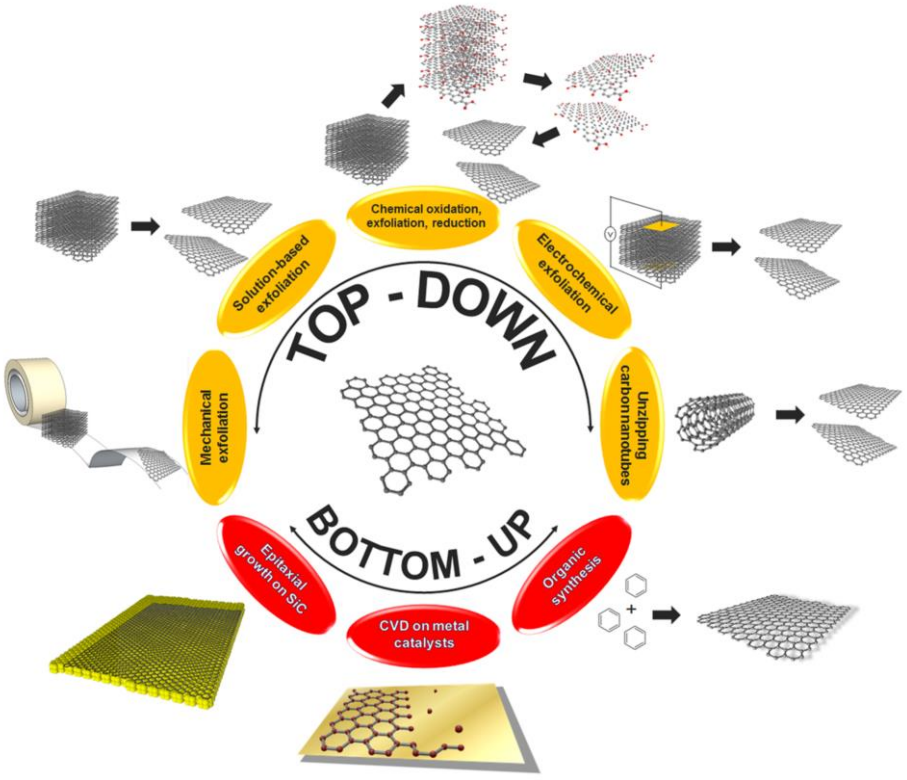

Figure 1.5.2 An overview of strategies for graphene synthesis [62]

1.5.2.1 Top-down methods

In most cases, the word “top-down” means graphene is produced from the exfoliation of a bulk of graphite. Graphite is the raw material, and the top-down methods generally are performed in mechanical, chemical and electrochemical processes. The key point for exfoliation is to overcome the van der Waals forces between each “graphene” layers. Besides, graphene can be obtained by opening the structure of carbon nanotubes.

Mechanical exfoliation. As known, single layer graphene was firstly exfoliated by Andre Geim and Konstantin Novoselov using adhesive tape [59]. The graphite with several layers was repeatedly flaked off, and single layer graphene was finally obtained and then shifted onto the wafer surface. This was a perfect example of mechanical methods and the gained single layer graphene kept the pristine properties of graphene, without bringing in any impurities. However, this pristine graphene was just only suitable for fundamental research due to the quite low yield and poor electrochemical activity [63].

Chemical oxidation exfoliation and reduction. Chemical oxidation methods are the most popular strategies to replace the mechanical method which use oxygen groups importation to weak the van der Waals forces. During the oxidation process of graphite, oxygen-containing groups are intercalated into graphite layer, which resulted in a complex of sp^3 and sp^2 hybridized carbon atoms. Excellent works have been done by

Brodie [64], Staudenmaier [65], Hofmann and Hummers [66] and Tour [67] to obtain graphene with chemical oxidation methods. Among them, Hummer's strategy is broadly accepted due to the low toxicity with the reagent of potassium permanganate ($KMnO_4$) and concentrated sulfuric acid (H_2SO_4). In fact, the products prepared by chemical oxidation methods are not called "graphene". They are the so-called graphene oxides, which can be reduced further to restore part of their original properties. However, the importation of oxygen groups and the structural failure is irreversible, resulting in more new properties and some of them can bring wide use in sensing.

Electrochemical exfoliation. Electrochemical exfoliation method shares the same thought to both mechanical and chemical exfoliations. It aims at the intercalations between graphite layers through applying anodic or cathodic potentials onto graphite working electrode immersing in specific aqueous or organic electrolytes. When the anodic potential is applied, the graphite is firstly oxidized by the positive potential and negatively charged ions in the solvent will intercalate between graphite layers. The van der Wall force becomes much lower and then another negative potential is needed to facilitate the complete exfoliation. Various kinds of electrolytes have been demonstrated valid, e.g., sulfuric acid [68], poly(styrenesulfonate) (PSS) [69], and sodium dodecyl sulfonate (SDS) [70]. Similar to chemical oxidation methods, the oxidation by application of positive potential leads to an abundance of oxygen groups and disruption of sp^2-hybridized carbon network. To eliminate this drawback, cathodic

reduction method was achieved by intercalation of H_3O+ ions [71], Li^+ ions and tetra-*n*-butylammonium (TBA^+) ions [72]. Zhong and co-workers developed a two-stage strategy that the graphite electrode was firstly expanded in Li+ ions, and followed by the second stage where the expanded graphite was exfoliated into graphene sheets by the introduction of TBA^+ ions at potential of -5V [72]. Electrochemical exfoliation methods are superior to other methods, and the most extraordinary advantage is that they are much more environment-friendly and controllable. The disadvantage is that although the tweak can be controlled by the applied potential, it is still hard to precisely exfoliate graphene sheets into homogeneous size and thickness. Moreover, the use of surfactants may functionalize the graphene sheets, and result in an irreversible change of electrochemical properties [73, 74].

1.5.2.2 Bottom-up methods

Bottom-up methods generally include chemical synthesis and chemical vapor deposition (CVD) approaches.

Chemical synthesis. The chemical synthesis method is to combine small polycyclic aromatic hydrocarbon molecules into a large piece of graphene. The fabrication is clean and scalable. However, when graphene grows into several nanometers, it becomes insoluble in both organic and inorganic solvent. This drawback hinders further growth and makes the growth more uncontrollable. Some efforts have been

reported that Mullen et.al synthesized graphene molecule including 222 carbons with an average size of 3.2 nm [75].

Chemical Vapor Deposition (CVD). CVD is the most popular bottom-up method for graphene synthesis. It is very promising due to the feasibility to achieve a single layer of graphene sheets with extremely high purity [76]. Compared to graphene products obtained by mechanical methods, it is very pity that CVD graphene has lower electronic properties [77]. However, this could not impede the wide use of CVD, which has been demonstrated the excellent performance in biosensing applications [78, 79].

1.5.2.3 Properties of graphene oxide materials

Properties of graphene oxide materials are primarily due to the atomic arrangement, size, and surface chemical groups. Since applications in electrochemistry are the scope of this thesis, properties which are related to electrochemical biosensing will be introduced in details.

- *Large surface-volume ratio*. The large surface-volume ratio is the basic similarities of all nanomaterials. Due to the small size in nanoscale and the high surface-volume ratio, the graphene materials will contact and react with reagent molecules around more readily [80]. Reactions become faster and efficient. What is more, according to AFM imaging, the thickness of graphene synthesized through any

methods is lower than 1nm [81], making it almost a kind of 2D material with the ideal surface-volume ratio.

- *Hydrophilicity*. Actually, the pristine graphene is hydrophobic, due to the perfect honeycomb lattice structure of sp^2 carbon atoms. However, chemical oxidation procedure gives graphene abundant oxygen groups at edges or in basal plane. These chemical groups are hydrophilic and make graphene well dispersed in aqueous or some organic solvent [82]. Great dispersion broadens the usability of graphene materials, especially in-vivo experiments since hydrophilicity is the basic character of a biocompatible material.

- *Multiple physical and chemical functionalizations*. Oxygen groups attached to sp^3 carbon atoms and sp^2 carbon atoms on the plane provide opportunities for chemical and physical functionalization. For chemical modification, carboxyl groups (-COOH) can react with amino groups ($-NH_2$) or thiol groups (-SH) through carbodiimide chemistry or maleimide chemistry, respectively. 1-ethyl-3-(3-dimethylaminopropyl) carbodiimide hydrochloride (EDC) and N-hydroxysuccinimide (NHS) are the reagents for these two chemical reactions [83]. Such reactions enable graphene integrated with DNA and proteins since NH_2 and SH groups exist in most biomolecules. Hydroxyl groups on graphene oxide surface can not react with NH_2 or SH groups directly, but they can be oxidized into carboxyl groups in the presence of strong oxidants such as nitric acid or concentrated sulfuric acid. Epoxy groups in graphene plane can be opened through

salinization reactions, e.g. (3-aminopropyl) triethoxysilane (APTES) for further immobilization with various biomolecules. For physical modification, π-π interaction and electrostatic interaction are the main approaches. ssDNA or peptides can adsorb onto graphene surface through π-π stacking. Graphene oxide is originally negatively charged, hence molecules with positive charges will interact with graphene oxide through electrostatic interaction [84].

- *Electrochemical properties*. The electrochemistry properties of graphene are mainly caused by inherent electrochemical activities and dopants/ impurities on graphene. Details are given in following 1.5.4 section.

1.5.3 Graphene based composites

As various types of graphene derivatives have been achieved, it is possible to synthesize graphene based composites with other materials to achieve different functionalities. Typically, graphene based composites can be achieved by decoration with organic polymers and metal nanomaterials [85]. For electrochemical biosensing, graphene-metal nanomaterial composites play an important role for the combination of both extraordinary electrochemical properties of graphene and metal nanomaterials. Therefore, the introduction is mainly focusing on metal related composites.

Two approaches, *ex-situ* linking and *in-situ* crystallization, are the primary synthesis methods of graphene-metal nanomaterials composites. *Ex-situ* linking

means graphene and metal nanomaterials are firstly synthesized separately, and then crosslinkers are imported for the combination. For instance, bovine serum albumin (BSA) was proved as a good linker for GO/rGO and AuNPs/AgNPs/PtNPs/PdNPs/LatexNPs [86]. BSA was adsorbed onto GO due to physical adsorption like π-π interaction and electrostatic interaction, while metal nanoparticles were attached to BSA though metal-sulfur chemical bonds. However, some drawbacks are still hard to be minimized because of the low amounts and non-uniform attachments of metal nanomaterials [87].

In contrast, *in-situ* crystallization method can significantly increase the surface coverage with a controllable size of metal nanoparticles. In a typical *in-situ* crystallization method, graphene materials and precursors of noble metals such as $HAuCl_4$ and H_2PtCl_6 are mixed together with special proportion, and then various methods based on chemical reduction, electroless deposition, thermal evaporation et.al are performed to achieve the graphene-metal nanomaterials composites [85]. The deposition of metal nanoparticles mainly takes place at oxygen group sites. Electrochemical biosensing primarily imported AuNPs, PtNPs and PdNPs for signal enhancement which has been partly introduced in section 1.4.3. Commonly AuNPs are reduced from $HAuCl_4$ in the present of citrate acid or $NaBH_4$ [88]. Obtained GO/AuNPs composites are used for attachment of antibodies, thiol-modified oligonucleotides through Au-S bond. Also, silver enhancement could happen at the AuNPs sites [89]. PtNPs are reduced from H_2PtCl_6. The procedure is very similar to

that of AuNPs, but interestingly that the synthesized PtNPs on graphene are much smaller than AuNPs. PtNPs are a good catalyst for H_2O_2 oxidation as mentioned before, and the function of PdNPs are very similar.

1.5.4 Electrochemistry of graphene materials

Electrochemistry of graphene materials can be summed up from the aspects of chemical composition and structure, synthesis strategies, or electrochemical activities generated. For instance, types and amounts of defects and oxygen groups vary significantly due to different preparing routes, and result in diverse electrochemical properties. Herein, an introduction focusing on electrochemical effects, such as heterogeneous electron transfer (HET), inherent electrochemical activity, and electrocatalysis effects is summarized.

Heterogeneous electron transfer (HET). HET is the electrons transfer between graphene sheets and molecules close to. Such electron transfer rate is related to the presence of defects, oxygen groups and impurities on planes and edges, as well as the chemical species existed in the electrolyte solution [90]. HET at graphene edges are much larger than that at graphene plane [91]. Generally, HET rates are positively correlated to the amounts of defects, therefore reduced graphene oxide (rGO) owns a greater HET rates than pristine graphene [92]. On the contrary, loading too many oxygen groups will obviously decrease HET rates, which means by the reduction of

such groups via electrochemical or chemical methods, the HET rate can be promoted [92]. Impurities doped on graphene surface act as another critical factor and can be divided into metallic and nonmetallic elements. Nitrogen and halogens are representatives of nonmetallic elements. Doped nitrogen acts as an electron donor which accelerate the heterogeneous electron transfer toward ferro/ferricyanide redox probes [93], while doped halogen provides an opposite function [94]. Metallic elements hardly exhibit influence on HET, but change the electrocatalytic behaviors which will be discussed later [95, 96]. Heterogeneous electron transfer also alters with different types of redox probes. For instance, some species like ascorbic acid and ferro/ferricyanide which are sensitive to the presence of oxygen groups will be affected by the oxidation and reduction of graphene [92], while compounds like $[Ru(NH_{3)6}]^{2+/3+}$, are insensitive, inversely [97].

Inherent electrochemical activity. Inherent electrochemical activity means the electrochemical reaction of graphene itself takes place. This is mainly due to the oxygen-containing groups on graphene sheets. Under particular potentials, oxygen groups such epoxide, peroxide, hydroxyl and carboxyl groups can be reduced. Typical these oxygen groups on graphene oxide have common reduction potentials. Carboxyl groups have the most extreme reduction potential around -1.8V, this may be due to the high degree of oxidation of -COOH [98]. Aldehyde has a reduction potential of -1.0V and peroxide is about - 0.7 [99]. The reduction potential also changes under different pH conditions and oxidation methods [100].

Electrocatalysis effects. Some of the graphene materials are regarded as electrocatalysts at first. The electrocatalytic activity was erroneously attributed to graphene materials themselves [101], This may be due to the high challenge to remove metal impurities. Unlike nonmetallic elements doped on graphene surface which have strong influences on heterogeneous electron transfer and inherent electrochemical activities. The electrocatalytic property is mainly caused by metal-based impurities. Ultrasonication treatments were found to have strong effects on the generation of metal impurities. Hence it was confirmed that the residual metallic impurities were responsible for the electrocatalytic effects [101]. It has been demonstrated that cumene hydroperoxide, glutathione, NaHS, and hydrazine can be catalyzed by metal-doped graphene [96].

1.5.5 Applications of graphene related materials in electrochemical biosensors

Due to the excellent and versatile characteristics of graphene related materials, tremendous interests have been attracted and widely research and applications have been done. Graphene based electrochemical biosensors are among these applications. Brief introduction of these applications is summarized with a classification on analytes. Analytes commonly consist of heavy metals, biomarkers, DNAs, proteins, and cells (bacterium).

1.5.5.1 Heavy metals

For heavy metals detections, voltammetric and amperometric techniques are mainly employed as basic approaches with introducing stripping strategies to achieve a lower limit of detections (LODs). Nanomaterials play a crucial role in the sensitivity enhancement for their faster electron transfer and mass transport rates, and enlarged surface area. Graphene materials with good electrochemical characters are deservedly regarded as an option for better sensing performance. For example, Li and his co-workers published a Pb^{2+} and Cd^{2+} biosensor using differential pulse anodic stripping voltammetry (DPASV) which was a technique combining pulse voltammetric method and stripping method [102]. Graphene oxide (GO) was proposed with nafion and the composites were fixed on working electrode. A low LOD of 0.02 μg/L was achieved.

1.5.5.2 Biomarkers

Biomarkers are a huge group which indicates directly or indirectly relevance to clinical diagnosis. Typically, biomarkers are small biomolecules, e.g. hydrogen peroxide (H_2O_2), glucose, NADH, dopamine(DA), uric acid (UA) and ascorbic acid (AA).

Glucose. Glucose is no doubt the most studied. Up to now, three generations of glucose electrochemical biosensors have been produced with relative mature applications in industry. At lab level, graphene also plays an important role to provide more sensitive electrode interfaces. In a typical design, graphene and glucose oxidase enzyme (GOx)

are firstly immobilized onto working electrode surface. Such design brings in two superiorities of graphene: the good biocompatibility which can ensure the highest enzyme activity, and a good electron transfer from the active center of enzymes to graphene on the electrode, which guarantees a quick electrochemical response. Lin et.al built a composite on the electrode with reduced graphene oxide, GOx and chitosan. Such glucose sensor reached a detection limit of 20 μM [103].

NADH and H_2O_2. NADH plays as an electroactive cofactor which reacts in all dehydrogenase process, including lactate, ethanol, and glucose. Different reduction methods of graphene have been studied for NADH redox behavior. Tang found the oxidation of NADH was remarkable shifted for around 30mV with the introduction of chemical reduced graphene oxide [104]. Li and co-workers proposed sensing platform with a LOD of 0.1μM with the assist of electrochemically reduced graphene oxide [105]. H_2O_2 is commonly appeared as a by-product of oxidases and horseradish peroxidase enzyme (HRP) is highly efficient to the decomposition of H_2O_2. Lu and coworkers built a platform with chemical reduced graphene oxide and cyclodextrin to combine with admantane-modified HRP, and achieved a limit of detection of 0.1μM [106].

Dopamine (DA). Dopamine is a neurotransmitter correlating to Parkinson's disease. It exists in serum samples with a low concentration around 0.01μM. Hence, very sensitive and high specific biosensors are needed for the detection in serum samples. However, the specificity is critical because the existing ascorbic acid (AA) and uric

acid (UA) are interfering substances because their oxidation potentials highly overlap. To distinguish them, graphene which was proved to be electrocatalytic just to DA in the presence of AA and DA provides great possibility in realizing a sensitive and highly specific detection. Shang et.al fabricated a microwave-plasma-enhanced CVD graphene based voltammetric biosensor for DA detection, and reached a LOD of 0.17μM with 1mM AA and 0.1mM UA coexisting [107].

1.5.5.3 DNA

DNA analysis is commonly achieved through two approaches. The first one is to directly detect the change of polynucleotides because they are internal negative charged and can attract or repel other charged redox probes. The other one is to label single strand DNA (ssDNA) probes and monitor the electroactivity change during DNA hybridization processes. The second method is always involved with DNA beacon or a sandwich structure. Various applications based on the second method have been reported. Dong's group achieved a ssDNA biosensor with the assistance of AuNPs and ERGO. ERGO was firstly deposited onto GCE surface, then $d(GT)_{29}$-SH oligonucleotides were dropped on and bound to graphene through π-π stacking. After that AuNPs modified with probe ssDNAs-SH were incubated with the electrode and attached on through Au-S chemical bond. Target ssDNAs labeled with biotin were then captured following by the attachment of HRP and streptavidin carried carbon nanospheres. By means of differential pulse voltammetry (DPV) detection of HRP catalyzing o-phenylenediamine and H_2O_2, a LOD of 5aM was realized [108].

Except the employment of graphene due to its remarkable properties as a platform for other modifications attachment, its inherent redox activities can be applied in biosensing field as well. Bonanni and co-workers fabricated a simple micro biosensor using GO nanoplatelets as electroactive labels [109]. Different DNA hybrids got with complementary, one mismatched and non-specific ssDNAs can sensitively and selectively distinguished by this platform.

1.5.5.4 Proteins

For protein detection, two main strategies are used with the assist of graphene materials. One is to simplify the fabrication only to capture target proteins without any secondary antibodies or sandwich structures involved. This method is easy to carry out, and the main purpose of the use of graphene is to enhance the electrochemical activity of the electrode surface, or to employ the inherent electroactivity of graphene sheets. Graphene modified on electrode surface can increase the surface superficial area, enabling more antibodies conjugation. Also, the electrochemical performance can be enhanced because of the rapid electrochemical response of graphene related materials. Particularly, graphene based composites are frequently applied, especially GO-AuNPs composites. Ma's group reported a carcinoembryonic antigen (CEA) biosensor with the deposition of GO-AuNPs-thionine on electrode surface [110]. Due to the chemoadsorption through Au-S bond, CEA antibodies were simply conjugated and able to capture target CEA. The voltammetric method was used for monitoring electrochemical signals, and LOD of 0.05fg/mL was achieved.

Secondary antibodies were frequently imported to achieve to sandwich structure. Herein the role of graphene is to load more secondary antibodies as well as some electrocatalysts which amplify electrochemical signals. Xie and co-workers built a voltammetric biosensor for the analysis of α-teroprotein (AFP) [111]. The electrocatalyst involved was HRP which could catalyze the oxygenolysis of H_2O_2 enhance the electrochemical signal through the presence of thionine. This sensor was capable for AFP detection low to 0.02ng/mL.

1.5.5.5 Cells

Two categories of cells are mostly intriguing in biosensing: cancer cells and bacteria. For cancer cells detection, circulating tumor cells have attracted tremendous attentions because they are promising for early detection of cancer. As reported in previous literature, it was demonstrated that at an early stage of cancer circulating tumor cells appeared in blood or lymph circulation system. However, the CTCs are mixed with an enormous number of normal cells and the concentration of CTCs is quite low, resulting in demand for high sensitive and selective detections. Yoon and co-workers fabricated a microfluidic device for CTC-specific capture [112]. A PDMS chamber was fixed on a silicon substrate with an inlet and an outlet. As analytic liquid flowed by, CTCs inside would be captured by antibodies immobilized on GO/Au patterns (**Figure 1.5.5**). GO was for plentiful chemical attachments of specific epithelial cell adhesion molecule (EpCAM) antibodies, while the flower-shaped gold pattern can improve the sensitivity because of the enhanced surface-volume ratio and

the approximate size to target cancer cells. As a result, a high sensitivity was achieved that 3-5 cells per milliliter in blood sample could be successfully separated.

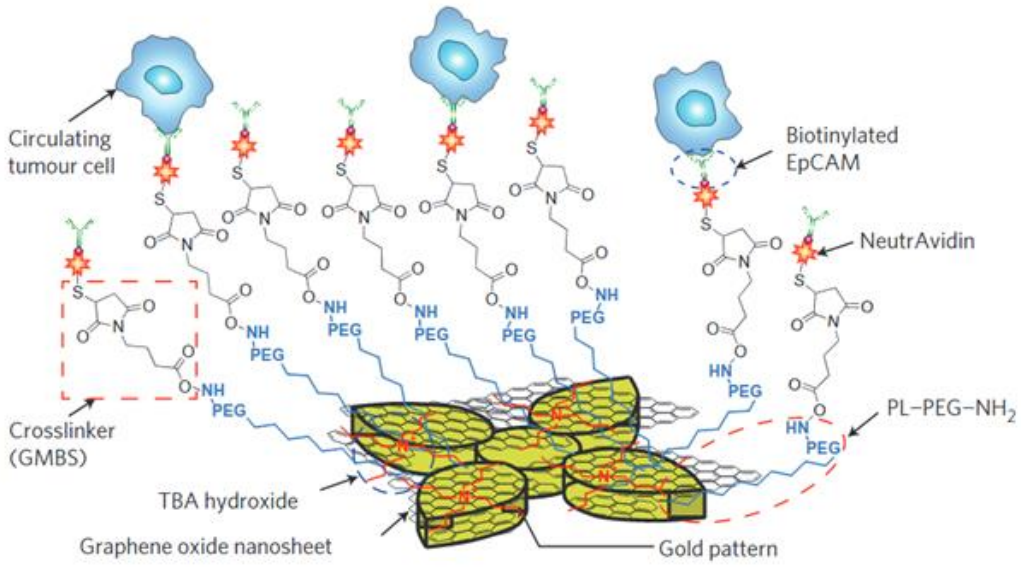

Figure 1.5.3 Conjugation between gold pattern, functionalized graphene oxide nanosheets and EpCAM antibodies[112]

Bacteria are another huge group for detection as mentioned in section 1.1. Various electrochemical devices have been fabricated with different electrochemical techniques, and some of them may import microfluidic technique. Examples of typical electrochemical biosensors for bacteria detection have been listed in section 1.2, so no more will be introduced here. The purpose to introduce graphene-based materials are the same to that of CTCs detections. Wan and co-workers reported a platform for bacteria detection with a sandwich structure and GO-mediated silver enhancement for signal amplification [113]. GO acted as a large carrier for anti-bacteria antibodies as well as the catalyst for Ag enhancer solution. Potentiometric stripping analysis (PSA) was performed as an analytic tool which could detect trace amounts of Ag ions. LOD

of this method was about 50 CFU/mL and effective detecting range was from 10^2 to 10^8 CFU/mL.

1.6 Nanoporous alumina membrane

1.6.1 Structure of nanoporous alumina membrane

As a subset of nanoporous materials, the nanoporous membrane has attracted tremendous attentions for its high surface-volume ratio as well as the capability for separation of small molecules. Moreover, the biocompatibility ensures it as a potential material to mimic cell membrane functions. It is very important that the pore sizes can be well controlled both on width and depth. Materials for nanoporous membrane generally are classified into organic and inorganic membranes. Organic membranes are made of polymers, through imprint technique or lithographic technique [114]. Inorganic membranes are mostly composed of metal oxides. As one of them, nanoporous alumina membrane is popular for its extraordinary properties.

Nanoporous alumina membrane is made of alumina oxide with a honeycomb-like structure (**Figure 1.6.1**). It is synthesized through an anodic etching process. In this process, pure aluminum is etched by the anode voltage in the present of the sulfuric solution, oxalic solution, or chromic solution. This method is well-established hence permits large scale productions with a low cost.

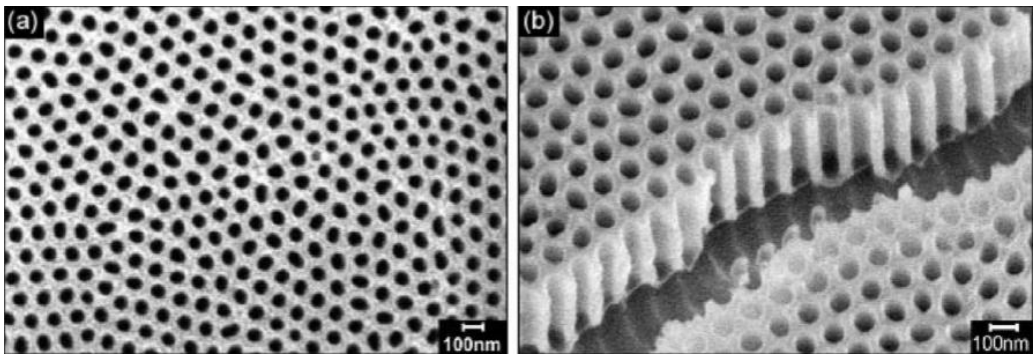

Figure 1.6.1 SEM images of nanoporous alumina nanotemplate. Plan view image of the membrane (a) and cross-section view of the membrane (b) [115]

During anodization process, the nanopore dimension is affected by many elements: electrolyte type and concentration, solution pH, anodizing potential, widening and anodizing time [116]. The diameter of nanopores varies from 20nm to 200nm while the depth can be even deep to 100μm [117].

1.6.2 Properties of nanoporous alumina membrane

The controllable size of alumina oxide nanopores enables nanoporous alumina membrane a versatile tool in biosensing area. The main superiorities of nanoporous alumina membrane are high surface-volume ratio and ease of modification.

High surface-volume ratio. Unlike traditional imperforate substrate, nanoporous alumina membrane is more like a 3D material with tons of nanopores. This feature greatly enhances the surface area of the membrane, because biological reactions can not only take place on membrane outside surface, but also inside nanochannels. Direct influence is that signals generated by biological recognition or catalysis can be magnified manifold.

Ease of modification. When applied in biosensors, nanoporous alumina membrane often performs as the substrate. Hence surface modification is highly needed for conjugations of antibodies or aptamers. Salinization is mostly used for nanoporous alumina membrane modification. Membranes are firstly treated with hydrogen peroxide, resulting in abundant hydroxyl groups on the membrane surface. Then silanes like 3-aminopropyltrimethoxysilzne (APTES) and (3-glycidoxypropyl) trimethoxysilane (GPMS) are mixed with treated nanoporous membranes. Chemical bonds are generated between hydroxyl groups on the membrane surface and silanes. As silanes are long chain molecules, amino groups (APTES) or epoxy groups (GPMS) are exposed outside and have the abilities to react with carboxyl groups or amino groups in biomolecules, respectively.

1.6.3 Application of nanoporous alumina membrane in electrochemical biosensing

Many electrochemical biosensors using nanoporous alumina membrane have been reported. Since the two projects concern about DNA and bacteria detection, applications in these two directions will be shortly summarized in this section.

DNA detection. For DNA detection, the fundamental idea is that probe single-strand DNAs are firstly linked to nanoporous alumina membrane both in channels and outside surface. After the hybridization of target DNAs, channels diameter is shortened and the ionic conductivity is hindered. Through measuring the impedance

change by the faradaic current, the captured of target DNA can be detected. For example, Deng and co-workers fabricated a simple electrochemical biosensor for DNA detection based on platinum modified nanoporous alumina membrane [118]. Platinum was deposited on both two sides of the membrane, acting as the working electrode and the counter electrode. When a droplet containing target DNAs incubated with membrane together, hybridizations happened inside, resulting in the conductivity change of nanoporous alumina membrane. A linear detection range from 10^{-12} to 10^{-6} M was achieved.

However, such methods are restricted by the nanoporous diameter which has to be comparable to the length of target DNAs. However, the length of DNAs varies much from a few nanometers to dozens of nanometers, and the sensitivity will be influenced significantly. As an improvement, a sandwich structure with signal amplification was reported by our group. The secondary probe DNAs were modified with AuNPs and would hybridize with captured target DNAs. After that, silver enhancement process was imported, resulting in silver blocking in nanopores. Impedance was massively decreased and the relative impedance decreased was proportional to target DNAs concentration.

Bacteria and cell detection. Unlike DNAs which are small to nano-scale, bacteria or cells are all in micro-scale which are much larger than the nanoporous size. Therefore, detections of target bacteria of cells take place at membrane surface with the help of antibodies or aptamers. When target cells are captured on the membrane, nanopores

are blocked and the conducting liquid can hardly pass through these channels, leading to impedance increase. Based on this principle, our group built a microfluidic device for real-time bacteria detection. A sensitive detection of *E. coli O157:H7* and *Staphylococcus aureus* with LOD of 10^2 CFU/mL were achieved and the detection process is real-time, which means the bacteria capture could be measured any time [119].

1.7 Objectives of the study

Specific objectives of part I include:

1) To establish a nanoporous alumina membrane based electrochemical biosensor with platinum nanoparticles (PtNPs) catalyzed precipitation as impedance signal enhancement for *E. coli O157:H7* gene detection;

2) To explore the impedance change generated by the formation of sandwich structure via hybridization of target gene sequences and secondary gene probe;

3) To explore optimal hybridization time of target gene sequences and precipitation caused by PtNPs;

4) To find out the sensitivity, limit of detection (LOD) as well as the specificity for detection of *E. coli O157:H7* gene sequence using nanoporous alumina membrane

based electrochemical biosensor with PtNPs catalyzed precipitation as impedance signal enhancement.

Specific objectives of part II include:

1) To establish a nanoporous alumina membrane based electrochemical biosensor with GO/Hemin catalyzed precipitation as impedance signal enhancement for *Salmonella enteritidis* bacteria detection;

2) To explore the impedance change generated by the formation of sandwich structure via target bacteria capturing and GO/Hemin/Antibody composites;

3) To explore the real-time capture of target *Salmonella enteridis* bacteria to optimize the capturing time;

4) To find out the sensitivity, limit of detection (LOD) as well as the specificity for detection of *Salmonella enteritidis* bacteria using nanoporous alumina membrane based electrochemical biosensor with GO/Hemin composites catalyzed precipitation as impedance signal enhancement.

Chapter 2 Methodology

2.1 Nanoporous alumina membrane based electrochemical biosensor with PtNPs tags for *E. coli O157:H7 gene* detection

2.1.1 Materials and instruments

Materials: Chloroplatinic acid (H_2PtCl_6), (3-glycidoxypropyl) trimethoxysilane (GPMS), Sodium citrate tribasic dehydrate ($C_6H_5Na_3O_7•2H_2O$), Sodium borohydride ($NaBH_4$), 4-Chloro-1-naphthol (4-CN) ($C_{10}H_7ClO$) were all purchased from Sigma Aldrich (St. Louis, MO, US). Dithiothreitol (DTT) ($C_4H_{10}O_2S_2$) was purchased from Thermo Scientific Pierce. Nanoporous alumina membranes (Whatman) (200nm, 13mm diameter) was supplied by GE Healthcare Life Sciences and Gel columns (illustra MicroSpin G-25 Columns) was from GE Healthcare (Piscataway, NJ, USA). Hydrogen peroxide (30%) was purchased from Advanced Technology & Industrial Co., Ltd. Polydimethylsiloxane (PDMS) was purchased from Sylgard 184 silicone elastomer kit (Dow Corning, USA). DNA sequences were all synthesized by Integrated DNA Technologies (IDT, Voralville, IA, USA), and are listed as follows:

DNA sequences: Target *E. coli O157:H7 gene* sequence [120]: 5'- TTT CAG GGA ATA ACA TTF CTG CAG GAT GGG CAA CTC TTG AGC TTC TGT AA-3'; 6 bases mismatched target gene sequence: 5'- TTT CAG CGA ATA ACA ATG CTG CAC GAT GGG CAT CTC TTG TGC TTC TGT TA- 3'; Non-target gene sequence: 5'-CCC AGA AAG GAT GAC GGA TCA AGT ATC ATT ACC TGT

GGT CTT GGT GAC CC- 3'; *E. coli O157:H7 gene* probe1: 5'- NH_2-TTA CAG AAG CTC AAG AGT TGC CCA T -3'; *E. coli O157:H7 gene* probe 2: 5'- CCT GCA GCA ATG TTA TTC CCT GAA A-SH -3'; Fluorescein modified Target *E. coli O157:H7 gene* sequence: 5'- FAM-TTT CAG GGA ATA ACA TTF CTG CAG GAT GGG CAA CTC TTG AGC TTC TGT AA-3'; Fluorescein modified non-target gene sequence: 5'-FAM-CCC AGA AAG GAT GAC GGA TCA AGT ATC ATT ACC TGT GGT CTT GGT GAC CC- 3'; Fluorescein modified *E. coli O157:H7 gene* probe1: 5'- NH_2-TTA CAG AAG CTC AAG AGT TGC CCA T-FAM -3'

Equipment: Au coating of samples was achieved by Bal-Tec SCD 005 Sputter Coater (Germany) and surface morphology characterization was by SEM (JEOL Model JSM-6490). TEM (JEOL-2100F) was used to characterize Platinum nanoparticles. Standard contact angle goniometer (ramé -hart Model 250, USA) was used for surface property characterization of a nanoporous alumina membrane. Fluorescence upright microscope (Nikon, ECLIPSE 80i, Japan) was used for fluorescence characterization. The measurement of surface charge of synthesized PtNP-oligonucleotides was obtained by a zeta potential analyzer (Zetasizer nano ZS, Malvern instruments Corporation). UV absorbance detection was achieved using a UV-Visible spectrophotometer (Ultrospec^{TM} 2100 pro, GE Healthcare). An electrochemical analyzer VersaSTAT3 (AMETEK) was used for electrochemical analysis (Princeton Applied Research USA).

2.1.2 Surface silanization of nanoporous alumina membrane

Surface silanization of nanoporous alumina membrane is the first step in both two projects. Silanization is the process to cover hydroxyl groups containing surface with organofunctional alkoxysilane molecules [121]. Mica or glass surfaces are mostly participated in while alkoxysilane molecules with alkoxy groups at one end can form covalent –Si-O-Si- bonds on these surfaces. At the other end, different silanes can provide various types of functional groups which have the potential to link with a variety of molecules. Hence, surface silanization is a kind of method for surface modification. In this project, GPMS was used as the silane for further linkage of amino group modified probe gene sequences. Chemical structure of GPMS is shown in **Figure 2.1.1**.

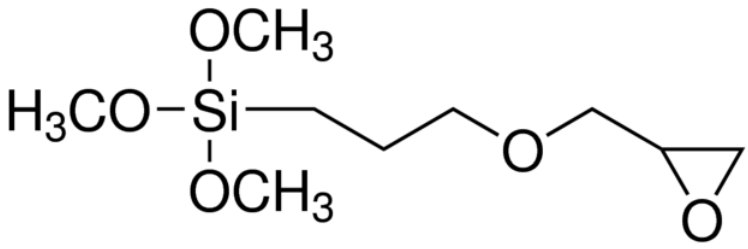

Figure 2.1.1 Chemical structure of (3-Glycidyloxypropyl)trimethoxysilane (GPMS)

Briefly, nanoporous alumina membrane was firstly treated with 30% H_2O_2 for the enrichment of hydroxyl groups. Under a constant heating for 30min at 250°C in H_2O_2 solution and then washed with DI water for several times, nanoporous alumina membrane was successfully hydroxylated. Membranes were dried next and immersed

in 2% GPMS which was dissolved in toluene solvent. After incubation in an oven at 65°C overnight, membranes were rinsed with toluene and ethanol, respectively, and the silanization of nanoporous alumina membrane was realized. Flow chart of the whole process is presented in **Figure 2.1.2**.

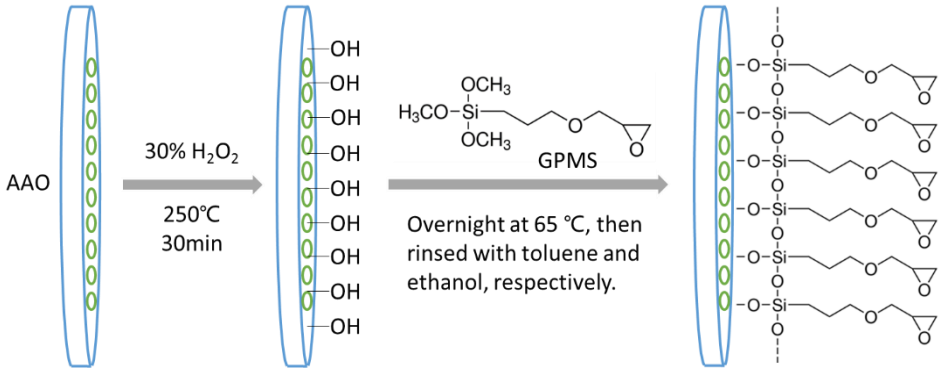

Figure 2.1.2 The whole process of surface silanization.

For the confirmation of the successful silanization of nanoporous alumina membrane, Ramé-Hart goniometer (NJ, USA) equipment was employed to measure the water contact angle of the treated surface (Figure 3.1.3). As the silanization process with GPMS could convert the hydrophilic surface to hydrophobic surface because the epoxy groups are much more hydrophobic than hydroxyl groups. A piece of nanoporous alumina membrane was placed on the specimen stage and a 10μL DI water was dropped on it. Then a camera was used to capture images and DROPimage Advanced 2.1 software was employed to calculate the water contact angle.

Figure 2.1.3 Image of Ramé-Hart goniometer (NJ, USA) equipment

2.1.3 Oligonucleotide probes immobilization

After the surface silanization with GPMS, oligonucleotide probes with amino groups were conjugated onto nanoporous alumina membrane surfaces. Nanoporous alumina membranes were firstly placed in petri dishes and amino group modified oligonucleotide probes were dissolved in 0.01M PBS buffer (PH 8.4) was a concentration of 1μM [122]. For each nanoporous alumina membrane piece, a 150μL droplet of oligonucleotide probes solution was spread on and incubated together for about 10h. Amino groups on oligonucleotides and epoxy groups on nanoporous alumina membrane would react with each other. Then the residual oligonucleotide solution was washed away for several times to ensure the unbound probes had been removed. The principle of this chemical reaction is shown in **Figure 2.1.4**.

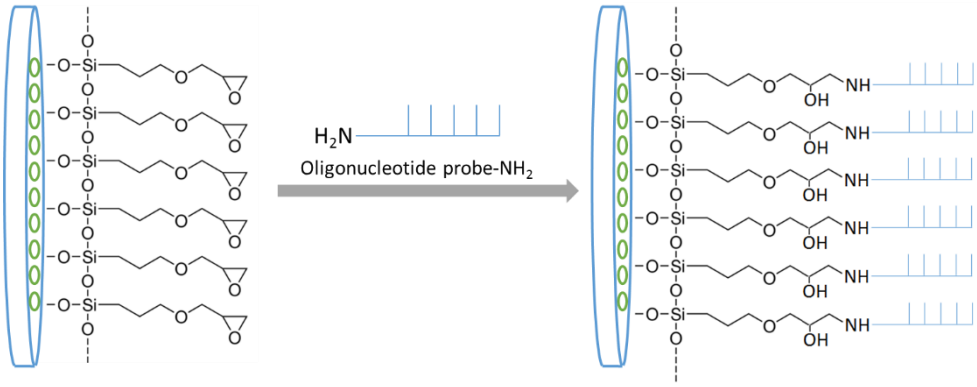

Figure 2.1.4 Scheme of amino group modified oligonucleotide probes conjugation on GPMS modified nanoporous alumina membrane

To verify the successful conjugation of oligonucleotide probes, Fluorescein amidite (FAM) modified oligonucleotide probes were introduced to conjugate with GPMS modified nanoporous alumina membrane. The concentrations of FAM-modified probes were 0.5, 1, 2μM, respectively, and oligonucleotide probes with no FAM-modified (2μM) were chosen as control groups. Other conditions were all the same. Fluorescent images were taken by Fluorescence microscope (Nikon, ECLIPSE 80i, Japan).

2.1.4 Fabrication of microfluidic chip integrated with nanoporous alumina

A simple microfluidic chamber was fabricated as the platform for target *E. coli O157:H7 gene* detection. Firstly, a complex stainless mold was placed in a cube chamber (**Figure 2.1.5a**). The mold is a combination of two cylinders with different diameters. The diameter of the small one is 5mm, which is just equal to the external

diameter of a typical glass carbon electrode (GCE). Then a mixture of sylgard 184 silicone elastomer base and curing agent (10:1) were mixed and poured into the cube chamber, then solidified under 65^0C for 2h (**Figure 2.1.5b**). After that, the obtained PDMS chamber could easily be separated from the cube with a complementary structure of previous stainless mold (**Figure 2.1.5c**). With the help of epoxy adhesive, oligonucleotide probes modified nanoporous alumina membrane could be fixed in the middle place of the PDMS chamber, resulting in a separation of upper and lower spaces (**Figure 2.1.5d**).

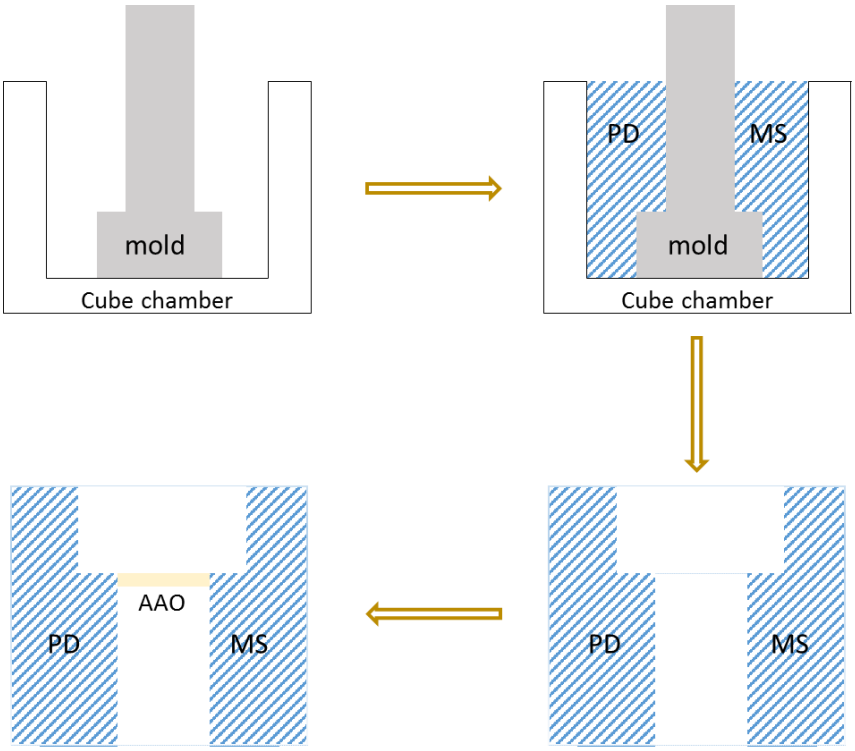

Figure 2.1.5 Fabrication process of microfluidic chip integrated with nanoporous alumina membranes.

2.1.5 PtNPs synthesis

Platinum nanoparticles (PtNPs) were synthesized from chloroplatinic acid (H_2PtCl_6) in the presence of sodium citrate and $NaBH_4$ as the reducing agents at room temperature [123]. Briefly, H_2PtCl_6 was firstly diluted into 15.0mL of DI water in a centrifuge tube to achieve a concentration of 500μM. The H_2PtCl_6 solution was kept under stirring, and 1.0mL of 50mM sodium citrate was added in. Then 500μL of 30mM $NaBH_4$ solution was dropped into the stirring solution discretely with a volume 5μL of each droplet. The tube cap was tightened and the stirring was kept for 30min. After 2h standing, PtNPs solution was achieved with an expected size of 4.0nm. Characterization of synthesized PtNPs was taken by TEM(JEOL-2100F) with an Oxford Instrument EDS system, and the operating voltage was 200 kV.

2.1.6 PtNP-oligonucleotide conjugation preparation

According to the reference reported by Alligrant's group, a simple method could be used to estimate the concentration of synthesized PtNPs solution [124]. A 4nm diameter PtNP is expected to include about 1800 Pt atoms [125]. Hence, the concentration of synthesized PtNPs was calculated to be around 500nM.

To achieve the PtNP-oligonucleotide conjugation, the ratio between PtNPs and oligonucleotides should be 25:1[124]. Before the mixture of PtNPs and thiol group modified *E. coli O157:H7 gene* probes, the gene sequences should be reduced firstly. This was because the modified thiol groups tended to be oxidized and left disulfide

bonds. 0.1 M DTT was used for the reduction of disulfide bonds for 30min. To avoid the interference of residual DTT, gel columns was used for the purification of *E. coli O157:H7 gene* probes. Then a 25:1 molar ratio of purification of *E. coli O157:H7 gene* probes and PtNPs was mixed to achieve PtNPs-oligonucleotides conjugations. After 2h mixture, the mixture was centrifuged at the speed of 13200rpm for 20min, then the precipitated PtNPs-oligonucleotides conjugates were resuspended in DI water. Zeta potential was measured of both PtNPs and PtNPs-oligonucleotides conjugates using Zetasizer nano ZS (Malvern instruments Corporation) equipment. **Figure 2.1.6** shows the sketch of formation of Pt-S bond between PtNP and thiol group modified oligonucleotides.

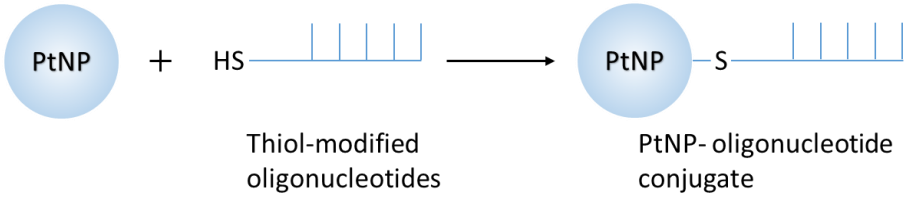

Figure 2.1.6 Formation of PtNP-oligonucleotide conjugates.

2.1.7 Target *E. coli O157:H7* gene capture

As the most critical procedure, characterization and optimization were taken at first. For the characterization, the fluorescent method was used to ensure target genes were hybridized with gene probes on nanoporous alumina membrane. FAM-modified target *E. coli O157:H7* gene sequences were chosen as experiment groups while FAM-modified non-target gene sequences were imported as control groups. After

nanoporous alumina membrane were successfully fixed in PDMS microfluidic chambers, a droplet of 150μL FAM-target/non-target gene sequences was spread on the membrane surface. The concentration was 1μM and the incubation time is 4h. Then the nanoporous alumina membranes were rinsed with DI water for several times. All these procedures were kept in a dark room to prevent photobleaching effect of FAM-modified gene sequences, which would affect the accuracy of analytical results.

Experiment groups and control groups in one particular experiment were observed and recorded by fluorescent microscopy, and then the fluorescent intensity was calculated by imageJ software. Optimization of the capturing time was performed next. 150μL FAM-target *E. coli O157:H7* gene sequences were added onto six PDMS chambers with reaction times of 1h, 2h, 3h, 4h, 5h, 6h. The concentration and procedures were all the same as previous experiments. The whole experiments were taken for three times for the accurate optimization.

2.1.8 Formation of a sandwich structure and precipitation catalysis

After target *E. coli O157:H7* genes capturing, PtNP-oligonucleotide conjugates were added into from a sandwich structure. Briefly, 150μL of 500nM PtNPs-oligonucleotides conjugates were dropped onto nanoporous alumina membrane for 4h, and then washed with DI water for three times. The concentration of PtNPs-oligonucleotides was defined by PtNPs, not oligonucleotides because the amounts of conjugated oligonucleotides were hard to estimate.

Precipitation catalyzed by PtNPs were followed in the present of H_2O_2 and 4-CN [126]. 4-CN was firstly dissolved in absolution ethanol and the concentration was 0.05M. Then 0.1 mL 4-CN solution was diluted in 5mL 0.01M PBS (PH=7.4), so the final concentration of 4-CN was 1mM. 30% H_2O_2 was diluted into 0.15mM and mixed with 1mM 4-CN solution. For the precipitation of 4-CN, nanoporous alumina membrane and electrode chamber was immersed in 150μL obtained solution for 15min. All the procedures of the *E. coli O157:H7 gene* electrochemical detection were shown in **Figure 2.1.7**.

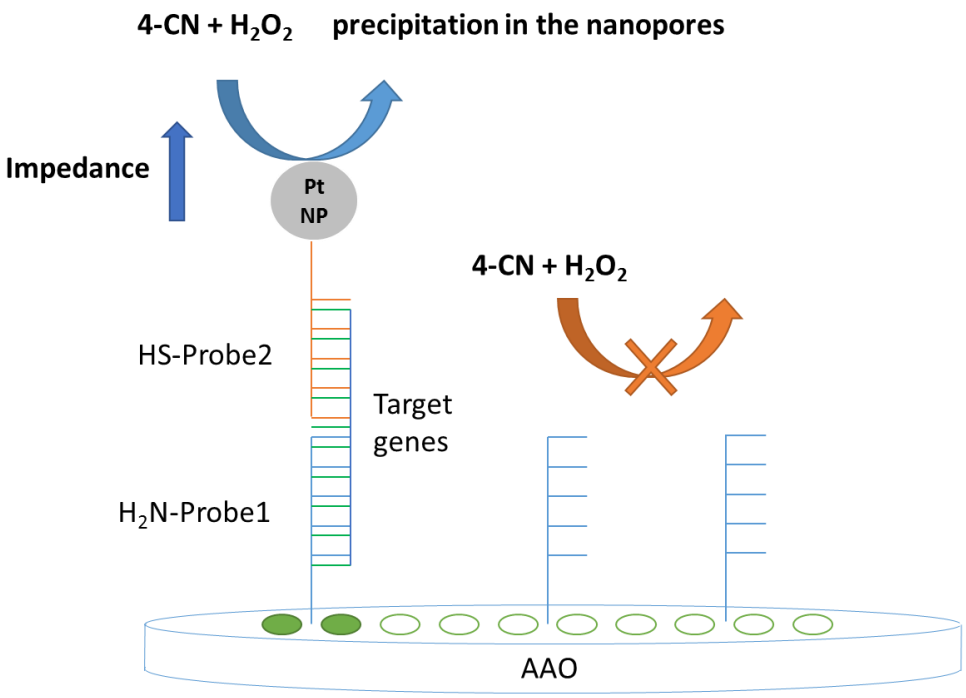

Figure 2.1.7 Sensing mechanism of *E. coli O157:H7 gene* detection

Optimization of the precipitation time was also performed using EIS method. 1μM target *E. coli O157:H7 genes* and 500nM PtNP-oligonucleotide conjugates were

imported and during the precipitation process, EIS was recorded every five minutes from 0min to 25min after 4-CN was first added in.

2.1.9 Electrochemical impedance spectroscopy for target *E. coli O157:H7 gene* detection

Impedimetric detection of target *E. coli O157:H7 genes* was conducted using electrochemical impedance spectroscopy (EIS). EIS was performed after each step with AC sweeps from 10kHz to 1Hz with an alternating voltage, 10 mV. A schematic diagram of the whole set-up is shown in **Figure 2.1.8**. The external diameter of GCE was equal to the internal diameter of the space under AAO membrane. Hence the PBS solution would not leak from the bottom. The other GCE was suspended beyond the nanoporous alumina membrane. When PBS solution was added in, upper GCE surface was immersed in PBS solution and the space between lower GCE and nanoporous alumina membrane was all fulfilled.

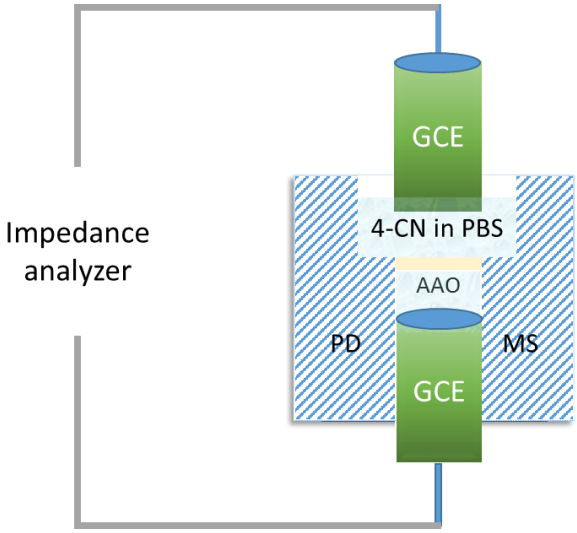

Figure 2.1.8 The set-up of whole detection system

Precipitation catalysis took place on AAO membrane, and hinder the electrons passing through. This set-up could ensure a real-time EIS detection since the electrodes could remain stationary during precipitation catalyzing step. To study the sensitivity of this platform, 0.1nM, 0.5nM, 1nM, 5nM, 10nM and 50nM target *E. coli O157:H7 gene* sequences were chosen with a volume of 150μL. Impedance data in the range from 10Hz to 100Hz indicated changes on nanoporous alumina membrane and the maximum relative change happened under 80Hz AC sweep. Since the base value of each nanoporous alumina membrane in different experiments varies, normalized impedance change (NIC) is introduced to minimize the deviation in different experiments.

The mathematical expression for NIC is shown in blow equation:

$$NIC = \frac{Z_{experiment} - Z_{control}}{Z_{control}} \times 100\%$$

All EIS measurements were taken by VersaSTAT3 (AMETEK) electrochemical workstation.

2.1.10 Specificity study of this fabricated *E. coli O157:H7 gene* electrochemical biosensor

For the specificity studies, non-target *E. coli O157:H7 gene* sequences and 6 base-mismatched *E. coli O157:H7 gene* sequences were imported, respectively. All

experiments for specificity study were conducted with the same concentration of origin target *E. coli O157:H7 gene* sequences. NIC at 80Hz was used for the evaluation of impedance increase at 0.1nM, 0.5nM, 1nM, 5nM, 10nM and 50nM.

2.2 Nanoporous alumina membrane based electrochemical biosensor with GO/Hemin-Antibody tags amplification for *Salmonella enteritidis* detection

2.2.1 Materials and instruments

Nanoporous alumina membranes (Whatman) (100 nm, 13mm diameter) was purchased from GE Healthcare Life Sciences. Graphene oxide (GO) (5mg/mL) was synthesized by Hummer's methods and purchased from Graphene supermarket. Hemin ($C_{34}H_{32}ClFeN_4O_4$) was purchased from Tokyo Chemical Industry Co., Ltd. 4-Chloro-1-naphthol (4-CN) ($C_{10}H_7ClO$) and Bovine Serum Albumin (BSA) was from Sigma Aldrich (St. Louis, MO, US). Hydrogen peroxide (30%) was purchased from Advanced Technology & Industrial Co., Ltd. Polydimethylsiloxane (PDMS) was purchased from Sylgard 184 silicone elastomer kit (Dow Corning, USA). Salmonella enteritidis mono-antibody (For *ompC antigen*) was supplied by Dr. Sheng Chen's groups, ABCT Department, the Hong Kong Polytechnic University.

Au coating of samples was achieved by Bal-Tec SCD 005 Sputter Coater (Germany) and surface morphology characterization was by SEM (JEOL Model JSM-

6490). TEM (JEOL-2100F) was used to characterize Graphene oxide. Standard contact angle goniometer (ramé -hart Model 250, USA) was for Surface property characterization of nanoporous alumina membrane, and Fluorescence microscope (Nikon, ECLIPSE 80i, Japan) was for Fluorescent characterization. The measurement of the surface charge of synthesized GO/Ab conjugates was obtained by Zetasizer nano ZS (Malvern instruments Corporation), and UV absorbance detection was achieved using Ultrospec^{TM} 2100 pro UV-Visible spectrophotometer (GE Healthcare). Electrochemical analyzer VersaSTAT3 (AMETEK) was from Princeton Applied Research (USA).

2.2.2 Antibody Immobilization on Nanoporous Alumina Membrane

For antibody immobilization, nanoporous alumina membrane was first modified with GPMS through silanization reaction. This was because that antibodies inherently consisted of amino groups which could covalently react with epoxy groups on GPMS molecules. The procedure of GPMS modification was totally the same to that in project one, taking about one night. Since antibodies were much more unstable and easily inactivated compared to oligonucleotides, the obtained GPMS modified nanoporous alumina membrane should be rinsed well to ensure all the organic molecules had been removed. After the GPMS modification process, nanoporous alumina membranes were then fixed in microfluidics chamber instead of antibodies immobilization on nanoporous alumina membrane. This was expected to save the high

cost of antibodies. The microfluidics chamber and the fabrication process were all the same to that in project one.

After the fabrication of nanoporous alumina membrane microfluidics chamber, 50μL of 100 ng/mL *S. enteritidis ompC* antibodies were dropped onto both sided of nanoporous alumina membrane, and incubated at 4°C overnight. Then 150μL 1% BSA was imported for 1h to prevent the non-specific adsorption of target bacteria. The scheme is shown in Figure 2.2.1.

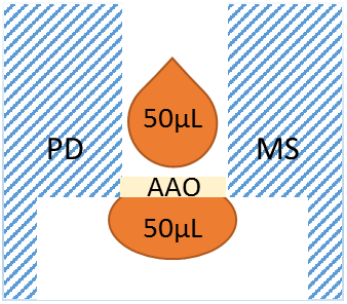

Figure 2.2.1 Scheme for *S. enteridis ompC* antibodies immobilization

For the confirmation that *S. enteridis ompC* antibodies were successfully immobilized onto nanoporous alumina surface as well as to find a relatively reasonable concentration, fluorescent labelled *S. enteridis ompC* antibodies were used as characterizations. Four different concentration (0, 50, 100 and 200 ng/mL) of antibodies were tried with the same reaction time, and then fluorescent microscopy was used for the observation.

2.2.3 Synthesis of GO/Hemin/-Antibody composites

Synthesis of GO/Hemin-Antibody composites were separated into two steps: the first is to synthesize GO-antibody composites, the next is to conjugate hemin onto the surface of GO/Ab composites.

For the first step, GO and antibodies were combined through the carbodiimide chemical reaction. The function of this reaction was to conjugate molecules covalently with carboxyl groups (-COOH) and amino groups ($-NH_2$). Briefly, Graphene oxide (GO) purchased from graphene supermarket was synthesized though Hummer's method. Then 1mL of 1mg/mL GO was incubated with 200μL 2mM NHS and 200μL 8mM EDC for 30min. During this step, the mixture was kept shaking. Then it was centrifuged at 13200rpm for 15min, and the supernatant was discarded while the deposits were resuspended in 1.0mL 0.01 PBS (PH=7.4). Since the treated GO was not so soluble in PBS solution, sonication was performed for 3min to recover the homogeneous dispersion. Then 10μL of 1.3mg/mL *S.enteridis ompC* antibodies was added in quickly and incubated at room temperature with continuous shaking. After 1h incubation, the mixture was centrifuged at 13200rpm and resuspended for three times, in order to remove the extra unbound antibodies. Then the deposits were incubated in 1.0mL 0.01M (PH=7.4) PBS containing 1% BSA for 30min, and centrifuged and resuspended in 0.01M PBS (PH=7.4) for the last time and stored in 4°C refrigerator.

Characterization of this step was performed using Zeta potential method through Zetasizer nano ZS (Malvern instruments Corporation). Zeta potentials of 0.1mg/mL GO dissolved in 0.01M PBS (PH=7.4) and 0.1mg/mL obtained GO-antibody composites in 0.01M PBS (PH=7.4) were measured and the peak potential was used for the comparison.

For the second step, Hemin was incubated with obtained GO-antibody composites to achieve the GO/Hemin-Ab composites. Firstly, 1mg Hemin was dissolved in 1.0mL 0.01M PBS(PH=7.4). Since hemin is not so water-soluble, 10μL ammonia solution was added in for solubility enhancement. Then 1mL 1.0mg/mL GO-antibody composites were mixed together and shaken for 3.5h [127]. 13200rpm centrifugation was then performed for 15min to separate the unbound hemin molecules, and the deposits were suspended in 1mL 0.01M PBS (PH=7.4) and stored in 4°C refrigerator for later use. The adsorption of hemin onto GO surface was mainly caused by π-π stacking interaction, since both GO and hemin molecules contained abundant π bonds. The sketch is shown in Figure 2.2.2 [58].

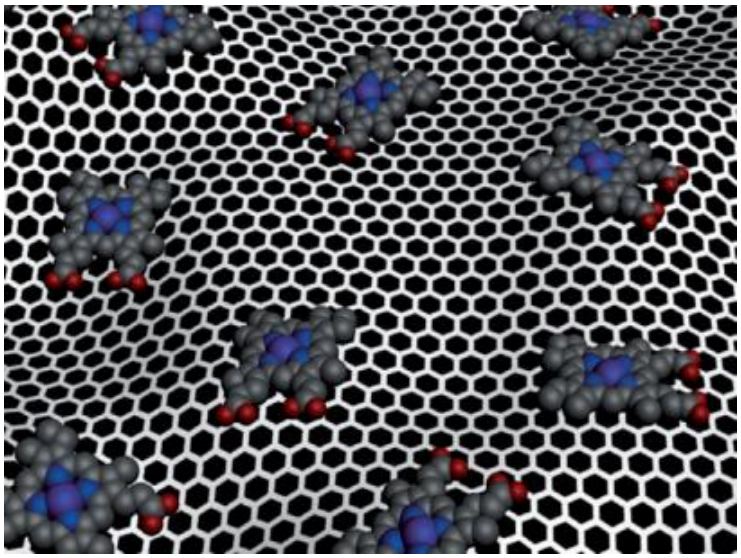

Figure 2.2.2 Formation of GO/Hemin conjugates through π-π stacking [58]

Characterization of this step was performed by measuring UV-Vis (200nm-800nm) absorbance through UltrospecTM 2100 pro UV-Visible spectrophotometer (GE Healthcare). Concentrations of GO/Ab composites and GO/Hemin-Ab composites were both 0.1mg/mL.

2.2.4 *Salmonella enteridis* captured on nanoporous alumina membrane

Firstly, the capturing of *S. enteridis* based on antibody-antigen binding was confirmed. Fluorescent microscopy and scanning electron microscopy were performed, respectively. After *S. enteridis ompC* antibodies were immobilized onto nanoporous alumina membrane, 150μL 10^5 CFU/mL *S. enteridis* were dropped on and incubated at room temperature for 1h. Then nanoporous alumina membrane was gently washed with PBS solution (PH=7.4), and then 50μL 0.1mg/mL FAM labelled

S. enteridis antibodies were dropped on and incubated for another 1h at room temperature, then the unbound antibodies were washed away by PBS solution (PH=7.4). In the control group, the different was that no *S. enteritidis* bacteria were added in. Fluorescent microscopy was imported to observe the fluorescent intensity and pictures were taken with a camera.

SEM was also performed for a more direct characterization. After 150μL 10^5 CFU/mL *S. enteridis* bacteria were captured by antibodies modified nanoporous alumina membrane, the membrane was rinsed, dried, and coated with a layer of gold by Bal-Tec SCD 005 Sputter Coater (Germany). Then the sample was observed by SEM in micro and nano scales. Electrochemical impedance spectrum (EIS) was used for further optimization of the capturing time. Since this microfluidics device enabled real-time detection of bacteria capturing, EIS sweeps from 10kHz to 1Hz were taken every 20min after *S. enteridis* bacteria were added in. Four different concentrations of target *S. enteridis* bacteria were chosen: 10^3, 10^4, 10^5, 10^6CFU/mL.

2.2.5 Formation of a sandwich structure and precipitation catalysis

After target *S. enteridis* bacteria were captured on the nanoporous membrane, a formation of the sandwich structure was followed by incubating GO/Hemin-Ab composites with captured bacteria together. A wash step was repeated for three times using PBS (PH=7.4) to ensure minimum unspecific bacteria were attached. Then a

150μL droplet of 0.1mg/mL obtained GO/Hemin-Ab composites solution were added on, and incubated with nanoporous alumina membrane at room temperature. After 40min incubation, the extra unreacted composites were washed away with PBS, and 450μL precipitation kits (1mM 4-CN, 0.15mM H_2O_2) were dropped on and under alumina nanoporous alumina membrane, and EIS measurement was taken then. After reaction for 15min, then EIS measurement was taken again.

EIS and SEM were imported for the characterization of this procedure. A 10^6 CFU/mL concentration of target *S. enteridis* bacteria were chosen and frequencies for EIS sweep were from 1Hz to 10kHz. SEM figures were also taken to directly observe the catalyzed precipitation covering nanopores on nanoporous alumina membrane. The whole sensing mechanism is shown in Figure 2.2.3.

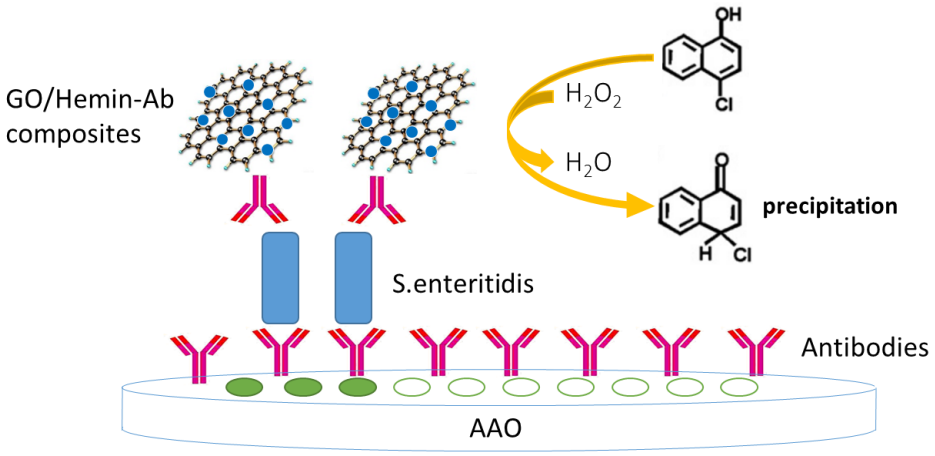

Figure 2.2.3 Sensing mechanism of *S. enteridis* bacteria detection

2.2.6 Electrochemical impedance spectroscopy for target *Salmonella enteridis* bacteria detection

Firstly, electrochemical impedance spectrum (EIS) was measured after each assembling step. To investigate the sensitivity of this sensing platform, concentration from 10^1 to 10^6 CFU/mL of target *S. enteridis* bacteria in a volume of 150μL were experimented, and the concentration of GO/Hemin-Ab composites was 0.1mg/mL and the volume was 150μL. The volume of precipitation kits (1mM 4-CN, 0.15mM H_2O_2 in 0.01M PBS) was totally 450μL and the precipitation time was 15min. EIS measurements were taken from 1Hz to 10kHz with an alternating voltage of 10mV. Impedance value at 50 Hz sweep was chosen for Normalized impedance change (NIC) calculation. At last, the linear detection range and limit of detection (LOD) was calculated using statistical methods.

For the specificity studies, *E. coli O157:H7* bacteria were imported. All experiments for specificity study were conducted with the same conditions of origin target *Salmonella enteridis* bacteria detection. NIC at 50Hz was also used for the evaluation of impedance increase at 10^1, 10^2, 10^3, 10^4, 10^5 and 10^6 CFU/mL in 0.01M PBS (PH=7.4).

Chapter 3 Results

3.1 Nanoporous alumina membrane based electrochemical biosensor with PtNPs tags for *E. coli O157:H7 gene* detection

3.1.1 Surface modification of nanoporous alumina membrane

Nanoporous alumina membrane surfaces are firstly modified with GPMS silane with epoxy groups for further DNA probes immobilization. As the first step of the whole platform construction, surface modification with GPMS silane through silanization process should be stable and strong enough for further attachment. Different from other silanization approaches on a glass slide with silanes such as APTES, the silanization reaction on nanoporous alumina membrane surface with GPMS silane needs a longer time because of the high surface to volume ratio of nanoporous alumina membrane as well as the relatively slow reaction rate of GPMS. Therefore, the characterization is highly needed to confirm an efficient and valid GPMS modification. Alumina oxide is intrinsically hydrophilic due to its metal oxide property. On the contrary, GPMS silane with epoxy groups makes it very hydrophobic. Hence, methods which are able to detect the surface wettability will be feasible to monitor this process by monitoring the surface wettability change.

A Ramé-Hart goniometer (NJ, USA) was used to measure the water contract angle of nanoporous alumina membrane before and after GPMS silane modification. As shown in representative photographs of **Figure 3.1.1**, a 10 μL volume of DI water

droplet quickly spread out on an untreated nanoporous alumina membrane with a low contact angle. However, the same volume of DI water on a GPMS modified nanoporous alumina membrane could hardly spread, leading to an obviously large water contact angle.

(a) **(b)**

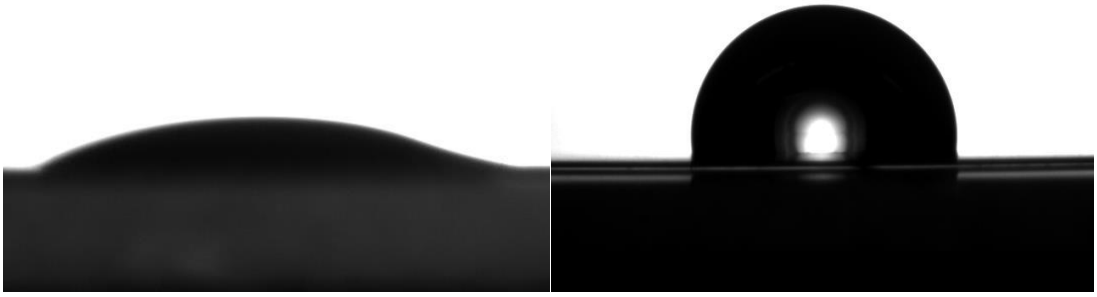

Figure 3.1.1 Change of nanoporous alumina membrane surface's water contact angle before (a) and after GPMS modification (b).

A histogram for the comparison of water contact angle before and after GPMS silanization is shown in **Figure 3.1.2**. Before surface silanization of GPMS, the water contact angle was averagely 15.4°, showing that the surface was quite hydrophilic. After the silanization, water contact angle became 114.5°, indicating the surface changed to hydrophobic. EIS was also taken as another characterization method, but the caused change can hardly be distinguished, which demonstrated that the silanization process did not obviously alter the impedance of the nanoporous membrane.

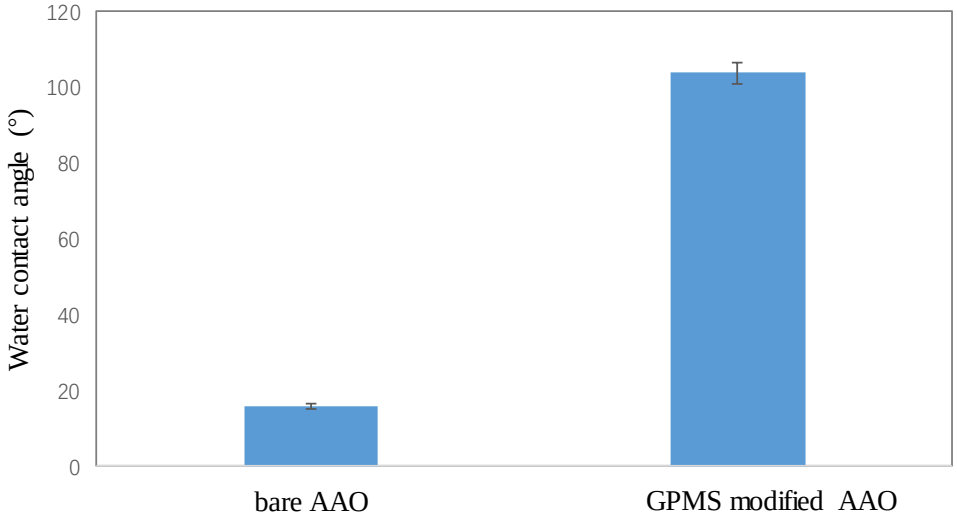

Figure 3.1.2 Average water contact angle before and after surface silanization.

3.1.2 Oligonucleotide probes immobilization on nanoporous alumina membrane

After silanization process with GPMS, amino group modified oligonucleotide probes was added to react with epoxy groups of attached GPMS on the nanoporous membrane. Fluorescence labelling method was used to confirm this immobilization. The confirmation of probes immobilization is critical to ensure the specificity of a DNA biosensor. These oligonucleotide probes were modified with amino groups at one end, and modified with FAM fluorescent dye at the other end. The concentrations of FAM labelled oligonucleotide probes were from 0.5 μM to 2 μM. After incubation with GPMS modified nanoporous alumina membrane for 10 h, fluorescence images were taken with a fluorescence microscope after washing with PBS buffer. The

fluorescence images were taken with the same exposure time and same excitation power. Oligonucleotide probes without FAM labelling were used as control groups, and the results were shown in **Figure 3.1.3 a, b, c and d**, respectively.

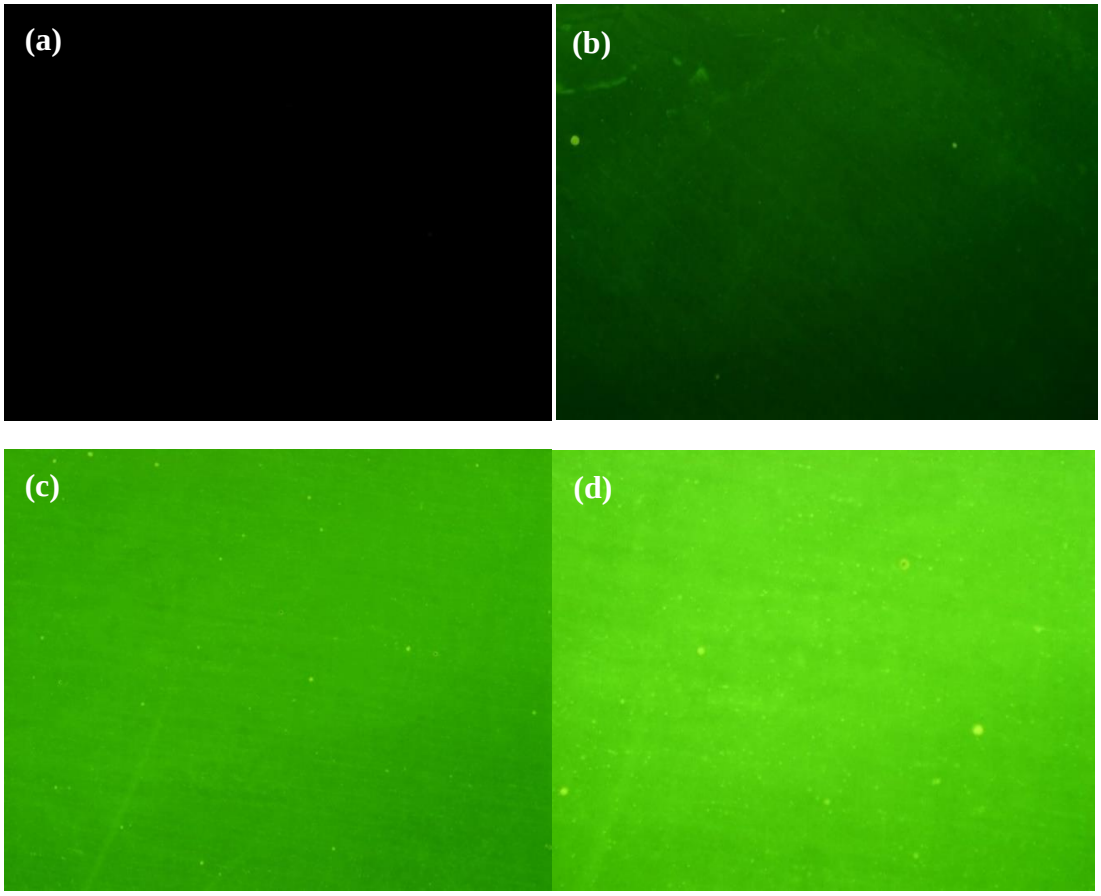

Figure 3.1.3 Fluorescent images of oligonucleotide probes immobilized on GPMS modified nanoporous alumina membrane with (a) control group at a concentration of 2 μM; FAM modified oligonucleotide probes at concentrations of (b) 0.5 μM, (c) 1 μM and (d) 2 μM, respectively.

As shown in **Figure 3.1.3**, it is obviously observed that FAM labelled oligonucleotide probes successfully immobilized, while the control group showed no obvious green signal. With the increase of the concentration of oligonucleotide probes, fluorescence intensity was enhanced significantly, which indicated more

oligonucleotide probes were immobilized on GPMS modified nanoporous membrane. Using imageJ software, the fluorescent intensities were calculated to be 0, 24.2, 72.3, 104.3, respectively. The covalent binding approach provides reliable and stable immobilization of oligonucleotide probes compared with physical adsorption approach.

3.1.3 PtNP-oligonucleotide probes conjugation

Bare platinum nanoparticles (PtNPs) were firstly synthesized from chloroplatinic acid (H_2PtCl_6) in the presence of sodium citrate and $NaBH_4$ as the reducing agents. The detailed synthesis process is introduced in the Methodology part. **Figure 3.1.4** shows the TEM images of synthesized PtNPs. As shown in **Figure 3.1.4a**, PtNPs were well monodispersed in water with an average size of 5±1 nm, which matched the results in the reference [124]. The PtNPs size is quite uniform with a narrow distribution range. The deviation of size may be due to the change of temperature or concentration of reagents during the process. **Figure 3.1.4a** shows an enlarged high resolution TEM (HRTEM) image of synthesized PtNPs. The synthesized PtNPs showed well rounded geometry.

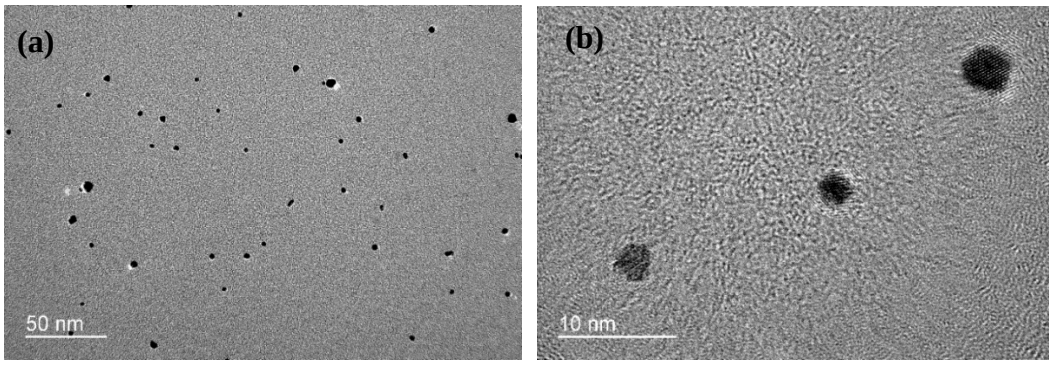

Figure 3.1.4 (a) TEM image of PtNPs dispersed in DI water with a scale bar of 50 nm; (b)TEM image of PtNPs dispersed in DI water with a scale bar of 10 nm

Then, the reporter probes modified with thiol groups were conjugated with PtNPs as the amplification tags. Zeta potential measurement was performed before and after PtNPs conjugation with the reporter probes. Zeta potential measurement was based on the surface electrical charge of nanoparticles. Nanoparticles with various surface groups will show various isoelectric points, resulting in a different surface charge in certain solution. As shown in **Figure 3.1.5**, the zeta potentials of bare PtNPs was around -37.7mV. After conjugation with oligonucleotide probes, the zeta potential of PtNPs shifted to -49.1mV due to negative charges carried by oligonucleotide probes. It was clear that a small shift of zeta potential value from bare PtNPs to PtNPs-oligonucleotide composites existed, which demonstrated the successful conjugation.

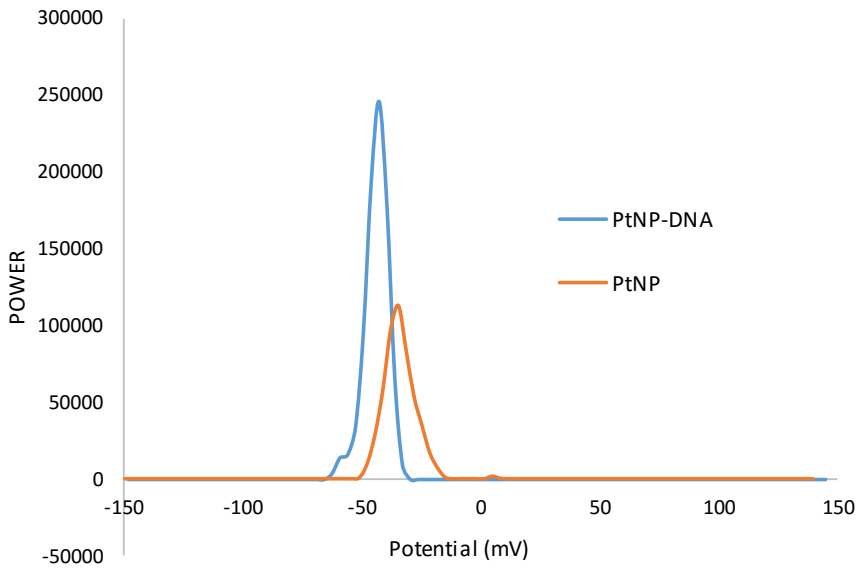

Figure 3.1.5 Zeta potential of bare PtNPs and PtNP-oligonucleotide probes in DI water.

3.1.4 Target *E. coli O157:H7 gene* captured by probes on nanoporous alumina membrane

Fluorescence labelling method was used with fluorescently labelled target genes for a direct characterization. EIS measurement for this step will be discussed in Section 3.1.5. A 150 μL volume of FAM labelled target *E. coli O157:H7* genes with a concentration of 1μM was dropped onto nanoporous alumina membrane. The same volume of FAM labelled non-target oligo with a concentration of 1 μM was used as a control. After a 4h DNA hybridization between capture probes and target genes or non-target oligos, fluorescence images were taken after PBS washing. As shown in **Figure 3.1.6b**, bright green emission indicated the successful FAM labelled target genes hybridization. By contrast, there were no obvious fluorescence signals for FAM

labelled non-target oligos, which demonstrated the specificity of the biosensor platform (**Figure 3.1.6a)**.

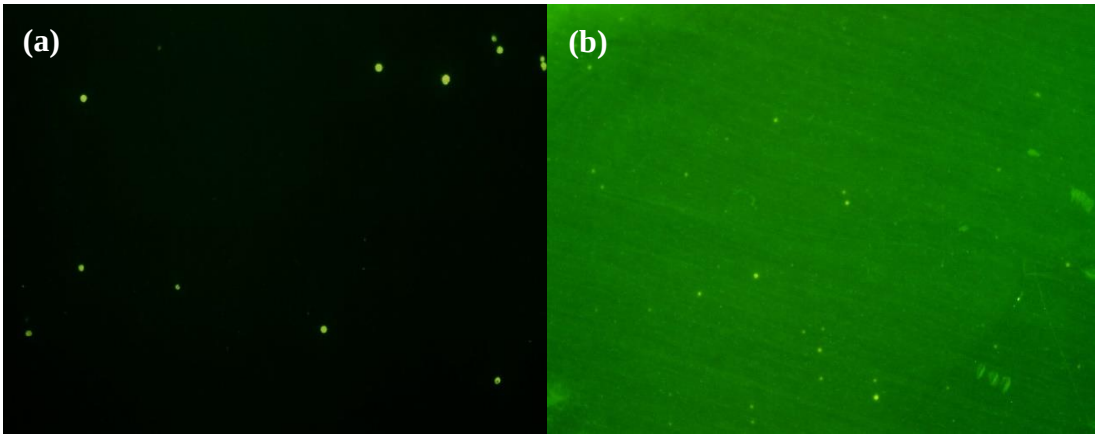

Figure 3.1.6 Fluorescence images of (a) FAM labelled non-target oligos captured by bio-functionalized nanoporous alumina membrane; (b) FAM labelled non-target oligoes. Both of them adopted a concentration of 1μM.

Capturing target *E. coli O157:H7* genes is an important step for the success of the whole biosensing platform. To get the optimal incubation time to ensure a high binding efficiency of target genes, the effect of incubation time on the fluorescence signals (which is correlated to the captured target oligos) was explored. Here, FAM labelled target *E. coli O157:H7* genes with a concentration of 1μM were used to hybridize with oligonucleotide probes on nanoporous membranes for different durations, and the comparison of their fluorescence intensity gave an assessment. As shown in **Figure 3.1.7**, the brightness increased as the reaction time extended. After 4h, the signal intensity did not increase any more, which meant that 4h was a roughly optimal time for incubation.

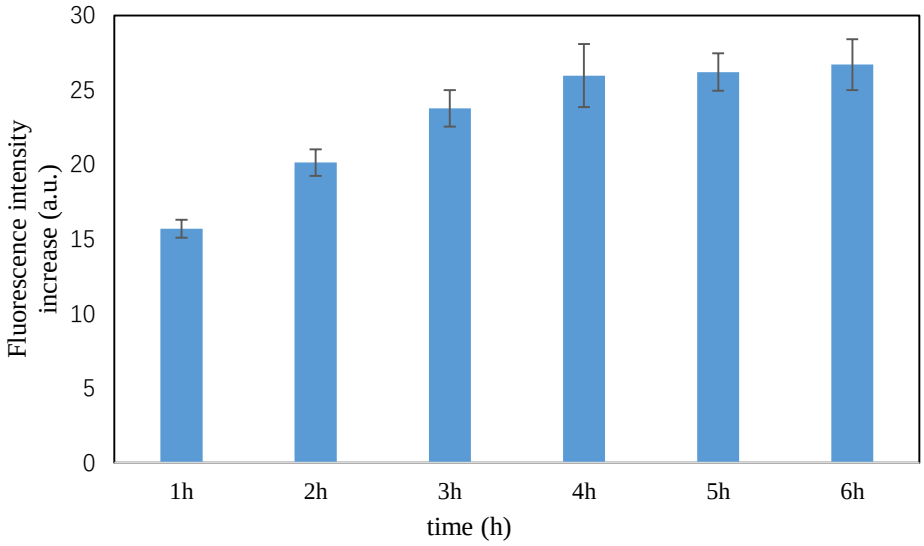

Figure 3.1.7 Fluorescence intensity change for 1h, 2h, 3h, 4h, 5h and 6h incubation with FAM labelled target oligos.

3.1.5 Target *E. coli O157:H7* gene detection with PtNPs based precipitation via EIS

3.1.5.1 Feasibility testing for the fabricated nanoporous membrane sensor

A sandwich structure with capture probe-target-reporter probe/PtNPs was formed in this procedure. Precipitation of 4-chloro-1-naphthol (4-CN) by conjugated PtNPs on nanoporous alumina membrane was then followed to amplify the signals by increasing the blocking degree of nanoporous membrane. **Figure 3.1.8** shows the SEM images before and after precipitation of insoluble 4-chloro-1-naphthol based on PtNPs catalysis. Compared with bare nanoporous alumina membrane, apparent precipitation

covered on the surface of the membrane was observed which could block the nanopores, leading to impedance signal amplification. SEM images are direct evidence to demonstrate the amplified blocking effect by PtNPs based precipitation of 4-CN.

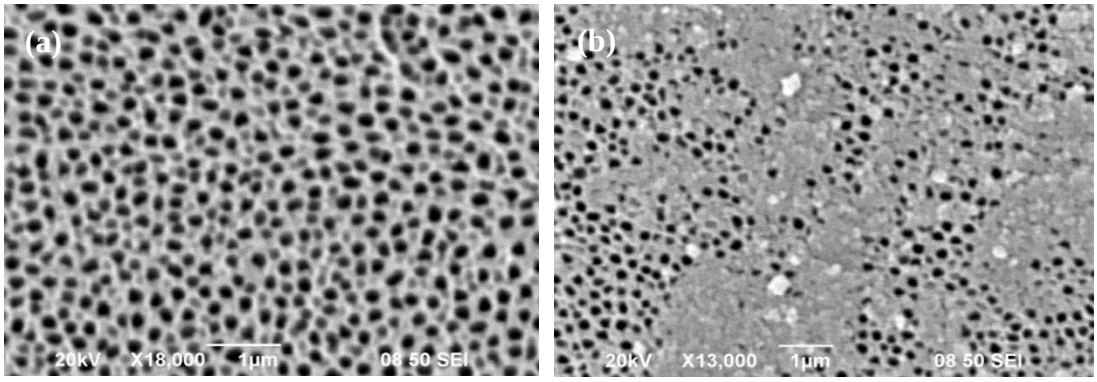

Figure 3.1.8 SEM characterizations before and after the PtNPs catalyzed precipitation of nanoporous alumina membrane surface

Electrochemical impedance spectroscopy (EIS) was then employed for target genes detection with PtNPs based precipitation for signal amplification. The impedance spectra of the nanoporous membrane with capture probes, immobilization with target oligos, conjugation with PtNPs labelled reporter probes and after PtNPs based precipitation are shown in **Figure 3.1.9**. The concentration of target DNAs was 1μM while the concentration of probe DNAs modified PtNPs was about 500 nM. It was observed that the impedance amplitude increased after target oligo immobilization and PtNPs labelled reporter probes conjugation. However, the impedance amplitude did not increase much due to the small size of target oligo and PtNPs (around 4 nm).

After PtNPs based precipitation, an obvious impedance amplitude increase was observed especially at low-frequency range, indicating the signal amplification effect of PtNPs based precipitation. After the PtNPs had catalyzed precipitation of insoluble 4-CN for 15min, the impedance of whole nanoporous alumina membrane increased significantly. The largest difference happens at 80 Hz EIS sweep. Since the purpose of precipitation procedure was to amplify the signals, impedance could be significantly enhanced and showed a direct correlation with the captured target gene.

The impedance amplitude changes were totally different under sweeps of various frequencies. Typically, the high-frequency part (100-10kHz), middle-frequency part (10-100Hz) and low-frequency part (1-10Hz) were dominated by different factors in the whole circuits. In the low-frequency region below 10 Hz, the impedance was mainly dominated by the two electrode surface. On the other side of the high-frequency region, the resistance of solution was the main cause to block the electron flowing. In the region various from 10Hz and 1kHz, nanoporous alumina membrane played the most important role in impedance domination. Hence, the impedance in this region was mainly concerned, and NIC was investigated as well.

Since the PtNPs based precipitation is critical for the enhancement of sensitivity, the precipitation time for induced precipitation needs to be investigated. For the exploration of appropriate reaction time, concentrations of target genes and PtNPs conjugated reporter probes remained unchanged. Impedance signals for precipitation at time 0 min, 5 min, 10 min, 15 min, 20 min and 25 min were measured and recorded

at 80 Hz, as shown in **Figure 3.1.10**. Results presented that impedance amplitude increased rapidly in the first 5 min, and then gradually increased to a plateau around 15 min. After 15 min, the impedance signal did not further increase, indicating that 15 min should be an appropriate time for efficient precipitation.

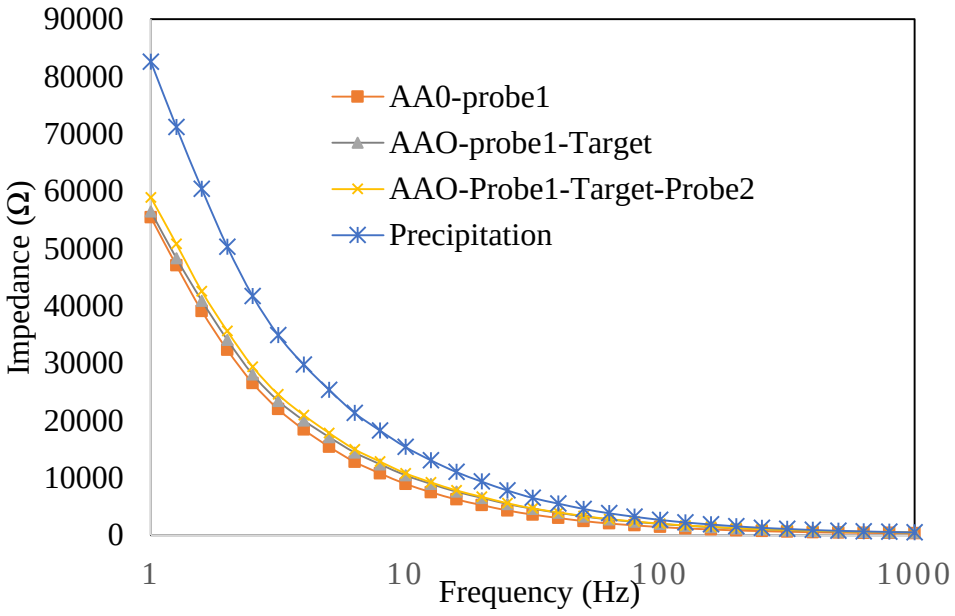

Figure 3.1.9 Electrochemical impedance spectra of oligonucleotide probes immobilization, target *E. coli O157:H7 genes* capturing, second PtNP-oligonucleotide immobilization and precipitation generated by PtNPs catalysis.

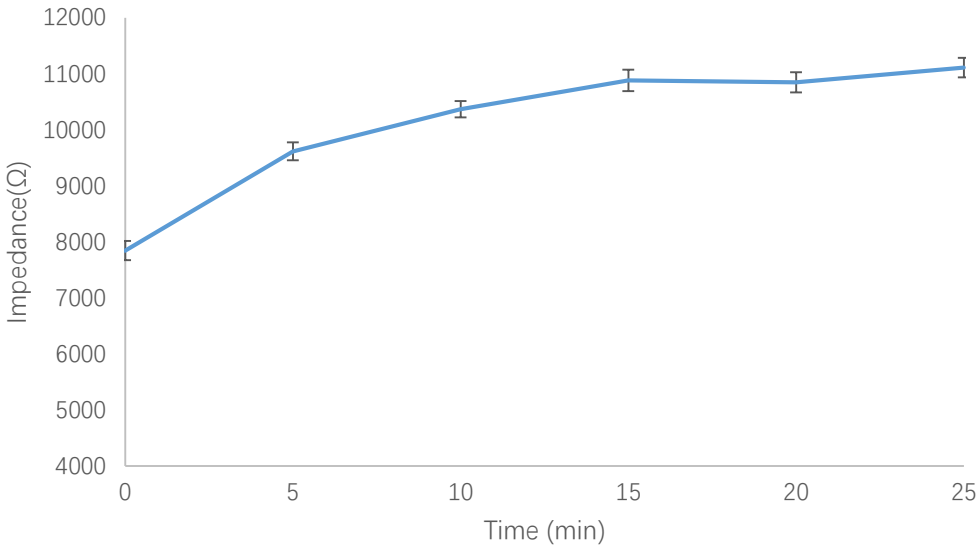

Figure 3.1.10 Time domains of impedance amplitude increase induced by PtNPs catalyzed 4-CN precipitation.

Then the fabricated nanoporous membrane sensor was used for *E. coli O157:H7* gene detection. Each step of characterization and optimization is to ensure the experiments were carried out in accordance with what we expected, as well as to shorten the fabrication time as much as possible with the unreduced sensitivity and specificity. After the design had been confirmed to be feasible, repetitive experiments were operated, intending to reach a high sensitivity with good specificity. The sensitivity was obtained from EIS data at 80 Hz scan, and the selectivity was guaranteed by testing other non-specific and 6 bases mismatched oligonucleotides.

3.1.5.2 Impedance measurement for different concentrations of *E. coli O157:H7* gene

Then, this nanoporous membrane based biosensor was used for different concentrations of *E. coli O157:H7* gene detection. As shown in **Figure 3.1.11**, impedance signals increased with the increased concentrations of target genes, especially in the low-frequency region. This was because oligonucleotides together with PtNPs based precipitation hindered the ion current flowing through the nanoporous membrane in the low-frequency domain. However, when the frequency was changed to a higher range, current could pass because of the polarization effect which enabled the oligonucleotides and precipitation “wall” vanished. This process was much likely to that of a capacitor in the circuit. Hence, the impedance value in the low-frequency region at 80 Hz was selected as the representative in impedance spectrum monitoring.

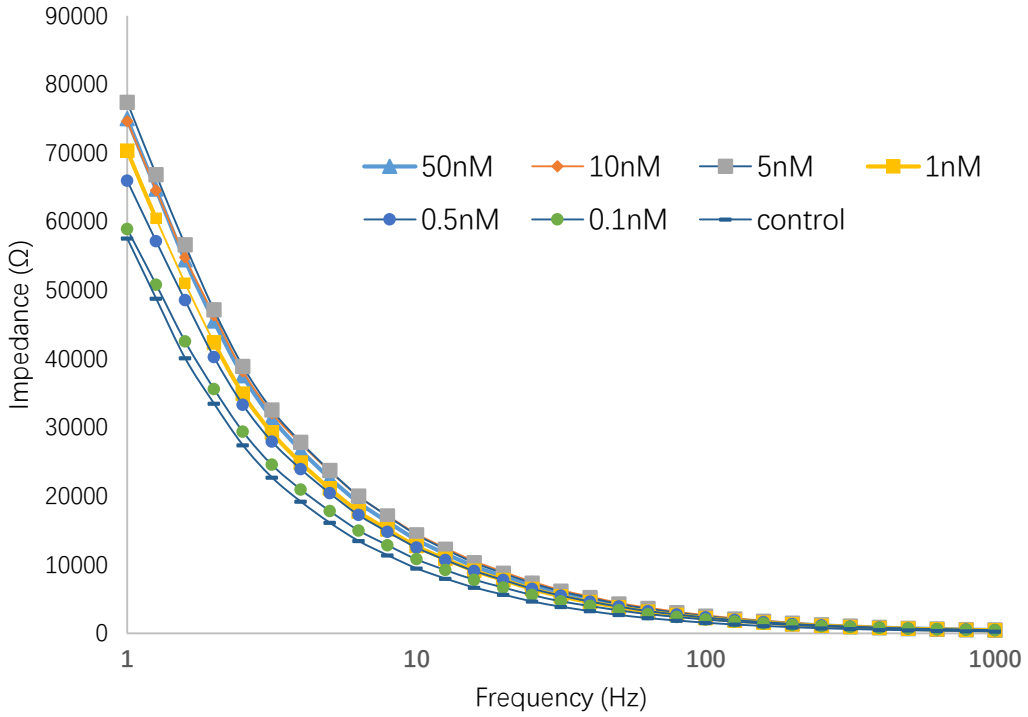

Figure 3.1.9 Impedance spectra of nanoporous membrane based biosensor for various concentrations of target genes.

As more and more target oligonucleotides were captured with conjugation with PtNPs labelled reporter probes and the followed catalyzed precipitation onto nanoporous alumina membrane surface, the generated impedance signals increased, especially under low-frequency sweeps. To avoid the variation for each nanoporous membrane based sensor, the normalized impedance change (NIC) was used to minimize the deviation in different experiments. The NIC is expressed by the following equation:

$$NIC = \frac{Z_{experiment} - Z_{control}}{Z_{control}} \times 100\%$$

Herein, the impedance signal without target genes and related precipitation was chosen as $Z_{control}$. The impedance signal after the precipitation process for various concentration of target genes was chosen as $Z_{experiment}$.

Figure 3.1.12 shows the NIC based impedance spectra for a series of target concentrations from 100 pM to 50 nM. Impedance spectrum of 0.1 nM, 0.5 nM, 1 nM, 5 nM, 10 nM and 50 nM after the precipitation are chosen to calculate the NIC signal. It was clearly observed that the change of blocking degree of nanoporous alumina membrane mainly influenced the EIS performance at low to medium frequency, leading to the relative impedance change mainly in the range 1 Hz to 1 kHz.

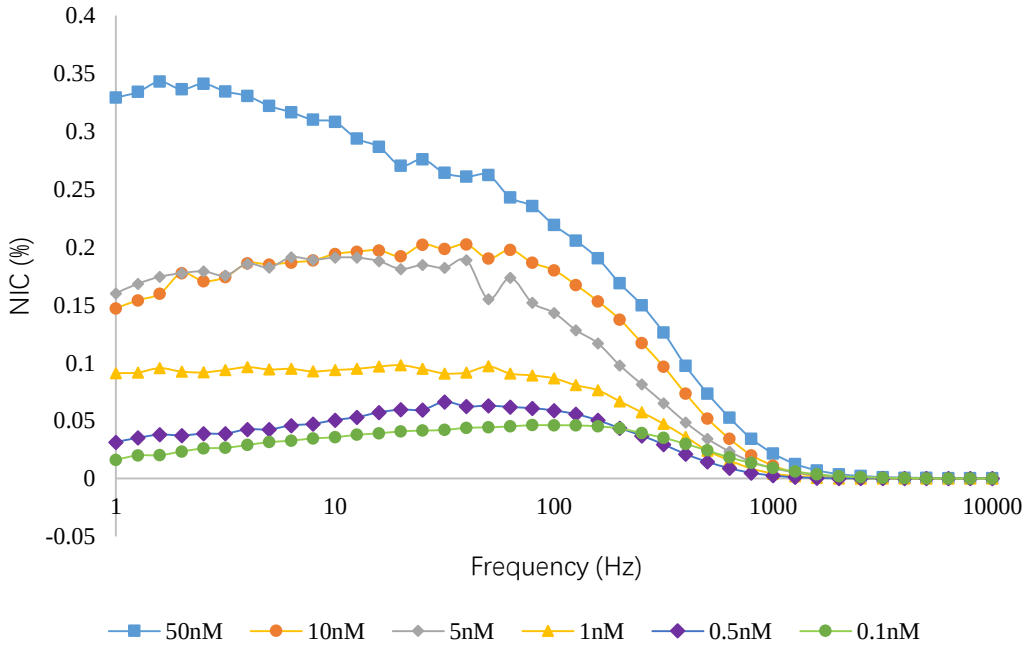

Figure 3.1.10 Normalized impedance change (NIC) from 1Hz to 10kHz with different concentrations of target *E. coli O157:H7 genes.*

As shown in **Figure 3.1.12**, the impedance amplitude reached the highest between 10 Hz and 100 Hz. According to the NIC-Frequency relational graph, for most cases, the maximum of NIC was between 30 Hz and 80 Hz and reached the maximum around 50 Hz except for 50 nM. Therefore, the frequency of 50 Hz was chosen as a characteristic frequency for the following impedance signal analysis with different concentration of target *E. coli O157:H7* genes.

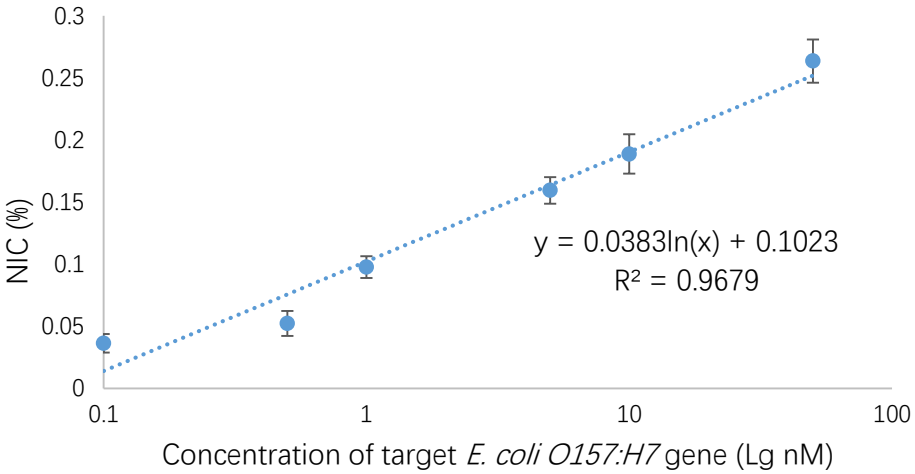

Figure 3.1.11 Normalized impedance change (NIC) at 50 Hz with different target *E. coli O157:H7 gene* concentrations.

As shown in **Fig 3.1.13**, the NIC at 50 Hz for *E. coli O157:H7* gene with concentrations of 0.1 nM was about 3.65 %. Then it increased to 5.25% for concentration of 0.5nM and 9.77% for concentration of 1nM. At a concentration of 5 nM, the NIC increased to around 15.95% and 18.89% for a concentration of 10 nM. When the concentration was 50 nM, the NIC was about 26.36%. The regression equation for NIC versus target *E. coli O157:H7 gene* concentrations from 0.1nM to

50nM is y = 0.0383ln(x) + 0.1023 with R^2 = 0.9707. The limit of detection is calculated to be 93.8 pM.

3.1.5.3 Impedance measurement for specificity testing

Specificity of this platform was also tested with non-specific oligonucleotides and 6 bases mismatched oligonucleotides. As shown in F**igure 3.1.14**, for the non-specific oligonucleotides groups, this platform exhibited a good selectivity for all the concentrations. The NIC of 50 nM non-specific oligonucleotides was 1.8%, which was even much lower than that of 0.1 nM target *E. coli O157:H7* gene. For the 6 bases mismatched oligonucleotides, the NIC signal was also much lower than that of target genes for all the concentrations. The NIC at 50 nM was about 4.6% which was only comparable to the NIC of target genes at 0.1nM. When the concentration was reduced to 10 nM, the NIC was as low as 2.38%.

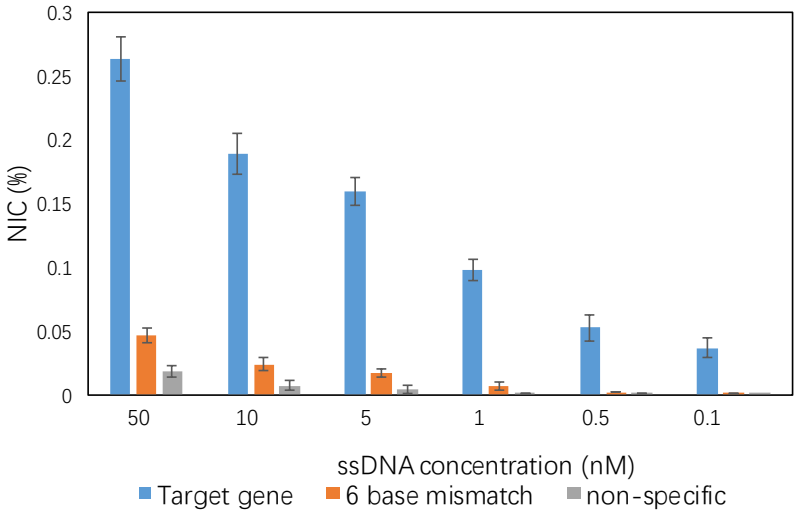

Figure 3.1.12 Impedance amplitude NIC for target gene, 6 base mismatch DNA and non-specific DNA

3.2 Nanoporous alumina membrane based electrochemical biosensor with graphene/hemin-antibody tags amplification for *Salmonella enteritidis* detection

3.2.1 Antibody immobilization on nanoporous alumina membrane

Immobilization of antibodies onto nanoporous alumina membrane is the first step in whole sensor fabrication. The procedure in this step was similar to that in the first project which immobilized oligonucleotide probes onto membrane surface. That conjugation of oligonucleotide probes was based on silanization reaction between amino groups on oligonucleotides and epoxy groups on GPMS. In this project, antibodies inherently contained amino groups, which were able to react with GPMS silane molecules directly. The conjugation of antibodies contained two steps: surface silanization of alumina oxide membrane and reaction between GPMS and antibodies. Characterization of surface silanization was also performed by measuring the water contact angles before and after surface silanization as shown in **Figure 3.1.1**, as well.

After the silanization of GPMS, a solution with 100 nM anti-salmonella antibodies was quickly dropped onto membrane surface and reacted at 4°C overnight. To validate the immobilization of antibodies onto membrane surface, fluorescence labelled antibodies were chosen for the characterization. FAM-modified anti-salmonella antibodies with concentrations of 50 nM, 100 nM, and 200 nM were used to react with nanoporous membranes overnight, respectively. Nanoporous membrane

without FAM labelled antibodies was chosen as a control group. The results are shown in **Figure 3.2.1**.

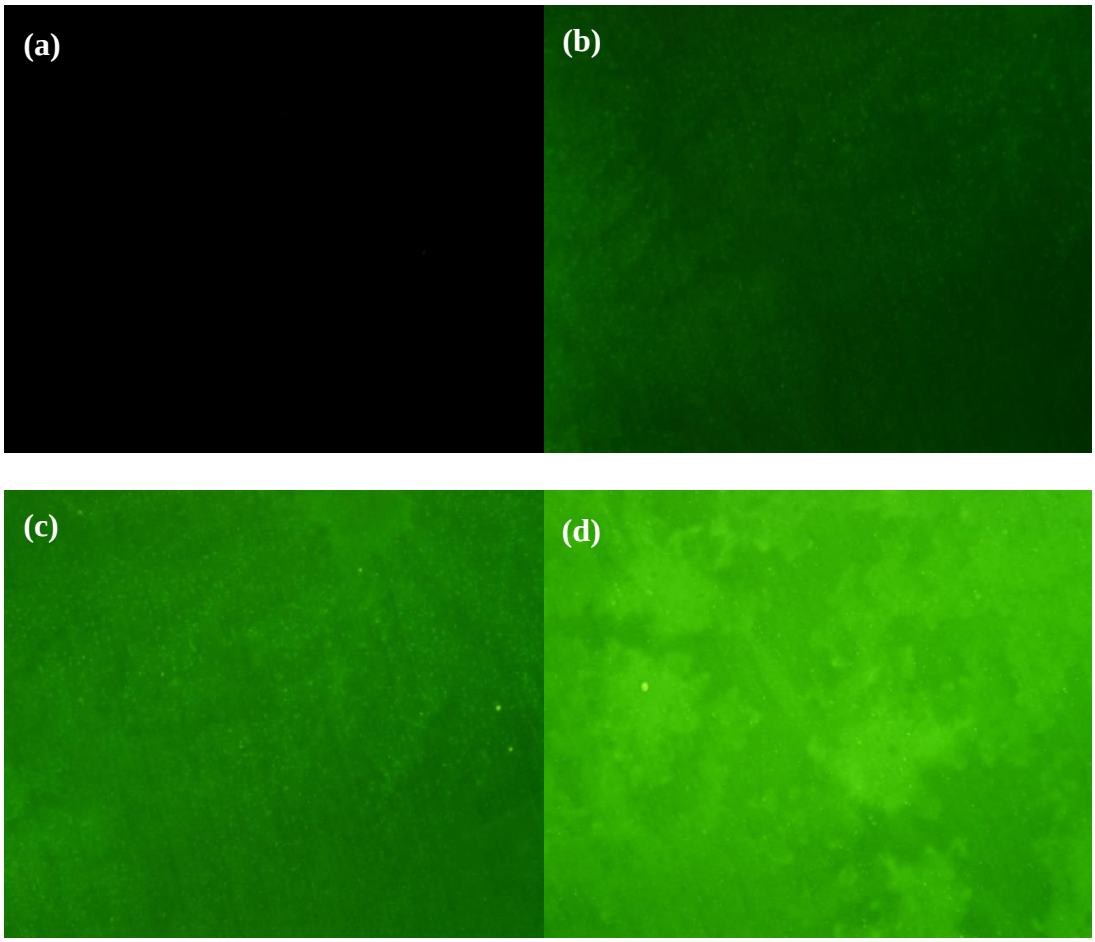

Figure 3.2.1 Fluorescent images of FAM-modified salmonella antibodies immobilized on GPMS modified alumina oxide membrane. The concentrations of FAM-modified antibodies were (a) 0 nM, (b) 50 nM, (c) 100 nM, (d) 200 nM, respectively.

Before observation through fluorescent microscopy, nanoporous alumina membrane was well washed with PBS solution, to wash away the unbounded antibodies. Using imageJ software, the fluorescent intensities were calculated to be 0, 23.1, 45.9, 76.0, respectively. As the concentration of antibodies increased, the fluorescence intensity became higher correlated to the original concentration of

antibodies, which demonstrated the antibodies were successfully attached onto the membrane. A concentration of 200 nM was chosen in the following experiments.

3.2.2 Synthesis of graphene-antibody/hemin composites

Synthesis of graphene-antibody/hemin composites is critical during the whole experiment process. The function of this composite is to act as amplification tags to attach onto captured salmonella bacteria to form a sandwich structure. Graphene/hemin hybrid nanosheets could be efficient catalysts for catalysis of insoluble 4-CN, leading to the impedance signal amplification on the nanoporous membrane. The formation of graphene/hemin-antibody composite ensured the specificity of this impedance signal amplification.

Graphene oxide (GO) nanosheets were firstly synthesized though Hummer's method. **Figure 3.2.2** shows the TEM image of GO nanosheets, where a single or a few layers of GO nanosheets were observed. The large 2D flat surface area makes GO a good platform for catalyst and biomolecule loading. GO was abundant of carboxyl groups (-COOH), which was facile to react with the amino groups ($-NH_2$) on antibodies. EDC and NHS were the reagents for carbodiimide chemical reactions which have been well developed. So, antibodies could be easily conjugated to GO surface. To characterize the antibodies immobilization on GO surface, zeta-potentials of GO were measured before and after antibodies immobilization. Since surface charges of anti-salmonella antibodies and GO might be different, zeta-potential could

be an indicator to demonstrate the immobilization. As shown in **Figure 3.2.3**, zeta potentials of GO and GO immobilized with antibody were different. Bare GO had a zeta potential at -49.9 mV in 0.01M PBS (pH=7.4) solution, while the zeta potential of GO-antibody composite was about -34.2 mV in the same solution. The difference of zeta-potential between GO and GO-antibody composites could be due to the lower surface charge density of antibodies compared with bare GO. When GO was covered with antibodies, the surface of GO-antibody composite became not so negative.

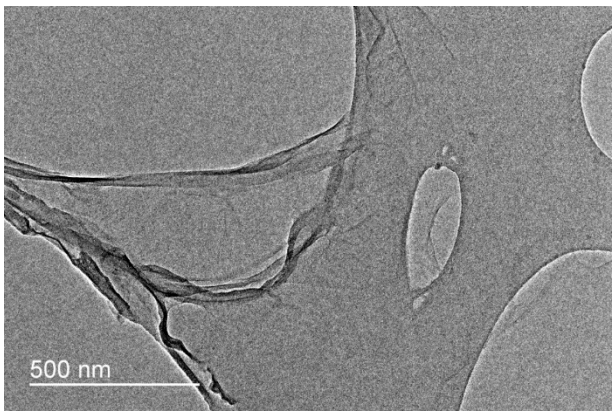

Figure 3.2.2 TEM image of graphene oxide synthesized by Hummer's method

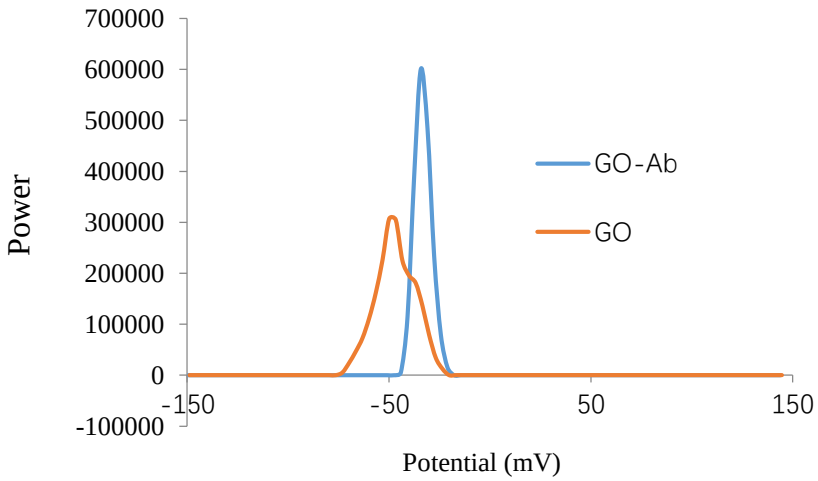

Figure 3.2.3 Zeta potential of GO and GO-antibody composites

After formation GO-antibody composite, hemin was then immobilized on GO surface via π-π stacking as well as electrostatic interaction. Firstly, hemin was dissolved in GO-antibody solution and reacted for 3 h. Then centrifugation was conducted to separate extra hemin from the synthesized GO-antibody/hemin composites because hemin was soluble micromolecule. The UV-Vis spectroscopy was used to characterize the formation process of GO-antibody/hemin composites. **Figure 3.2.4** shows the UV-Vis spectrum of GO, Hemin, and GO/Hemin-Ab. Hemin had its own absorption peak around 375 nm, while GO has an absorbance peak at 227 nm. Therefore, if hemin was attached onto GO surface, the original peak of GO was remained, while the spectrum at 400 nm was enhanced. A little shift was obtained from 375 nm to 400 nm due to the bathochromic shift (25 nm). Both zeta potential and UV-Vis spectrum methods proved the successful synthesis of GO-antibody/hemin composites.

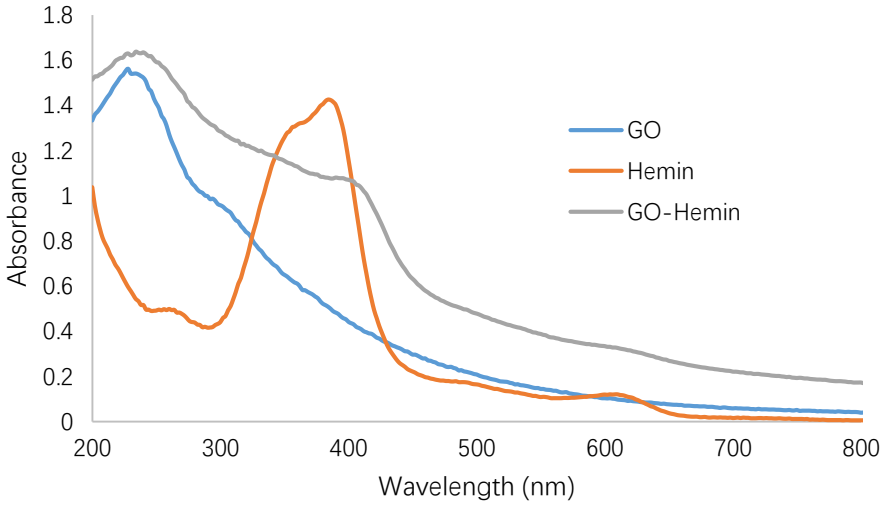

Figure 3.2.4 UV-Vis spectrum of GO, Hemin, and GO-antibody/hemin composites

3.2.3 *Salmonella enteritidis* captured on nanoporous alumina membrane

The functionalized nanoporous membrane sensor was then tested for *Salmonella enteritidis* bacteria capture. Fluorescence labelling sandwich method was used for monitor the bacteria capture process. Firstly, target bacteria solution was incubated was nanoporous alumina membrane for 1h. After the *S. enteritidis* bacteria had been captured on nanoporous alumina membrane, FAM labelled anti-salmonella antibody was dropped onto membrane surface to bind specifically with *S. enteritidis* bacteria to form a sandwich structure. Since one bacterium had plentiful binding sites for specific antibodies, the conjugation of FAM-modified antibodies could be facile and fast.

Figure 3.2.5 show the fluorescence images of functionalized nanoporous membrane with 0 CFU/mL and 10^5 CFU/mL Salmonella. As shown in **Figure 3.2.5a**, fluorescence could hardly be seen when no *S. enteritidis* bacteria were dropped onto nanoporous membrane after the careful washing off unbound bacteria and FAM-antibodies. However, when 150 μL solution with 10^5 CFU/mL Salmonella bacteria was added and followed by washing, many fluorescence dots were found which were related to the fluorescence labelled bacteria (**Figure 3.2.5b)**. The results demonstrated that 1) the anti-salmonella antibody was effective for *S. enteritidis* bacteria capture and labeling, and 2) FAM labelled antibodies could barely attach onto membrane surface through non-specific adsorption after careful rinsing and covalently bonded antibodies could firmly bind with the membrane surface.

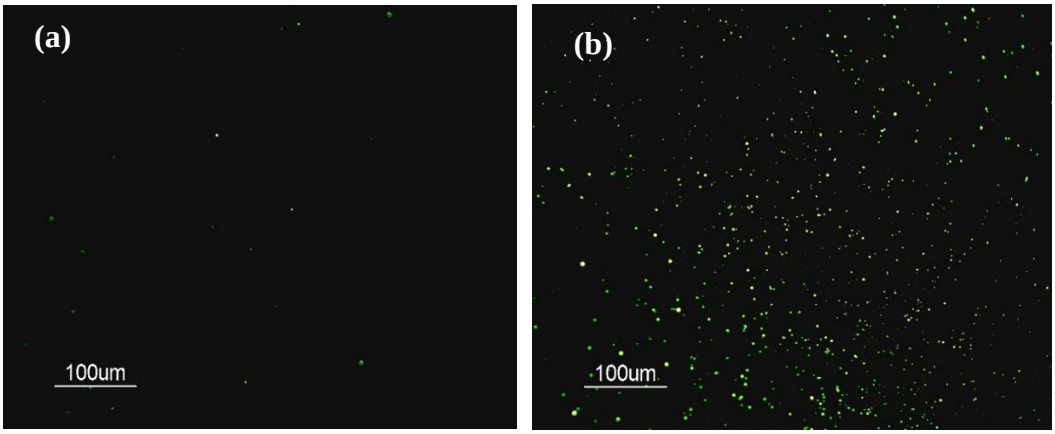

Figure 3.2.5 Fluorescent image of (a) no salmonella bacteria captured by nanoporous alumina membrane (b) 10^5 CFU/mL Salmonella bacteria captured by nanoporous alumina membrane.

SEM images were then taken as another visual confirmation for the bacteria capturing. SEM of nanoporous alumina membrane with no salmonella bacteria is shown in **Figure 3.2.6 (a)**, while SEM of the nanoporous membrane with captured salmonella bacteria is shown in **Figure 3.2.6 (b).** The size of nanopores on the membrane was selected around 200 nm in **Figure 3.2.6 (a)**. It was clearly observed that traditional rod-shape salmonella bacteria captured on the nanoporous membrane. Captured bacteria could be seen on nanoporous alumina membrane with kept morphology and the size around1-2 μm, which was consistent with the known morphology and size of *S. enteritidis* bacteria.

SEM photographs were also taken for GO-antibody/hemin based precipitation on the nanoporous membrane (**Figure 3.2.7**). It was clearly seen that after GO-antibody/hemin based precipitation, more areas of the nanoporous membrane was covered by deposited insoluble 4-CN by GO/hemin based catalysis. It was expected

that the impedance signal could be largely enhanced due to the increased blocking degree of nanoporous membrane.

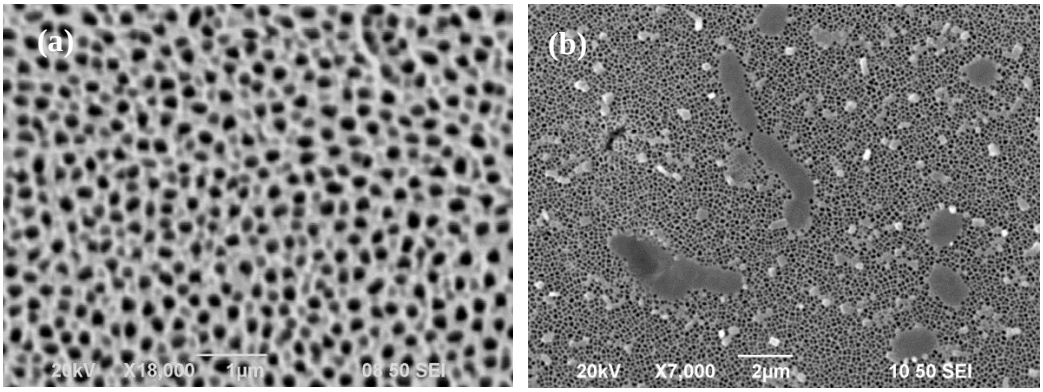

Figure 3.2.6 (a) SEM of bare nanoporous alumina membrane and (b) nanoporous alumina membrane with captured salmonella bacteria

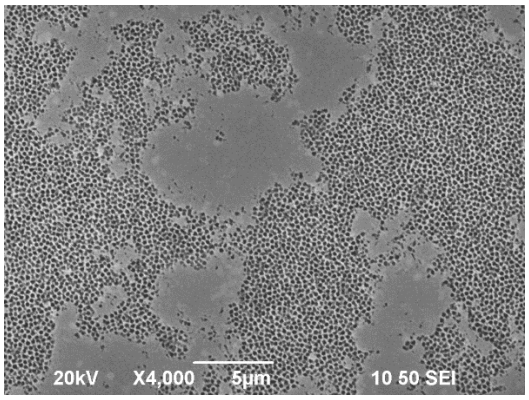

Figure 3.2.7 SEM characterizations after the GO/Hemin catalyzed precipitation of nanoporous alumina membrane surface

3.2.4 Impedance sensing for Salmonella bacteria

After verifying the feasibility of this design and optimizing committed steps during the whole procedure, impedance sensing for Salmonella bacteria using functionalized nanoporous membrane was performed via EIS spectroscopy. The

sensitivity, limit of detection, and specificity of this biosensor were explored. The specificity of this biosensor was tested with another type of bacteria *E. coli*.

3.2.4.1 Impedance spectrum monitoring for *Salmonella enteritidis* bacteria detection

Except for fluorescence, electronic microscopy, UV-Vis spectrum or surface charge strategies, impedance spectrum was also performed to monitor each step in whole *S. enteritidis* bacteria detection process. The concentration of *S. enteritidis* bacteria was 10^6 CFU/mL and 150 μL 0.1mg/mL GO-antibody/hemin composite solution was dropped onto nanoporous alumina membrane and reacted for 1h. After careful rinsing, EIS was taken after each step, and the increase is shown in the **Figure 3.2.8** (grey curve to yellow curve). **Figure 3.2.8** shows impedance spectra with scans from 1 Hz to 10 kHz were measured for bare AAO, AAO with immobilized antibodies; antibody functionalized AAO with bacteria capture, the formation of sandwich structure by conjugation with GO-antibody/hemin, and amplification after precipitation. It was observed that the impedance signal did not change much when antibodies were firstly immobilized on the membrane surface. Then, impedance kept increasing with target capturing, GO-antibody/hemin conjugation and precipitation because more and more substance covered on the nanoporous membrane surface. Especially, significant increases of impedance signal were observed after *S. enteritidis* bacteria capturing and precipitation catalysis.

The step of capturing salmonella bacteria obviously increased the impedance signal. Since the size of a salmonella bacterium was around 1-2 μm while the size of nanopores on alumina membrane was about 200 nm, the nanopores could be blocked by the covered bacteria on the top. The captured salmonella bacteria blocked the nanopores channels and hindered the electron movements and the increase of impedance was clear and convictive.

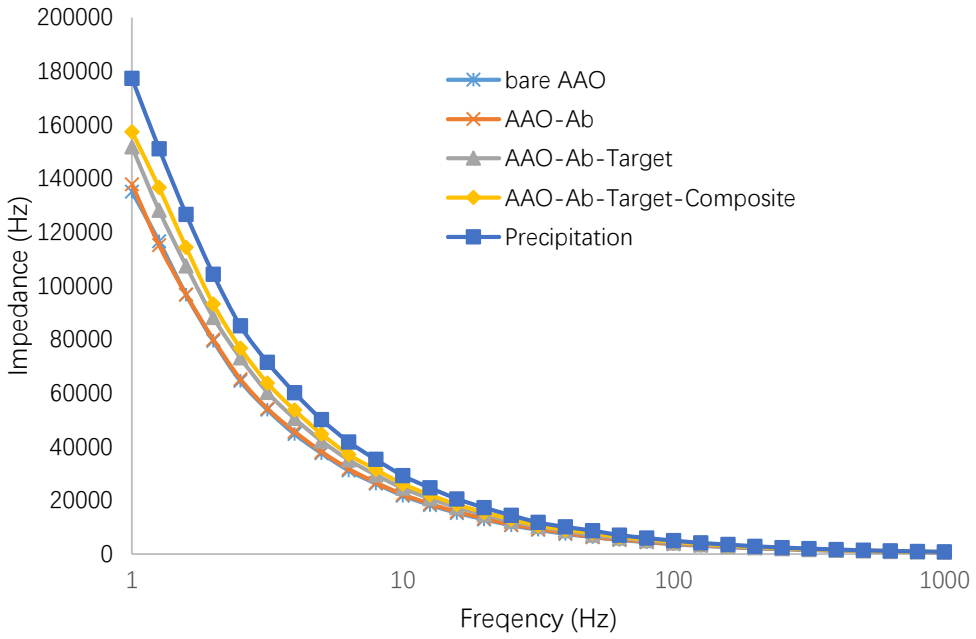

Figure 3.2.8 Original electrochemical impedance spectra of antibody modification, salmonella bacteria capturing, GO/Hemin-Ab composites, as well as precipitation catalysis generated by GO/Hemin composites.

For the step of conjugation of GO-antibody/hemin composite on bacteria, the impedance amplitude did not change too much. Compared to *S. enteritidis* bacteria, the size of GO-antibody/hemin composite is much smaller and not so capable of hindering the ion current flowing. In **Figure 3.2.8**, an obvious increase of impedance

still can be observed, although the amount is not as much as that in bacteria capturing procedure. After precipitation, a large impedance signal increase was observed due to more blocking areas of nanoporous membrane. The EIS results here demonstrated the GO-antibody/hemin composite based precipitation could largely increase the sensitivity for bacteria detection.

3.2.4.2 Impedance measurement of different concentrations of Salmonella bacteria

Impedance measurement for various concentrations of salmonella bacteria was then performed. **Figure 3.2.9** shows the impedance spectra for various concentrations from 10 to 10^6 CFU/mL. It was observed that impedance signals of nanoporous membranes increased with the increasing of bacteria concentrations, especially in low-frequency range. Back to the model circuit, the membrane part was represented by Rc and Cc in parallel, which was predominant under low-frequency sweeps because the bacteria and precipitation "wall" vanished. Therefore, the experimental data matched the theoretical data.

Normalized impedance change (NIC) was also employed for further analysis of precipitation effect and the appropriate frequency which exhibited largest NIC. **Figure 3.2.10** shows the calculated NIC from 10 to 10^6 CFU/mL. Similar to that in oligonucleotides platform which had the highest NIC at 50 Hz, the most obvious

change of NIC in this platform was around 50 Hz. Therefore, impedances obtained under 50 Hz sweeps were chosen for the calculation of the sensitivity for this sensing platform. As shown in **Figure 3.2.11**. NIC at 50 Hz for salmonella bacteria concentration of 10 CFU/mL was about 1.20%. Then it increases to 11.41% for concentration of 10^2 CFU/mL and 20.19% for concentration of 10^3 CFU/mL. At concentration of 10^4 CFU/mL, the NIC increases to around 27.96% and 33.84% for concentration of 10^5 CFU/mL. When the concentration is 10^6 CFU/mL, the NIC is about 37.45%. The regression equation for NIC versus salmonella bacteria concentrations from 10^1 CFU/mL to 10^6 CFU/mL was y = 0.0318ln(x) - 0.0362 with R^2 = 0.9751. The limit of detection was calculated to be 12 CFU/mL.

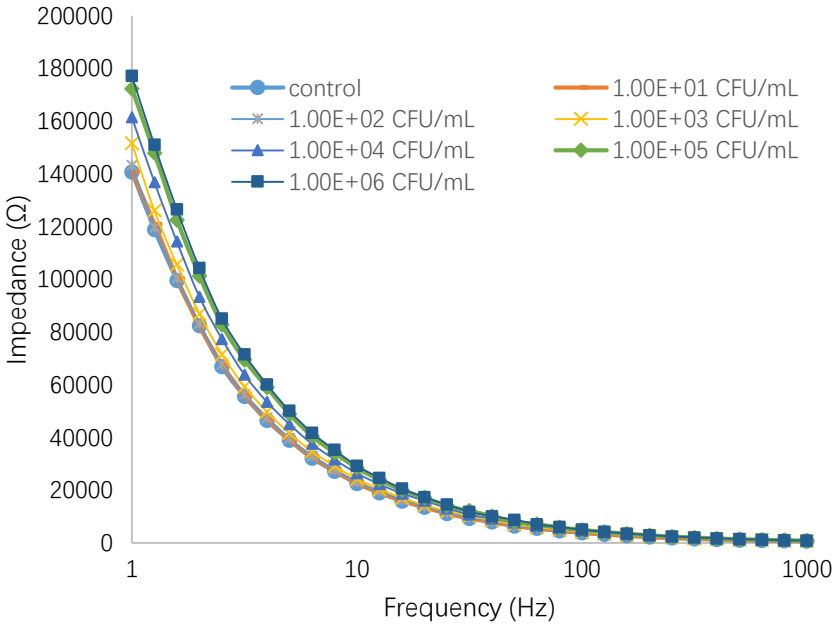

Figure 3.2.9 Impedance spectra with various target bacteria concentrations from 10 to 10^6 CFU/mL

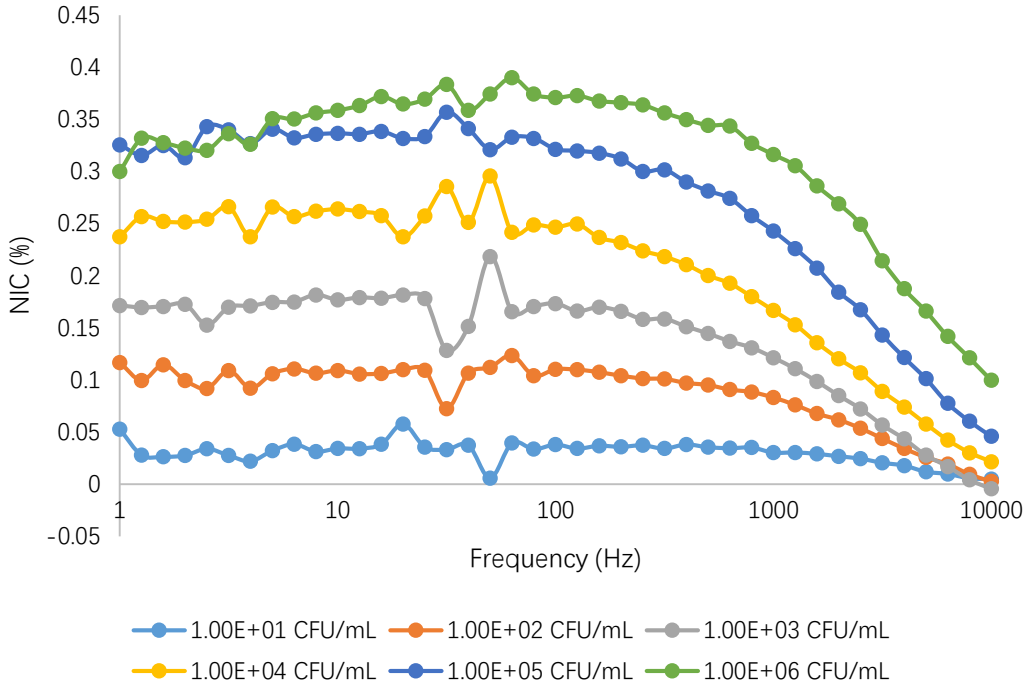

Figure 3.2.70 Normalized impedance change (NIC) from 1Hz to 10 kHz with different concentrations of target salmonella bacteria after precipitation.

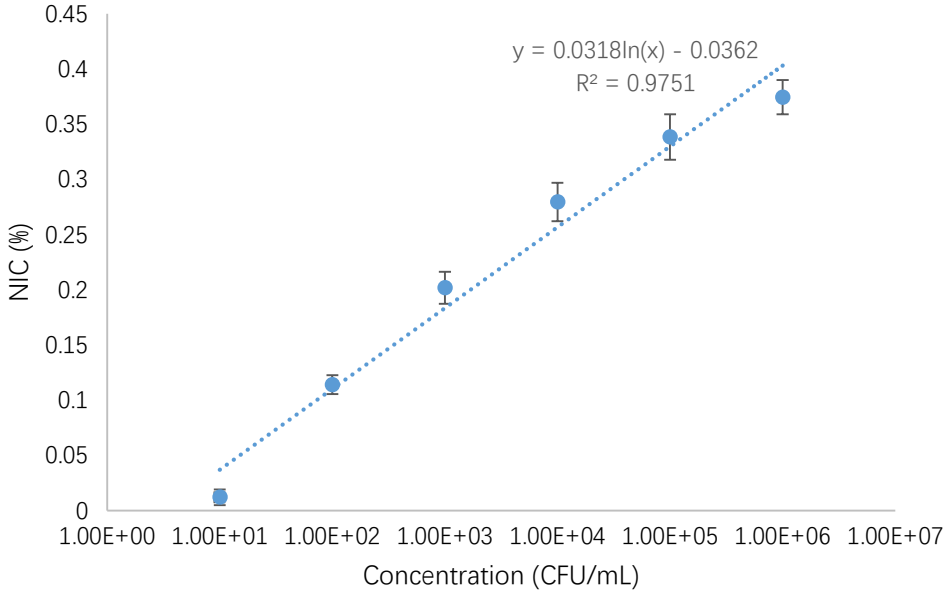

Figure 3.2.11 Normalized impedance change (NIC) at 50 Hz with different target salmonella bacteria concentrations.

The response of the nanoporous membrane based biosensor for various bacteria concentrations was also explored. The reaction conditions were all the same as the previous experiments and EIS was taken every five minutes. As shown in **Figure 3.2.12**, impedance amplitude increased gradually to the maximum for all the concentrations from 10^3 to 10^6 CFU/mL after target *S. enteritidis* bacteria solution was dropped onto the nanoporous alumina membrane for 40 min. Therefore, it could be concluded that 40 min was an appropriate time for salmonella bacteria capturing, which met the requirement of a fast and valid detection.

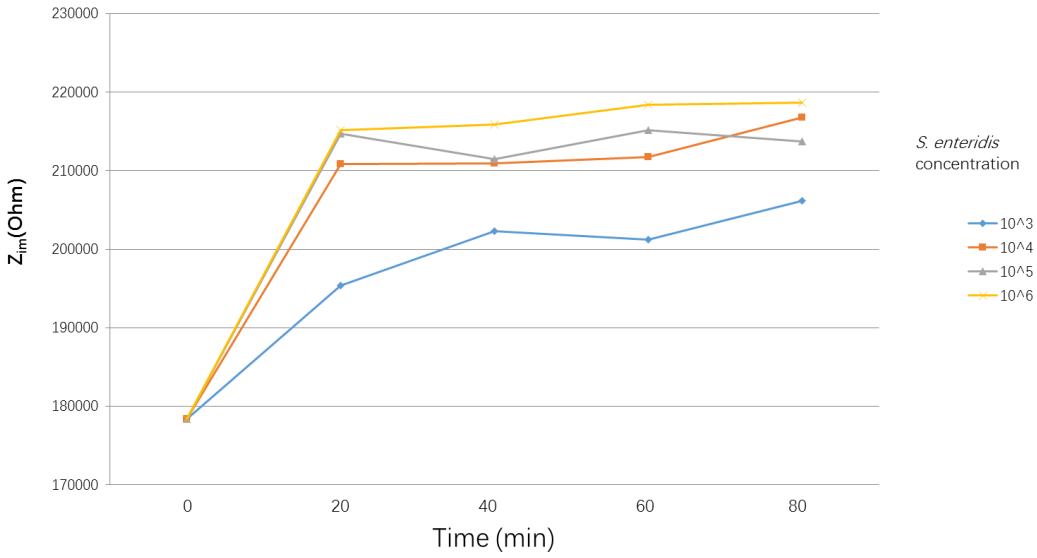

Figure 3.2.12 Time response of antibody-bacteria recognition for various bacteria concentrations

3.2.4.3 Impedance measurement for specificity testing

Cross-reactivity in antibodies was critical in immunoassays. Although one particular type of antibody could only recognize and combine with specific target antigen theoretically, physical adsorption caused by Van der Waals' force or electrostatic force could be the interference factor which causes non-specific binding. Hence, specificity studies are highly in need to explore whether cross-reactions on unspecific bacteria would happen.

E. coli O157:H7 bacteria were selected as the control group for specific testing. As shown in **Figure 3.2.13**, target salmonella bacteria groups show obvious high impedance signals compared with control group of *E. coli O157:H7* bacteria for the concentrations from 10^2 to 10^6 CFU/mL. For interferential *E. coli O157:H7* bacteria, NIC in the range from 10 to 10^6 was quite low. While target salmonella bacteria at a concentration of 10 CFU/mL had a quite large relative standard deviation, which could not clearly differentiate from a control group of *E. coli O157:H7* bacteria. Therefore, the specificity of this salmonella bacteria detection was considered to be good in the range from 10^2 to 10^6 CFU/mL.

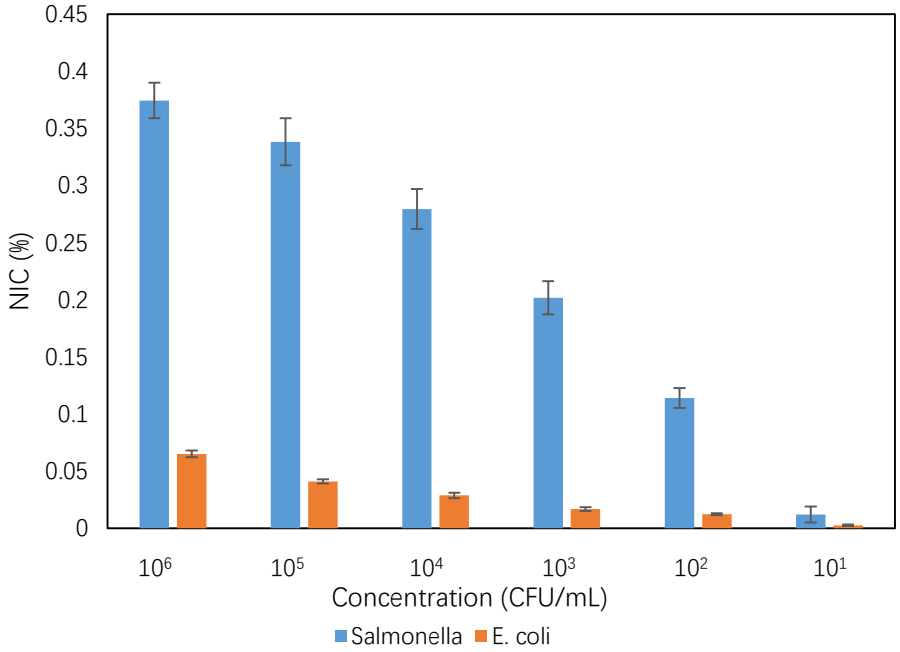

Figure 3.2.8 Impedance amplitude NIC for target salmonella and non-specific *E. coli O157:H7* bacteria.

Chapter 4 Discussion and future work

An ideal biosensor should consist of these features: high sensitivity and excellent selectivity, low cost, fast detection, easy to operate, portability and no requirement of bulky and expensive instruments, good repeatability and stability. Hence, the discussion of our two projects including electrochemical biosensors for *E. coli O157:H7* gene detection and *Salmonella enteritidis* bacteria detection are based on these aspects.

4.1 Immobilization of *E. coli O157:H7 gene* probes or *Salmonella enteritidis* bacteria antibodies on nanoporous alumina membrane

Typically, two approaches are mainly used to achieve the immobilization of gene probes or antibodies: one is through covalent binding, and the other one is through non-covalent binding which is caused by physical adsorption. Each of them has its advantages and disadvantages. For immobilizations through covalent binding, the most prominent superiority is the stability. Covalent binding is based on chemical reaction, so it is essentially a stable chemical bond. Compared to physical bonds, chemical bonds are very strong and stable under various conditions such as different pH, temperature, ion strength, or constant physical stirring or washing. However, drawbacks existed as well. First of all, covalent binding is a relatively complicated chemical synthesis process. Many chemicals are involved, which may destroy the

structures of reagents. This issue is especially critical in bio-related reactions because biomolecules such as proteins, oligonucleotides, or cells are very unstable and easy to bed denatured. Furthermore, covalent binding through the original chemical groups on biomolecules may lead to the loss of functions. Another drawback is the less flexibility of chemical bonds. In some cases, the binding molecules need to be released under certain conditions or reactions, but the covalent chemical bond is hard to be destructed.

In electrochemical biosensing, antibodies or aptamers which have the bio-recognition functions are generally attached to working electrodes as the first step. Compared with physical adsorption, biomolecules attachment through covalent binding may hinder the electron transfer on electrodes surface and decrease the conductivity of electrode surface, which may weaken the electrochemical performances. For instance, ITO electrodes are widely used in electrochemical sensing as well as electrochemiluminescence sensing. The abundant hydroxyl groups enable ITO electrodes covalently bound to various molecules through silanization reactions. However, after silane modification, the conductivity of ITO electrode may decrease significantly, leading to insensitive reactions under electrochemical changes.

Physical adsorption is based on Van der Waals' forces, which is typically caused by hydrophily/ hydrophobicity and surface charge. Particles with opposite charges or similar hydrophilic properties tend to aggregate. Compared to chemical bond forces, Van der Waals' forces are much weaker. Hence the washing step may lead to the exfoliations. Furthermore, surface charges are affected by environment parameters

such as pH values. A positively charged molecule in the low pH environment may turn into negatively charged one in the high pH environment. Hence physical adsorption is also unstable under varying pH conditions. Advantages of physical adsorption are that it can keep the intrinsic electrochemical performance of electrodes and the bio-functions of biomolecules.

In our two projects, covalent binding was chosen for oligonucleotides and antibodies attachments. This was decided mainly based on the concerns of sensitivity and stability. For the stability, covalent binding is much stronger and more stable compared to physical binding. Multiple washing steps are performed during the whole fabrication procedures which need a stable bonding force. Moreover, the sandwich structures were formed during the sensor establishment, which was mainly based on the first antibody immobilization and second antibodies conjugation. Hence, strong binding is critical for the stability of this sandwich structures. Fortunately, unlike other electrochemical biosensors whose modification processes took place on working electrode surfaces with the negative influence on the electrochemical performance of the sensor, covalent modification on nanoporous alumina membranes will not change the electrochemical performance since nanoporous alumina membrane is intrinsically non-conductive and the impedance signal is mainly based on the blocking degree of nanopores. Hence the adverse impacts of covalently binding for the traditional electrodes can be ignored for our experiment.

4.2 Nanopores size effect

Three nanopores' sizes of nanoporous alumina membranes are commercially available: 200nm, 100nm, 20nm. For *E. coli O157:H7 genes* detection, small nanopores of nanoporous alumina membranes were commonly chosen to achieve a best hindering of electron mobility. Oligonucleotides are long chain molecules with phosphate backbones. The size of an oligonucleotides molecule can be roughly estimated by the amount of bases. The distance between two bases is about 0.34 nm. Hence a 50-bases oligonucleotides molecule is about 17 nm. Detection without any further amplifications is suitable to use nanoporous alumina membranes with small size. This is because that the similar sizes of nanopores and oligonucleotides will lead to a high blocking degree of nanopores for high sensitivity.

However, small-sized nanoporous alumina membrane has its limitation for a more general detection of various length oligonucleotides. When nanopores and oligonucleotides have similar sizes, it will be quite difficult for oligonucleotides to go inside the nanopores due to the hydrodynamic effect. To facilitate the entering of oligonucleotides, the nanopores should be much larger than the oligonucleotides. When target oligonucleotides are much smaller than the nanopore size, the electron mobility in nanopores will not be hindered obviously, leading to a less-than-ideal performance. Hence such a method with matching pore size with oligonucleotide size is not a good choice for oligonucleotides detection.

Therefore, in our projects, detections using a sandwich structure with an amplification tag will greatly enhance the sensitivity and feasibility to various lengths of target oligonucleotides. Since an amplification process is performed to fill the whole nanopore, the size of nanopores can be chosen much larger and the oligonucleotides capturing is not limited inside nanopores. Even though the oligonucleotides capturing happens on nanoporous alumina membrane, the signal amplification can be applied and provides an excellent sensitivity. Hence, in the first project, large nanoporous alumina membrane (200nm) were used, and theoretically oligos smaller than this size could be detected. However, no further comparison between 100 nm and 200 nm nanoporous membrane were conducted, as well as the comparisons between precipitation inside nanopores and on the membrane surface. Future works will focus on these two aspects to build a better oligonucleotides detecting platform with better performance.

Although the depth of nanopores could not be altered, it still needs some discussions. To achive a higher LOD, the length of nanopores should be as small as possible. Hence, when very few target oligos were added in and caused the blockage, more amounts of nanopores could be obstructed, leading to the large change of impedance. Moreover, when the length of nanopores is small, the basic impedance is small as well, which is also favorable to better the sensitivity. To achieve a wide detection range, the depth can be larger to prevent the full blockage of nanopores.

4.3 Selection of amplification methods and tags

Many methods and tags have been reported for signal amplification. For instance, our group built a microfluidics device for DNA detection based on silver enhancement [122]. The secondary oligonucleotides probes were modified with gold nanoparticles (AuNPs), and during the amplification process, silver was deposited around AuNPs to achieve a Ag-Au shell-core structure. The volume of this shell-core composites was much larger than that of small AuNPs whose size is typically around 13nm. If the silver enhancement took place inside nanoporous, the space for electron floating would be significantly blocked, leading to a great increase of the impedance (**Figure 4.3.1**).

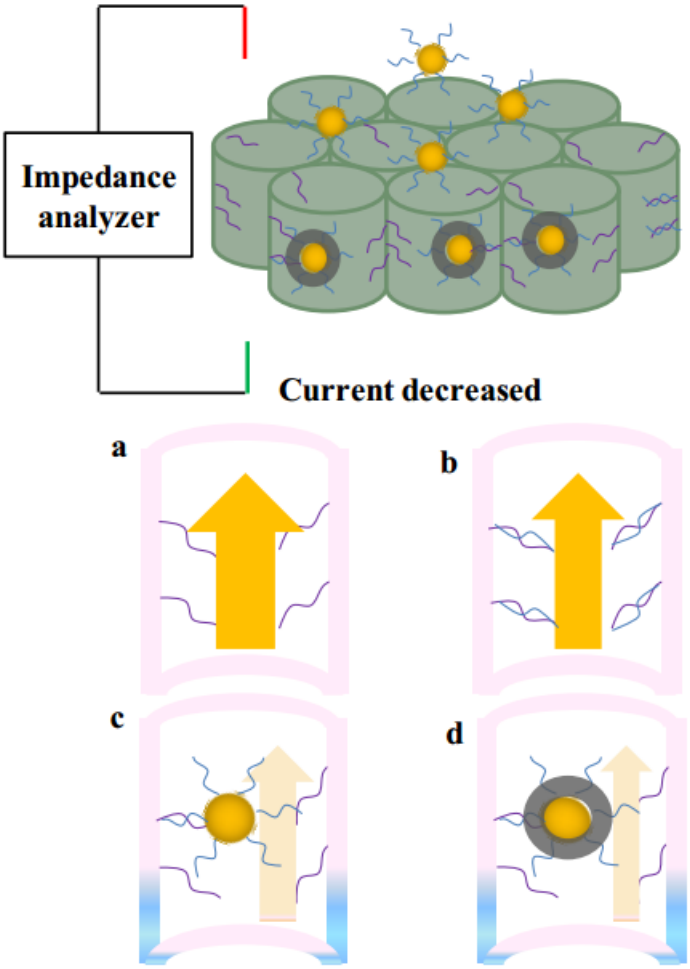

Figure 4.3.1 Sensing principle of nanoporous membrane impedance sensor based on silver enhancement amplification. (a) (b) (c) and (d) show the impedance gradually decreases in each experimental step and each the largest after silver enhancement reaction [122].

This method was proved excellent for oligonucleotides detection. However, several limitations were existed and needed to be improved. The function of silver enhancement was to block the nanoporous channels and hinder the electron transfer. However, gold and silver were conductive material intrinsically, and this hampered the efforts for blocking ion current through the nanopores. To design a better amplification tag, catalyzed precipitation of non-conductive 4-CN was chosen with

the catalysts of PtNPs and GO/hemin. The precipitation products of 4-CN were not conductive, which met the requirement of electron hindering. During the precipitation reaction, sediments were deposited onto membrane surface and inside nanopores, which significantly enhance the impedance signals.

Moreover, since the precipitation reaction was based in the presence of H_2O_2, this platform could be potentially performed as a biosensor for H_2O_2 detection. A simple detection can be designed as following: H_2O_2 catalysts such as HRP or PtNPs can be firstly modified inside nanoporous alumina membrane. When 4-CN is added into PBS solution containing H_2O_2, precipitation will be deposited inside nanopores in the presence of H_2O_2, leading to the increasing impedance between working electrode and the counter electrode. The impedance increase is proportional to the concentration of target H_2O_2.

4.4 Synthesis of GO/Hemin-antibody composites

In the composites of GO/Hemin-antibody, GO plays a role as the nanocarrier for the attachment of antibodies and hemin biomolecules. Since GO is abundant of oxygen containing groups and has a large surface-volume ratio, antibodies could be immobilized on though covalent binding and a high loading capacity of hemin biomolecules would be achieved.

For the synthesis of GO-antibody/hemin composites, the synthesis approach was initially designed to attach hemin in GO surface firstly and then to conjugate antibodies onto the surface of obtained GO/hemin composites. However, there were some difficulties to conjugate antibody firstly and the final synthesis approach adopted conjugation of antibody on GO at the first step. The reason could be explained as following.

When the attachment of antibodies was achieved through covalent binding, EDC/NHS had to be used to activate carboxyl groups on GO firstly. However, hemin itself also consisted of carboxyl groups (**Figure 4.4.1**), and the activation of hemin was unavoidable to lose the catalytic property. If the attachment of antibodies was achieved through physical adsorption, since both of hemin and antibody attachments are based on π-π stacking interaction, a competitive relation existed and influenced the amount of attached hemin and antibodies (**Figure 4.4.2**). Also, the later adsorption of BSA for passivation was another competitor.

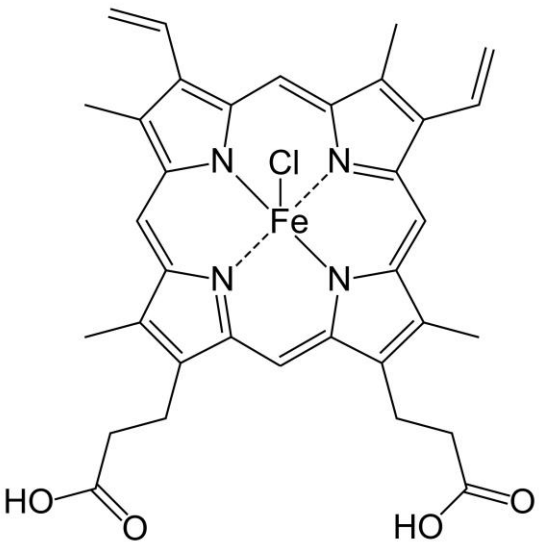

Figure 4.4.1 Skeletal formula of hemin molecule

Therefore, a covalent binding method of antibody was conducted firstly, and the concentration of ammonium hydroxide was reduced. Results showed that the activity of antibodies remained which could be used to capture salmonella bacteria. However, the potential quantification of the decrease of the antibody activity during the whole conjugation process was not tested, and future experiments can be conducted for the evaluation.

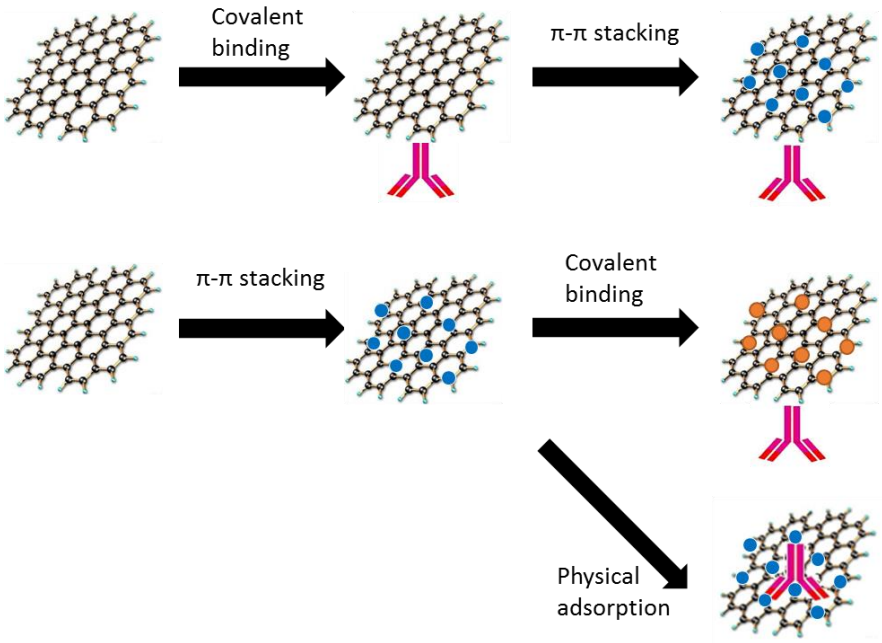

Figure 4.4.2 Three strategies to synthesize GO/Hemin-Antibody composites

4.5 Sample volume and sensing area effects

For *Salmonella enteritidis* bacteria detection, when the concentration of target *Salmonella enteritidis* bacteria was low to 10 CFU/mL, a 150 μL sample averagely contains 1~2 bacteria. Since the distribution of bacteria was quite random in the solution when the sample volume was very small, it was very possible that no bacteria existed in the 150 μL sample to be tested. Moreover, compared to the small volume of a few bacteria, sensing area of nanoporous alumina membrane is too large to sense effectively. Therefore, future improvement of sensitivity can be achieved through decreasing the sensing area on membranes as well as increasing the sample volume.

Microfluidics-based detecting system integrated with nanoporous membranes can be a good alternative. For the sample volume issue, since the detection process inside microfluidics will be conducted with a flowing solution sample, the sample volume can be much larger. Moreover, the detecting time will not be increased much because the small channels in a typical microfluidics device enable the rapid detection. This is due to the small height of the microfluidic channels, leading to a higher probability for bacteria to contact with the bottom sensing surface. For the portability concern, the small size of a microfluidics device makes it very promising as well.

4.6 Improvement to achieve fast detection

An excellent sensing platform should not only be sensitive and specific but also be very fast to provide a quick response. Compared to other reported devices with no

sandwich structure for signal amplification, fabrication of these two biosensors in this thesis are much more complicated. Therefore, assembling time is a critical issue and need to be shortened as much as possible. For the *E. coli O157:H7 genes* detection, the target genes capturing time as well as the time of precipitation were studied in details. The target genes' hybridization was found to be close to saturation after 4h, and the later hybridization of Pt-oligonucleotides probes was therefore performed for 4 h. More future work is needed for the time optimization to achieve fast-response electrochemical biosensors for gene and bacteria detection.

5. Conclusion

Nanoporous alumina membrane based electrochemical biosensors were developed for *E. coli O157:H7 genes* detection with PtNPs tags for signal amplification and *Salmonella enteritidis* bacteria detection with GO/hemin composites tags for signal amplification, respectively. The research consists of two parts.

The first part was to fabricate a nanoporous alumina membrane based impedimetric biosensor for *E. coli O157:H7 genes* detection. A sandwich structure was formed via the co-hybridization of target genes and gene probes on the membrane as well as another gene probe conjugated with PtNPs. The purpose of conjugation of PtNPs on gene probes was to catalyze soluble 4-CN into insoluble 4-CN in the presence of hydrogen peroxide. The catalyzed insoluble 4-CN would precipitate onto nanoporous alumina membrane surface and into nanopores, resulting in significant

impedance increase. This platform was proved to be feasible and efficient for *E. coli O157:H7 genes* detection and the detection was conducted by electrochemical impedance spectroscopy method. A limit of detection (LOD) of 93.8pM was achieved. The specificity study was conducted with non-target genes and 6 bases mismatched genes. The results demonstrated good sequence selectivity of this impedimetric biosensor.

The second part was to fabricate a nanoporous alumina membrane based impedimetric biosensor for *Salmonella enteritidis* bacteria detection. A sandwich structure was formed via the specific co-attachments of target *S. enteritidis* bacteria and antibody probes on the membrane as well as GO-antibody/hemin composites. GO/Hemin-Ab composites were attached onto captured bacteria to catalyze soluble 4-CN into insoluble products. The basic principle was the same to that in the first part. A LOD of 12 CFU/mL was achieved and the selectivity was proved good using *E. coli* bacteria as the control groups.

Reference

[1] Leonard P, Hearty S, Brennan J, Dunne L, Quinn J, Chakraborty T, et al. Advances in biosensors for detection of pathogens in food and water. Enzyme Microb Tech. 2003;32:3-13.

[2] Ivnitski D, Abdel-Hamid I, Atanasov P, Wilkins E. Biosensors for detection of pathogenic bacteria. Biosens Bioelectron. 1999;14:599-624.

[3] Swaminathan B, Feng P. Rapid Detection of Food-Borne Pathogenic Bacteria. Annu Rev Microbiol. 1994;48:401-26.

[4] de Boer E, Beumer RR. Methodology for detection and typing of foodborne microorganisms. Int J Food Microbiol. 1999;50:119-30.

[5] Krambeck C, Krambeck HJ, Overbeck J. Microcomputer-Assisted Biomass Determination of Plankton Bacteria on Scanning Electron-Micrographs. Appl Environ Microb. 1981;42:142-9.

[6] Borsheim KY, Bratbak G, Heldal M. Enumeration and Biomass Estimation of Planktonic Bacteria and Viruses by Transmission Electron-Microscopy. Appl Environ Microb. 1990;56:352-6.

[7] Loferer-Krossbacher M, Klima J, Psenner R. Determination of bacterial cell dry mass by transmission electron microscopy and densitometric image analysis. Appl Environ Microb. 1998;64:688-94.

[8] Howell SW, Inerowicz HD, Regnier FE, Reifenberger R. Patterned protein microarrays for bacterial detection. Langmuir. 2003;19:436-9.

[9] Johnson RP, Durham RJ, Johnson ST, Macdonald LA, Jeffrey SR, Butman BT. Detection of Escherichia-Coli O157-H7 in Meat by an Enzyme-Linked-Immunosorbent-Assay, Ehec-Tek. Appl Environ Microb. 1995;61:386-8.

[10] Gehring AG, Patterson DL, Tu SI. Use of a light-addressable potentiometric sensor for the detection of Escherichia coli O157 : H7. Anal Biochem. 1998;258:293-8.

[11] Ke DB, Menard C, Picard FJ, Boissinot M, Ouellette M, Roy PH, et al. Development of conventional and real-time PCR assays for the rapid detection of group B streptococci. Clin Chem. 2000;46:324-31.

[12] Jofre A, Martin B, Garriga M, Hugas M, Pla M, Rodriguez-Lazaro D, et al. Simultaneous detection of Listeria monocytogenes and Salmonella by multiplex PCR in cooked ham. Food Microbiol. 2005;22:109-15.

[13] Lazcka O, Del Campo FJ, Munoz FX. Pathogen detection: A perspective of traditional methods and biosensors. Biosens Bioelectron. 2007;22:1205-17.

[14] Waswa J, Irudayaraj J, DebRoy C. Direct detection of E-Coli O157 : H7 in selected food systems by a surface plasmon resonance biosensor. Lwt-Food Sci Technol. 2007;40:187-92.

[15] Selvin PR, Ha T, Enderle T, Ogletree DF, Chemla DS, Weiss S. Fluorescence resonance energy transfer between a single donor and a single acceptor molecule. Biophys J. 1996;70:Wp302-Wp.

[16] Shi JY, Chan CY, Pang YT, Ye WW, Tian F, Lyu J, et al. A fluorescence resonance energy transfer (FRET) biosensor based on graphene quantum dots (GQDs) and gold nanoparticles (AuNPs) for the detection of mecA gene sequence of Staphylococcus aureus. Biosens Bioelectron. 2015;67:595-600.

[17] Su XL, Li YB. A self-assembled monolayer-based piezoelectric immunosensor for rapid detection of Escherichia coli O157 : H7. Biosens Bioelectron. 2004;19:563-74.

[18] Funes-Huacca M, Wu A, Szepesvari E, Rajendran P, Kwan-Wong N, Razgulin A, et al. Portable self-contained cultures for phage and bacteria made of paper and tape. Lab Chip. 2012;12:4269-78.

[19] Brett CMA, Oliveira-Brett AM. Electrochemical sensing in solution-origins, applications and future perspectives. J Solid State Electr. 2011;15:1487-94.

[20] Brett CMA. Electroanalytical techniques for the future: The challenges of miniaturization and of real-time measurements. Electroanal. 1999;11:1013-6.

[21] Ostwald W. Electrochemistry: history and theory: Smithsonian Institution and the National Science Foundation; 1980.

[22] Thevenot DR, Toth K, Durst RA, Wilson GS. Electrochemical biosensors: recommended definitions and classification. Biosens Bioelectron. 2001;16:121-31.

[23] Wang J. Analytical electrochemistry: John Wiley & Sons; 2006.

[24] Buck RP, Lindner E. Recommendations for nomenclature of ionselective electrodes (IUPAC Recommendations 1994). Pure Appl Chem. 1994;66:2527-36.

[25] Scholz F. From the Leiden jar to the discovery of the glass electrode by Max Cremer. J Solid State Electr. 2011;15:5-14.

[26] Wang J, Cai XH, Fernandes JR, Ozsoz M, Grant DH. Adsorptive potentiometric stripping analysis of trace tamoxifen at a glassy carbon electrode. Talanta. 1997;45:273-8.

[27] Bonfil Y, Brand M, Kirowa-Eisner E. Trace determination of mercury by anodic stripping voltammetry at the rotating gold electrode. Anal Chim Acta. 2000;424:65-76.

[28] Arevalo MC, Luna AMC, Arevalo A, Arvia AJ. Voltammetric Approach to Multicomponent Electrochemical Systems at Platinum-Electrode Surfaces. J Electroanal Chem. 1992;330:595-614.

[29] Thevenot DR, Sternberg R, Coulet PR, Laurent J, Gautheron DC. Enzyme Collagen Membrane for Electrochemical Determination of Glucose. Anal Chem. 1979;51:96-100.

[30] Wollenberger U, Schubert F, Pfeiffer D, Scheller FW. Enhancing Biosensor Performance Using Multienzyme Systems. Trends Biotechnol. 1993;11:255-62.

[31] Fang YX, Zhang D, Qin X, Miao ZY, Takahashi S, Anzai J, et al. A non-enzymatic hydrogen peroxide sensor based on poly(vinyl alcohol)-multiwalled carbon nanotubes-platinum nanoparticles hybrids modified glassy carbon electrode. Electrochim Acta. 2012;70:266-71.

[32] Maduralveeran G, Ramaraj R. Gold nanoparticles embedded in silica sol-gel matrix as an amperometric sensor for hydrogen peroxide. J Electroanal Chem. 2007;608:52-8.

[33] Travascio P, Witting PK, Mauk AG, Sen D. The peroxidase activity of a hemin-DNA oligonucleotide complex: Free radical damage to specific guanine bases of the DNA. J Am Chem Soc. 2001;123:1337-48.

[34] Farjami E, Clima L, Gothelf K, Ferapontova EE. "Off On" Electrochemical Hairpin-DNA-Based Genosensor for Cancer Diagnostics. Anal Chem. 2011;83:1594-602.

[35] Bock LC, Griffin LC, Latham JA, Vermaas EH, Toole JJ. Selection of Single-Stranded-DNA Molecules That Bind and Inhibit Human Thrombin. Nature. 1992;355:564-6.

[36] Weiss S, Proske D, Neumann M, Groschup MH, Kretzschmar HA, Famulok M, et al. RNA aptamers specifically interact with the prion protein PrP. J Virol. 1997;71:8790-7.

[37] Lauhon CT, Szostak JW. Rna Aptamers That Bind Flavin and Nicotinamide Redox Cofactors. J Am Chem Soc. 1995;117:1246-57.

[38] Lorsch JR, Szostak JW. In-Vitro Selection of Rna Aptamers Specific for Cyanocobalamin. Biochemistry-Us. 1994;33:973-82.

[39] Huizenga DE, Szostak JW. A DNA Aptamer That Binds Adenosine and Atp. Biochemistry-Us. 1995;34:656-65.

[40] Stoltenburg R, Reinemann C, Strehlitz B. SELEX-A (r)evolutionary method to generate high-affinity nucleic acid ligands. Biomol Eng. 2007;24:381-403.

[41] Tombelli S, Minunni A, Mascini A. Analytical applications of aptamers. Biosens Bioelectron. 2005;20:2424-34.

[42] Orazem ME, Tribollet B. Electrochemical impedance spectroscopy: John Wiley & Sons; 2011.

[43] Ferapontova EE, Olsen EM, Gothelf KV. An RNA aptamer-based electrochemical biosensor for detection of theophylline in serum. J Am Chem Soc. 2008;130:4256-+.

[44] Xuan F, Luo XT, Hsing IM. Ultrasensitive Solution-Phase Electrochemical Molecular Beacon-Based DNA Detection with Signal Amplification by Exonuclease III-Assisted Target Recycling. Anal Chem. 2012;84:5216-20.

[45] Shervedani RK, Mehrjardi AH, Zamiri N. A novel method for glucose determination based on electrochemical impedance spectroscopy using glucose oxidase self-assembled biosensor. Bioelectrochemistry. 2006;69:201-8.

[46] Shamsipur M, Asgari M, Maragheh MG, Moosavi-Movahedi AA. A novel impedimetric nanobiosensor for low level determination of hydrogen peroxide based on biocatalysis of catalase. Bioelectrochemistry. 2012;83:31-7.

[47] Patolsky F, Katz E, Willner I. Amplified DNA detection by electrogenerated biochemiluminescence and by the catalyzed precipitation of an insoluble product on electrodes in the presence of the doxorubicin intercalator. Angew Chem Int Edit. 2002;41:3398-+.

[48] Chen W, Cai S, Ren QQ, Wen W, Zhao YD. Recent advances in electrochemical sensing for hydrogen peroxide: a review. Analyst. 2012;137:49-58.

[49] Narayanan R, El-Sayed MA. Shape-dependent catalytic activity of platinum nanoparticles in colloidal solution. Nano Lett. 2004;4:1343-8.

[50] Yao SJ, Xu JH, Wang Y, Chen XX, Xu YX, Hu SS. A highly sensitive hydrogen peroxide amperometric sensor based on MnO2 nanoparticles and dihexadecyl hydrogen phosphate composite film. Anal Chim Acta. 2006;557:78-84.

[51] Salimi A, Hallaj R, Soltanian S, Mamkhezri H. Nanomolar detection of hydrogen peroxide on glassy carbon electrode modified with electrodeposited cobalt oxide nanoparticles. Anal Chim Acta. 2007;594:24-31.

[52] Miao XM, Yuan R, Chai YQ, Shi YT, Yuan YY. Direct electrocatalytic reduction of hydrogen peroxide based on Nafion and copper oxide nanoparticles modified Pt electrode. J Electroanal Chem. 2008;612:157-63.

[53] Elzanowska H, Abu-Irhayem E, Skrzynecka B, Birss VI. Hydrogen peroxide detection at electrochemically and sol-gel derived Ir oxide films. Electroanal. 2004;16:478-90.

[54] Jiang LC, Zhang WD. Electrodeposition of TiO2 Nanoparticles on Multiwalled Carbon Nanotube Arrays for Hydrogen Peroxide Sensing. Electroanal. 2009;21:988-93.

[55] Wang J, Musameh M. Carbon nanotube/teflon composite electrochemical sensors and biosensors. Anal Chem. 2003;75:2075-9.

[56] Zhou M, Zhai YM, Dong SJ. Electrochemical Sensing and Biosensing Platform Based on Chemically Reduced Graphene Oxide. Anal Chem. 2009;81:5603-13.

[57] Hou L, Gao ZQ, Xu MD, Cao X, Wu XP, Chen GN, et al. DNAzyme-functionalized gold-palladium hybrid nanostructures for triple signal amplification of impedimetric immunosensor. Biosens Bioelectron. 2014;54:365-71.

[58] Xue T, Jiang S, Qu YQ, Su Q, Cheng R, Dubin S, et al. Graphene-Supported Hemin as a Highly Active Biomimetic Oxidation Catalyst. Angew Chem Int Edit. 2012;51:3822-5.

[59] Novoselov KS, Geim AK, Morozov SV, Jiang D, Zhang Y, Dubonos SV, et al. Electric field effect in atomically thin carbon films. Science. 2004;306:666-9.

[60] Yu HT, Xu PC, Lee DW, Li XX. Porous-layered stack of functionalized AuNP-rGO (gold nanoparticles-reduced graphene oxide) nanosheets as a sensing material for the micro-gravimetric detection of chemical vapor. J Mater Chem A. 2013;1:4444-50.

[61] Compton OC, Nguyen ST. Graphene Oxide, Highly Reduced Graphene Oxide, and Graphene: Versatile Building Blocks for Carbon-Based Materials. Small. 2010;6:711-23.

[62] Ambrosi A, Chua CK, Bonanni A, Pumera M. Electrochemistry of Graphene and Related Materials. Chem Rev. 2014;114:7150-88.

[63] Meyer JC, Geim AK, Katsnelson MI, Novoselov KS, Booth TJ, Roth S. The structure of suspended graphene sheets. Nature. 2007;446:60-3.

[64] Brodie B. Sur le poids atomique du graphite. Ann Chim Phys. 1860;59:e472.

[65] Staudenmaier L. Verfahren zur darstellung der graphitsäure. Berichte der deutschen chemischen Gesellschaft. 1898;31:1481-7.

[66] Hummers WS, Offeman RE. Preparation of Graphitic Oxide. J Am Chem Soc. 1958;80:1339-.

[67] Marcano DC, Kosynkin DV, Berlin JM, Sinitskii A, Sun ZZ, Slesarev A, et al. Improved Synthesis of Graphene Oxide. Acs Nano. 2010;4:4806-14.

[68] Jnioui A, Metrot A, Storck A. Electrochemical production of graphite salts using a three-dimensional electrode of graphite particles. Electrochim Acta. 1982;27:1247-52.

[69] Wang GX, Wang B, Park J, Wang Y, Sun B, Yao J. Highly efficient and large-scale synthesis of graphene by electrolytic exfoliation. Carbon. 2009;47:3242-6.

[70] Alanyalioglu M, Segura JJ, Oro-Sole J, Casan-Pastor N. The synthesis of graphene sheets with controlled thickness and order using surfactant-assisted electrochemical processes. Carbon. 2012;50:142-52.

[71] Morales GM, Schifani P, Ellis G, Ballesteros C, Martinez G, Barbero C, et al. High-quality few layer graphene produced by electrochemical intercalation and microwave-assisted expansion of graphite. Carbon. 2011;49:2809-16.

[72] Wang JZ, Manga KK, Bao QL, Loh KP. High-Yield Synthesis of Few-Layer Graphene Flakes through Electrochemical Expansion of Graphite in Propylene Carbonate Electrolyte. J Am Chem Soc. 2011;133:8888-91.

[73] Bonanni A, Pumera M. Surfactants used for dispersion of graphenes exhibit strong influence on electrochemical impedance spectroscopic response. Electrochem Commun. 2012;16:19-21.

[74] Brownson DAC, Banks CE. Graphene electrochemistry: Surfactants inherent to graphene inhibit metal analysis. Electrochem Commun. 2011;13:111-3.

[75] Cai JM, Ruffieux P, Jaafar R, Bieri M, Braun T, Blankenburg S, et al. Atomically precise bottom-up fabrication of graphene nanoribbons. Nature. 2010;466:470-3.

[76] Novoselov KS, Fal'ko VI, Colombo L, Gellert PR, Schwab MG, Kim K. A roadmap for graphene. Nature. 2012;490:192-200.

[77] Farmer DB, Chiu HY, Lin YM, Jenkins KA, Xia FN, Avouris P. Utilization of a Buffered Dielectric to Achieve High Field-Effect Carrier Mobility in Graphene Transistors. Nano Lett. 2009;9:4474-8.

[78] Li XS, Zhu YW, Cai WW, Borysiak M, Han BY, Chen D, et al. Transfer of Large-Area Graphene Films for High-Performance Transparent Conductive Electrodes. Nano Lett. 2009;9:4359-63.

[79] Ambrosi A, Pumera M. Electrochemistry at CVD Grown Multilayer Graphene Transferred onto Flexible Substrates. J Phys Chem C. 2013;117:2053-8.

[80] Huang P, Xu C, Lin J, Wang C, Wang XS, Zhang CL, et al. Folic Acid-conjugated Graphene Oxide loaded with Photosensitizers for Targeting Photodynamic Therapy. Theranostics. 2011;1:240-50.

[81] Paredes JI, Villar-Rodil S, Solis-Fernandez P, Martinez-Alonso A, Tascon JMD. Atomic Force and Scanning Tunneling Microscopy Imaging of Graphene Nanosheets Derived from Graphite Oxide. Langmuir. 2009;25:5957-68.

[82] Paredes JI, Villar-Rodil S, Martinez-Alonso A, Tascon JMD. Graphene oxide dispersions in organic solvents. Langmuir. 2008;24:10560-4.

[83] Umasankar Y, Unnikrishnan B, Chen SM, Ting TW. Graphene impregnated with horseradish peroxidase multimer for the determination of hydrogen peroxide. Anal Methods-Uk. 2012;4:3653-60.

[84] Wu M, Kempaiah R, Huang PJJ, Maheshwari V, Liu JW. Adsorption and Desorption of DNA on Graphene Oxide Studied by Fluorescently Labeled Oligonucleotides. Langmuir. 2011;27:2731-8.

[85] Huang X, Qi XY, Boey F, Zhang H. Graphene-based composites. Chem Soc Rev. 2012;41:666-86.

[86] Liu JB, Fu SH, Yuan B, Li YL, Deng ZX. Toward a Universal "Adhesive Nanosheet" for the Assembly of Multiple Nanoparticles Based on a Protein-Induced Reduction/Decoration of Graphene Oxide. J Am Chem Soc. 2010;132:7279-+.

[87] Huang J, Zhang LM, Chen BA, Ji N, Chen FH, Zhang Y, et al. Nanocomposites of size-controlled gold nanoparticles and graphene oxide: Formation and applications in SERS and catalysis. Nanoscale. 2010;2:2733-8.

[88] Brust M, Walker M, Bethell D, Schiffrin DJ, Whyman R. Synthesis of thiol-derivatised gold nanoparticles in a two-phase liquid–liquid system. J Chem Soc, Chem Commun. 1994:801-2.

[89] Liang RQ, Tan CY, Ruan KC. Colorimetric detection of protein microarrays based on nanogold probe coupled with silver enhancement. J Immunol Methods. 2004;285:157-63.

[90] Pumera M. Graphene-based nanomaterials and their electrochemistry. Chem Soc Rev. 2010;39:4146-57.

[91] Davies TJ, Hyde ME, Compton RG. Nanotrench arrays reveal insight into graphite electrochemistry. Angew Chem Int Edit. 2005;44:5121-6.

[92] Ambrosi A, Bonanni A, Sofer Z, Cross JS, Pumera M. Electrochemistry at Chemically Modified Graphenes. Chem-Eur J. 2011;17:10763-70.

[93] Poh HL, Simek P, Sofer Z, Tomandl I, Pumera M. Boron and nitrogen doping of graphene via thermal exfoliation of graphite oxide in a BF3 or NH3 atmosphere: contrasting properties. J Mater Chem A. 2013;1:13146-53.

[94] Poh HL, Simek P, Sofer Z, Pumera M. Halogenation of Graphene with Chlorine, Bromine, or Iodine by Exfoliation in a Halogen Atmosphere. Chem-Eur J. 2013;19:2655-62.

[95] Chee SY, Pumera M. Metal-based impurities in graphenes: application for electroanalysis. Analyst. 2012;137:2039-41.

[96] Wong CHA, Chua CK, Khezri B, Webster RD, Pumera M. Graphene Oxide Nanoribbons from the Oxidative Opening of Carbon Nanotubes Retain Electrochemically Active Metallic Impurities. Angew Chem Int Edit. 2013;52:8685-8.

[97] Moo JGS, Ambrosi A, Bonanni A, Pumera M. Inherent Electrochemistry and Activation of Chemically Modified Graphenes for Electrochemical Applications. Chem-Asian J. 2012;7:759-70.

[98] Eng AYS, Ambrosi A, Chua CK, Sanek F, Sofer Z, Pumera M. Unusual Inherent Electrochemistry of Graphene Oxides Prepared Using Permanganate Oxidants. Chem-Eur J. 2013;19:12673-83.

[99] Chua CK, Sofer Z, Pumera M. Graphite oxides: effects of permanganate and chlorate oxidants on the oxygen composition. Chemistry–A European Journal. 2012;18:13453-9.

[100] Zhou M, Wang YL, Zhai YM, Zhai JF, Ren W, Wang FA, et al. Controlled Synthesis of Large-Area and Patterned Electrochemically Reduced Graphene Oxide Films. Chem-Eur J. 2009;15:6116-20.

[101] Toh RJ, Pumera M. Metallic impurities availability in reduced graphene is greatly enhanced by its ultrasonication. Faraday Discuss. 2013;164:275-82.

[102] Li J, Guo SJ, Zhai YM, Wang EK. Nafion-graphene nanocomposite film as enhanced sensing platform for ultrasensitive determination of cadmium. Electrochem Commun. 2009;11:1085-8.

[103] Kang XH, Wang J, Wu H, Aksay IA, Liu J, Lin YH. Glucose Oxidase-graphene-chitosan modified electrode for direct electrochemistry and glucose sensing. Biosens Bioelectron. 2009;25:901-5.

[104] Tang LH, Wang Y, Li YM, Feng HB, Lu J, Li JH. Preparation, Structure, and Electrochemical Properties of Reduced Graphene Sheet Films. Adv Funct Mater. 2009;19:2782-9.

[105] Li Z, Huang Y, Chen L, Qin XL, Huang Z, Zhou YP, et al. Amperometric biosensor for NADH and ethanol based on electroreduced graphene oxide-polythionine nanocomposite film. Sensor Actuat B-Chem. 2013;181:280-7.

[106] Lu LM, Qiu XL, Zhang XB, Shen GL, Tan WH, Yu RQ. Supramolecular assembly of enzyme on functionalized graphene for electrochemical biosensing. Biosens Bioelectron. 2013;45:102-7.

[107] Shang NG, Papakonstantinou P, McMullan M, Chu M, Stamboulis A, Potenza A, et al. Catalyst-Free Efficient Growth, Orientation and Biosensing Properties of Multilayer Graphene Nanoflake Films with Sharp Edge Planes. Adv Funct Mater. 2008;18:3506-14.

[108] Dong HF, Zhu Z, Ju HX, Yan F. Triplex signal amplification for electrochemical DNA biosensing by coupling probe-gold nanoparticles-graphene modified electrode with enzyme functionalized carbon sphere as tracer. Biosens Bioelectron. 2012;33:228-32.

[109] Bonanni A, Chua CK, Zhao GJ, Sofer Z, Pumera M. Inherently Electroactive Graphene Oxide Nanoplatelets As Labels for Single Nucleotide Polymorphism Detection. Acs Nano. 2012;6:8546-51.

[110] Han JM, Ma J, Ma ZF. One-step synthesis of graphene oxide-thionine-Au nanocomposites and its application for electrochemical immunosensing. Biosens Bioelectron. 2013;47:243-7.

[111] Du D, Zou ZX, Shin YS, Wang J, Wu H, Engelhard MH, et al. Sensitive Immunosensor for Cancer Biomarker Based on Dual Signal Amplification Strategy of Graphene Sheets and Multienzyme Functionalized Carbon Nanospheres. Anal Chem. 2010;82:2989-95.

[112] Yoon HJ, Kim TH, Zhang Z, Azizi E, Pham TM, Paoletti C, et al. Sensitive capture of circulating tumour cells by functionalized graphene oxide nanosheets (vol 8, pg 735, 2013). Nat Nanotechnol. 2013;8.

[113] Wan Y, Wang Y, Wu JJ, Zhag D. Graphene Oxide Sheet-Mediated Silver Enhancement for Application to Electrochemical Biosensors. Anal Chem. 2011;83:648-53.

[114] Bernards DA, Desai TA. Nanoscale porosity in polymer films: fabrication and therapeutic applications. Soft Matter. 2010;6:1621-31.

[115] Gultepe E, Nagesha D, Menon L, Busnaina A, Sridhar S. High-throughput assembly of nanoelements in nanoporous alumina templates. Appl Phys Lett. 2007;90.

[116] Park JW, Park SS, Kim Y, Kim I, Ha CS. Mesoporous silica nanolayers infiltrated with hole-transporting molecules for hybrid organic light-emitting devices. Acs Nano. 2008;2:1137-42.

[117] O'sullivan J, Wood G. The morphology and mechanism of formation of porous anodic films on aluminium. Proceedings of the Royal Society of London A:

Mathematical, Physical and Engineering Sciences: The Royal Society; 1970. p. 511-43.

[118] Deng JJ, Toh CS. Impedimetric DNA Biosensor Based on a Nanoporous Alumina Membrane for the Detection of the Specific Oligonucleotide Sequence of Dengue Virus. Sensors-Basel. 2013;13:7774-85.

[119] Tian F, Lyu J, Shi JY, Tan F, Yang M. A polymeric microfluidic device integrated with nanoporous alumina membranes for simultaneous detection of multiple foodborne pathogens. Sensor Actuat B-Chem. 2016;225:312-8.

[120] Chan KY, Ye WW, Zhang Y, Xiao LD, Leung PHM, Li Y, et al. Ultrasensitive detection of E. coli O157:H7 with biofunctional magnetic bead concentration via nanoporous membrane based electrochemical immunosensor. Biosens Bioelectron. 2013;41:532-7.

[121] Hermanson GT. Bioconjugate techniques: Academic press; 2013.

[122] Ye WW, Shi JY, Chan CY, Zhang Y, Yang M. A nanoporous membrane based impedance sensing platform for DNA sensing with gold nanoparticle amplification. Sensor Actuat B-Chem. 2014;193:877-82.

[123] Chow KF, Mavre F, Crooks RM. Wireless electrochemical DNA microarray sensor. J Am Chem Soc. 2008;130:7544-+.

[124] Alligrant TM, Nettleton EG, Crooks RM. Electrochemical detection of individual DNA hybridization events. Lab on a Chip. 2013;13:349-54.

[125] Jentys A. Estimation of mean size and shape of small metal particles by EXAFS. Phys Chem Chem Phys. 1999;1:4059-63.

[126] Hou L, Cui Y, Xu M, Gao Z, Huang J, Tang D. Graphene oxide-labeled sandwich-type impedimetric immunoassay with sensitive enhancement based on enzymatic 4-chloro-1-naphthol oxidation. Biosensors and Bioelectronics. 2013;47:149-56.

[127] Guo YJ, Deng L, Li J, Guo SJ, Wang EK, Dong SJ. Hemin-Graphene Hybrid Nanosheets with Intrinsic Peroxidase-like Activity for Label-free Colorimetric Detection of Single-Nucleotide Polymorphism. Acs Nano. 2011;5:1282-90.